THE ASEAN JOURNAL OF RADIOLOGY

January-April 2012
Volume XVIII Number I
ISSN 0859 144X

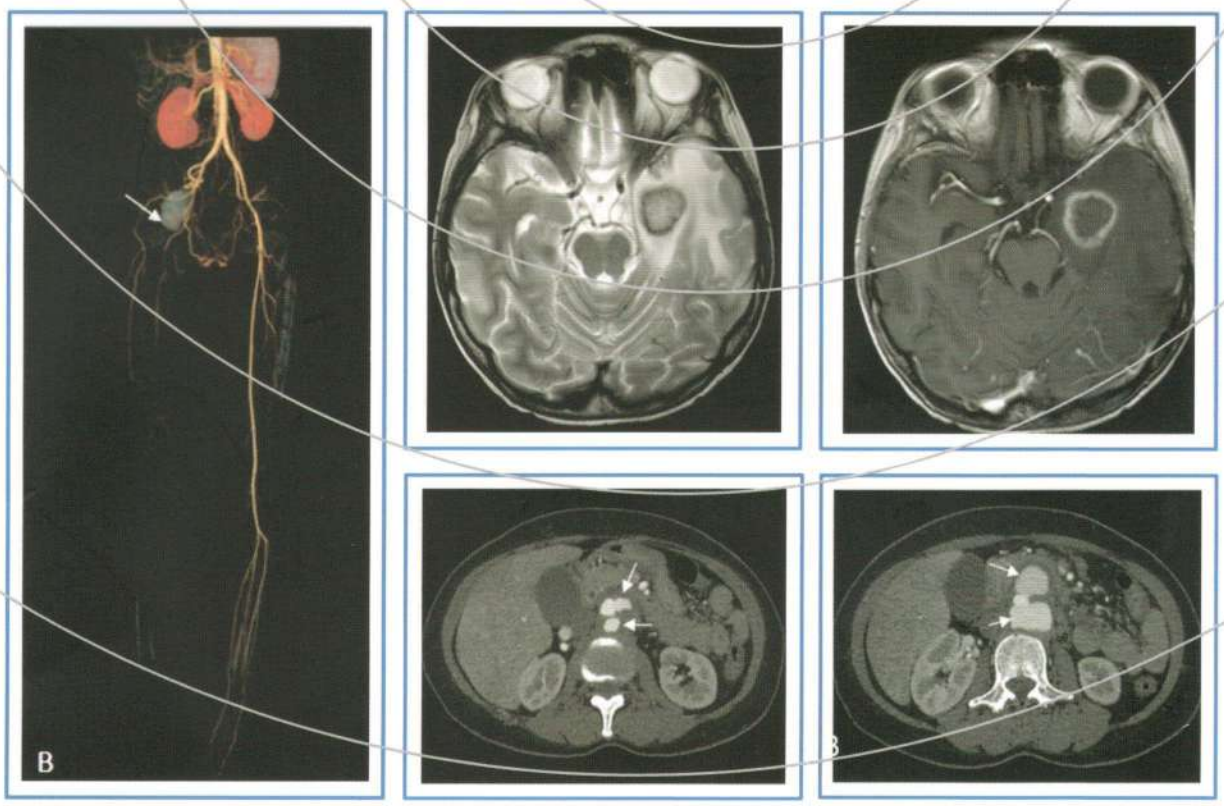

Published by

Royal College of Radiologists of Thailand

and

Radiological Society of Thailand

Bangkok, Thailand.

THE **ASEAN JOURNAL** OF **RADIOLOGY**
January-April 2012, Volume XVIII No.I

The Committee of Royal College of Radiologists of Thailand

Apr 2011-Mar 2013

President:	Permyot	Kosolbhand
Vice-president:	Sirintara	Singhara Na Ayudya
Secretariat General:	Pongdej	Pongsuwan
Vice-secretary General:	Alongkorn	Kiatdilokrath
Treasurer:	Krisdee	Prabhassawat
Academic president:	Anchalee	Churojana
House Master & Social Programme:	Kiat	Arjhansiri
Secretary:	Vithya	Varavithya
Registrar:	Pisit	Wattanaruangkowit
Committee:	Poonsook	Jitnuson
	Chamaree	Chuapatcharasopon
	Chantima	Rongviriyapanich
	Nitra	Piyaviseipat

The Committee of Radiological Society of Thailand

Apr 2011-Mar 2013

President:	Permyot	Kosolbhand
Vice-president:	Sirintara	Singhara Na Ayudya
Secretariat General:	Pongdej	Pongsuwan
Treasurer:	Krisdee	Prabhassawat
Academic president:	Anchalee	Churojana
House Master&Social Programme:	Kiat	Arjhansiri
Committee:	Poonsook	Jitnuson
	Chamaree	Chuapatcharasopon
	Chantima	Rongviriyapanich
	Nitra	Piyaviseipat
	Amphai	Uraiverotchanakorn

The Journal of the Royal College of Radiologists & Radiological Society of Thailand

(2011 - 2013)

Office:

1. Department of Radiology, Faculty of medicine, Ramathibodi hospital 270, Rama VI Road, Toong Phayathai, Ratchathewi, Bangkok, 10400
   Tel 02-2011259#110, Fax 02-2011297
   E-mail Sirintarapongpech2@hotmail.com

2. The Royal college of Radiologists & Radiological society of Thailand. 9th Floor, Royal Golden Jubilee Building, 2 Soi Soonvijai, Petchburi Road, Bankok, 10320
   Tel 02-7165963, Fax 02-7165964
   E-mail rcrtthailand@gmail.com

Contents

Original Article

Case Report and Review Literature

Case Report

THE ASEAN JOURNAL OF RADIOLOGY 2012: 18(1): 1-8 1

Original Article

The Comparison of %Ejection Fraction Between 4D MSPECT and Myometrix in Gated Myocardial SPECT

Taratip Narawong, M.Sc.

Division of Nuclear Medicine, Department of Radiology, Rajavithi Hospital, Bangkok 10400, Thailand

Abstract

Objective: To compare the %Ejection Fraction (%EF) between 4D MSPECT and Myometrix software in Gated Myocardial SPECT for a one day protocol study in Rajavithi hospital.

Materials and Methods: The 100 retrospective data of the Gated Myocardial SPECT from the suspected Coronary Artery Disease patients during July to October 2011 was reanalyzed by an experienced operator. Two software i.e, 4D MSPECT and Myometrix were used. The reconstruction parameters for rest study was OSEM/MLEM 2 iterations 10 subsets with no attenuation correction and the post filter of 3D Butterworth at critical frequency of 0.548 power 12.6. The reconstruction parameters for stress study was OSEM/ MLEM 2 iterations 10 subsets and the post filter of 3D Butterworth at critical frequency of 0.45 power 10. The %EF, end diastolic volume (EDV) and end systolic volume (ESV) were compared between each software. A two tailed pair t-test was used to test the statistically significant difference in these three value for both intraoperator and interoperator studies.

Results: The average age of the patient was 63.9±12.1 (mean±SD) with 44 female and 56 male. In intraoperator study, the mean %EF of 4DMSPECT showed the good correlation with Myometrix for both rest and stress study (r=0.95 and r=0.96, respectively.) In interoperator study, the mean %EF of 4DMSPECT also gave the good correlation with Myometrix for both rest and stress study (r=0.99 and r=0.99, respectively). The statistical test between two software showed no significant difference. ($p>0.05$).

Conclusion: The %EF from both software gave the good correlation. Since these two software packages used different algorithm so it did not recommend to interchange between these two software.

Keywords: Ejection Fraction, Gated Myocardial SPECT, 4DMSPECT, Myometrix

Introduction

Gated Myocardial perfusion SPECT (GSPECT) is the routine Nuclear Medicine study for assessment of the Coronary Artery Disease(CAD) because of several factors as follows; first it is a simple method which can be finished within a single study. Second, the Tc-99m labeled perfusion tracers allow ECG gating with flexible acquisition protocols. Third, the fast acquisition and processing by the advance mutidetectors SPECT makes this technique simple, practical and user friendly in clinical setting. Fourth, GSPECT measurements have been extensively validated against many other standard cardiac imaging modalities,[1] such as the good correlation with echocardiography[2,3] or Magnetic Resonance Imaging[4-6] or even the comparison between each software packages.[7,8] Though there were several publications about the study of the software packages but those were the study about Emory Cardiac Toolbox (ECTb) and Myometrix or ECTb and 4D MSPECT. The purpose of this retrospective study is to compare the %EF from 4D MSPECT and Myometrix in the suspected CAD patients.

Materials and Methods

Study population

Reviewed the patient file of the suspected Coronary Artery Disease (CAD) patients who underwent Tc-99m MIBI Gated Myocardial SPECT (GSPECT) from July to October 2011. The data which had a complete study i.e., rest and stress data, were included in this study. Other uncompleted data were excluded such as the patient who could not do the stress study.

Gated SPECT acquisition

A one day rest/stress protocol using 370/1110 MBq of Tc-99m MIBI was performed in every patient. Both acquisitions began 60-90 minutes after Tc-99m MIBI injection. All studies used a dual-headed GE-Infinia SPECT system (GE Medical Systems, Milwaukee, WI, USA) equipped with Low Energy High Resolution collimator. The acquisition protocol for rest study was step-and-shoot with 25 second per view, total 60 views, 3 angle per view, total 180 angle. Matrix size of 64 x 64, ECG gating acquired 8 frames per cardiac cycle, zoom 1.3 and no attenuation and scatter correction were applied. The stress study protocol was the same as rest study except the time per view was reduced to be 20 second per view.

Image reconstruction

The reconstruction parameters for all rest studies were OSEM/MLEM 2 iterations 10 subsets with no attenuation correction and the post filter of 3D Butterworth at critical frequency of 0.548 power 12.6. The reconstruction parameters for all stress studies were OSEM/MLEM 2 iterations 10 subsets and the post filter of 3D Butterworth at critical frequency of 0.45 power 10. The experienced operator reanalyzed all data and compared the value of %EF, EDV and ESV of Myometrix with 4DMSPECT software packages for the intraoperator study. For interoperator study, the previous %EF, EDV and ESV were recorded and compared with the second reconstruction analysis by the experienced operator for both rest and stress study.

Statistical analysis

The patient data were presented as mean± SD. Moreover, the correlation between each software packages was presented. The paired student's t-test was used to analyze the statistically signifi-

cant difference at the 95% confidence. A p-value of less than 0.05 was considered as statistically significant.

Ethics

This study was approved by the Rajavithi hospital ethics committee.

Results

There were 100 patients with average age of 63.9±12.1 (44 female and 56 male). The patient characteristics were shown in table 1.

The result of the intraoperator study for the comparison between two software was shown in table 2. The %EF, EDV(ml) and ESV(ml) were presented in mean±SD for both rest and stress study.

The result of the interoperator study for the comparison between two software was shown in table 3. The %EF, EDV(ml) and ESV(ml) was presented in mean±SD for both rest and stress study.

The correlation analysis and the statistically significance test (p-value) were shown in table 4 for intraoperator and in table 5 for interoperator comparison. All parameters were compared such as %EF, EDV(ml) and ESV(ml), rest and stress study for both 4D MSPECT and Myometrix software.

Discussion

As the previous study showed that 4D MSPECT gave the most reliable data compared with other software package when using the software phantom.[9] But because of the display format which is not suitable for the needs of the physicians in the Rajavithi hospital and they prefer the display format of the Myometrix software than 4D MSPECT. Therefore, this study used the 4D MSPECT as the gold

Table 1 Patient characteristics (n=100)

Characteristics	No. of patients
Mean age±SD (year)	63.9±12.1 (range 24-87)
Gender : Male	56 (56%)
: Female	44 (44%)

Table 2 Mean, standard deviation(SD), and range of %EF, EDV and ESV calculated by 4DMSPECT and Myometrix in intraoperator comparison.

parameter	Mean±SD (range)	
	4DMSPECT	Myometrix
Rest Study		
%EF	56.80±18.89 (19-92)	50.24±19.37 (9-87)
EDV(ml)	117.11±78.40 (33-457)	107.89±79.84 (28-553)
ESV(ml)	61.79±67.02 (3-325)	65.84±77.05 (4-505)
Stress study		
%EF	53.77±19.55 (18-91)	49.34±19.72 (4-85)
EDV(ml)	124.90±86.75 (36-564)	110.95±81.63 (30-558)
ESV(ml)	71.16±78.54 (3-461)	68.70±77.82 (4-489)

Table 3 Mean, standard deviation (SD), and range of %EF, EDV and ESV calculated by 4DMSPECT and Myometrix in interoperator study.

parameter		mean±SD (range)	
		first analysis	second analysis
Rest Study			
%EF	4DMSPECT	56.77±18.77 (19-92)	56.80±18.89 (19-92)
	Myometrix	50.45±19.61 (8-87)	50.24±19.37 (9-87)
EDV(ml)	4DMSPECT	116.71±77.37 (33-457)	117.11±78.40 (33-457)
	Myometrix	107.44±79.49 (28-553)	107.89±79.82 (28-553)
ESV(ml)	4DMSPECT	61.79±66.53 (3-325)	61.79±67.02 (3-325)
	Myometrix	65.38±76.66 (4-505)	65.84±77.05 (4-505)
Stress study			
%EF	4DMSPECT	54.05±19.42 (18-91)	53.77±19.55 (18-91)
	Myometrix	49.42±19.88 (5-85)	49.34±19.71 (4-85)
EDV(ml)	4DMSPECT	123.31±86.29 (36-564)	124.93±86.75 (36-564)
	Myometrix	110.34±81.02 (30-558)	110.95±81.63 (30-558)
ESV(ml)	4DMSPECT	69.79±77.89 (3-461)	71.16±78.54 (3-461)
	Myometrix	67.19±75.81 (4-489)	68.70±77.82 (4-489)

Table 4 Correlation analysis and the p-value for the statistical significant difference analysis for intraoperator study between 4D MSPECT and Myometrix

	Pearson correlation	p-value
Rest study		
%EF	0.95	0.98
EDV(ml)	0.97	0.68
ESV(ml)	0.95	0.49
Stress study		
%EF	0.96	0.91
EDV(ml)	0.99	0.81
ESV(ml)	0.99	0.41

Table 5 Correlation analysis and the p-value for the statistical significant difference analysis for interoperator study between the first and second analysis for 4D MSPECT and Myometrix

	Pearson correlation		p-value	
	4D MSPECT	Myometrix	4D MSPECT	Myometrix
Rest study				
%EF	0.99	0.99	0.32	0.35
EDV(ml)	0.99	0.99	0.33	0.33
ESV(ml)	0.99	0.99	0.32	0.33
Stress study				
%EF	0.99	0.99	0.36	0.33
EDV(ml)	0.99	0.99	0.37	0.34
ESV(ml)	0.99	0.99	0.36	0.37

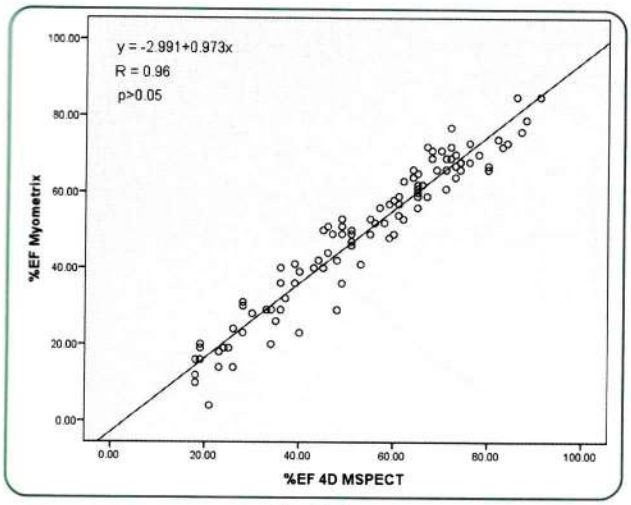

Fig.1(a)

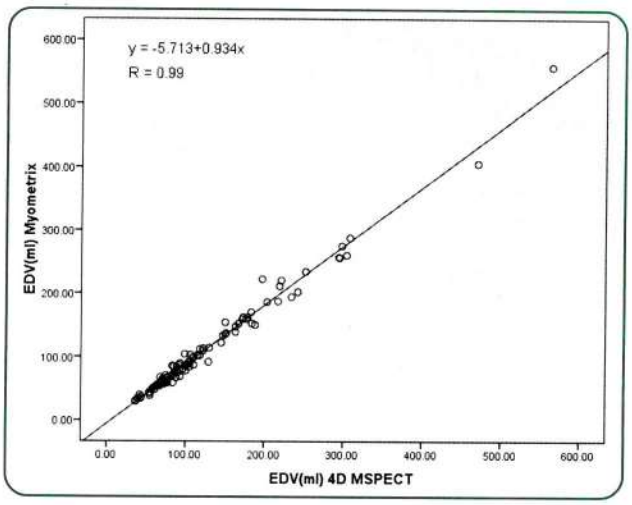

Fig.1(b)

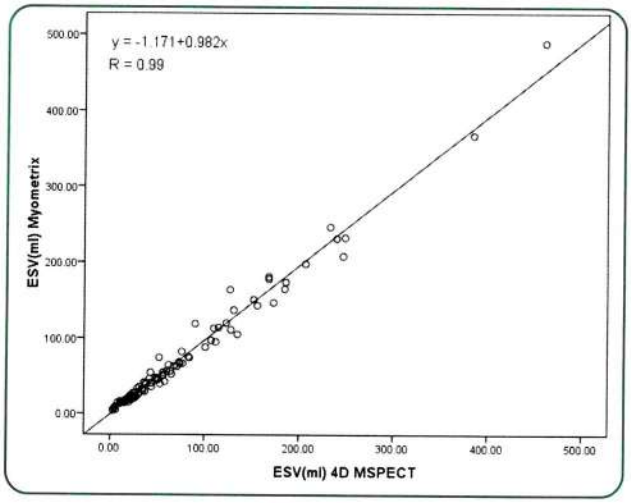

Fig.1(c)

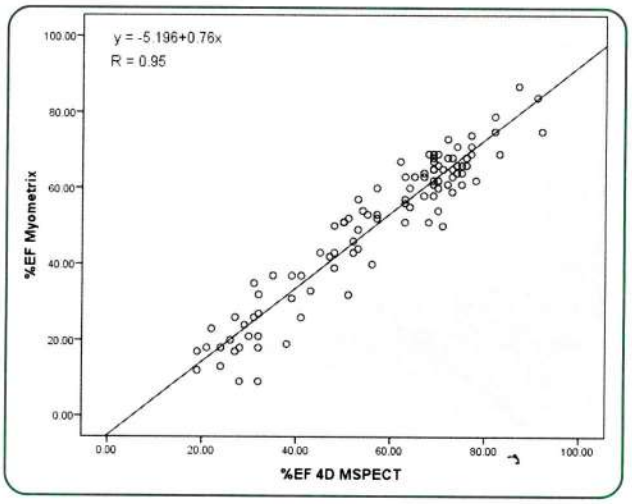

Fig.1(d)

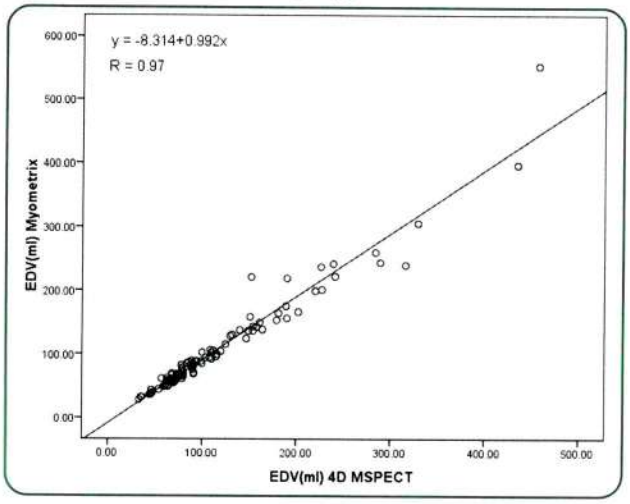

Fig.1(e)

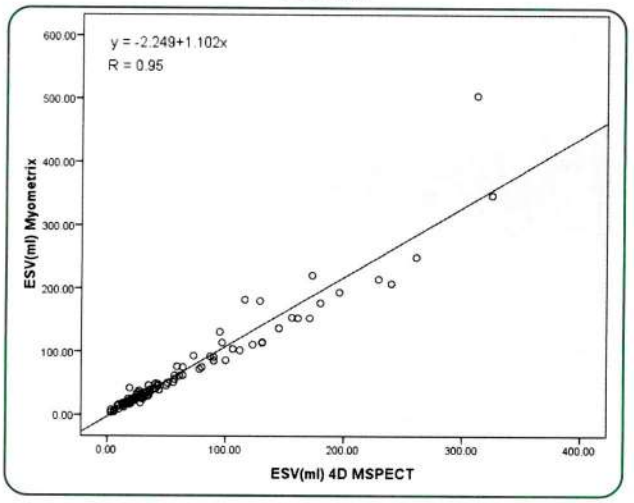

Fig.1(f)

Fig.1 Correlation analysis of %EF (a), EDV(ml) (b) and ESV(ml) (c) calculated by 4D MSPECT and Myometrix for stress study and correlation analysis of %EF (d), EDV(ml) (e), and ESV(ml) (f) for rest study in Intraoperator comparison.

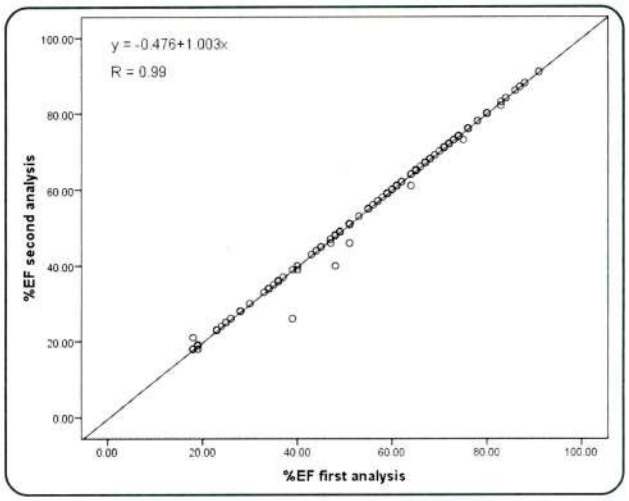

Fig.2(a)

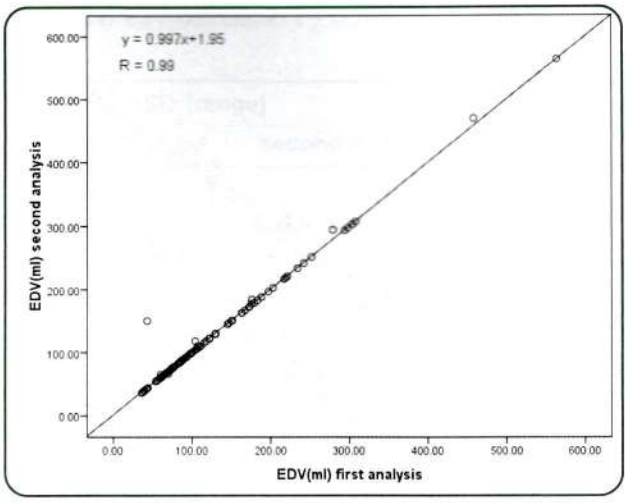

Fig.2(b)

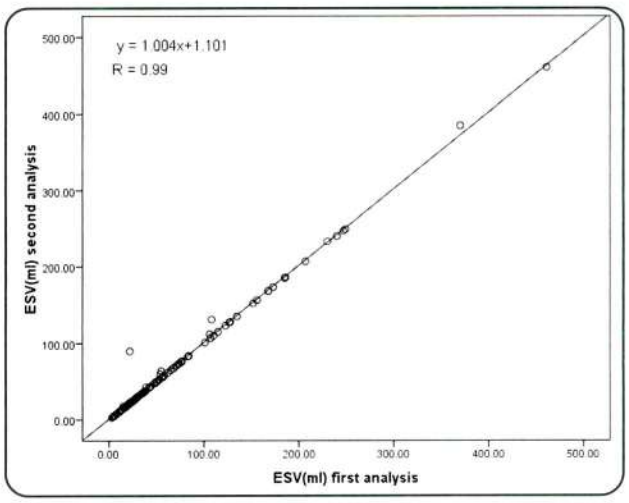

Fig.2(c)

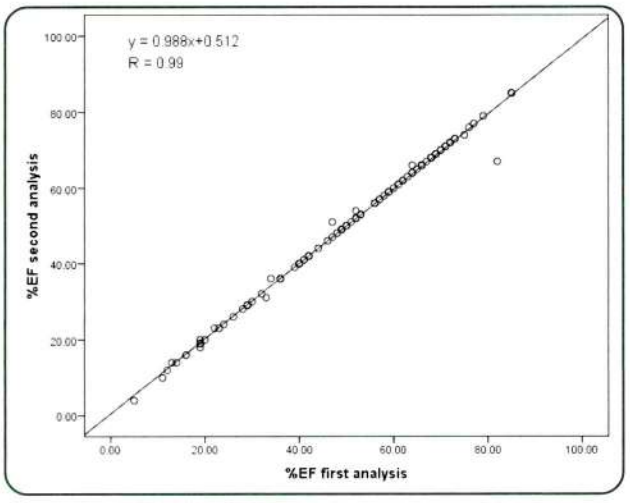

Fig.2(d)

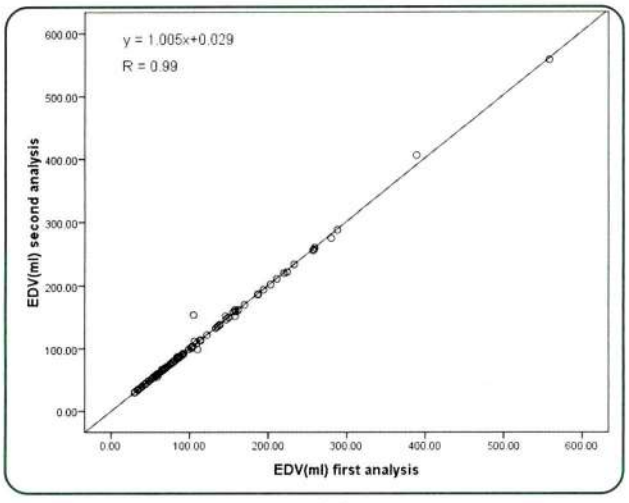

Fig.2(e)

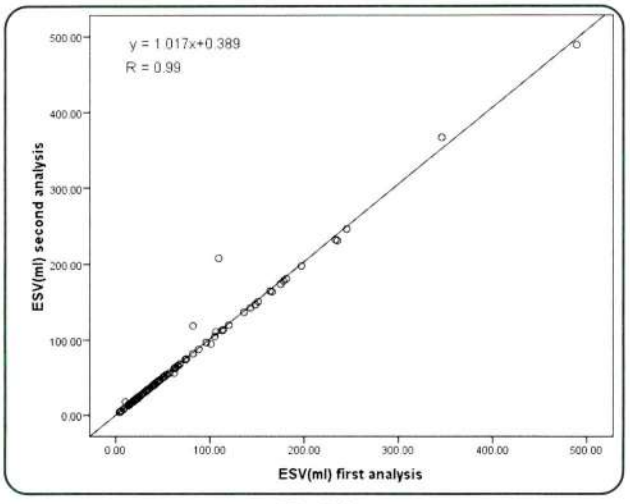

Fig.2(f)

Fig.2 Correlation analysis of %EF (a), EDV(ml) (b) and ESV(ml) (c) calculated by 4D MSPECT and correlation analysis of %EF(d), EDV(ml)(e), and ESV(ml) (f) calculated by Myometrix for stress study in Interoperator comparison.

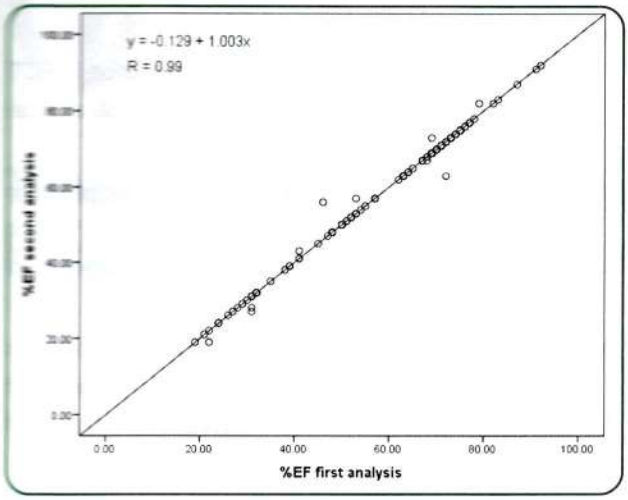

Fig.3(a)

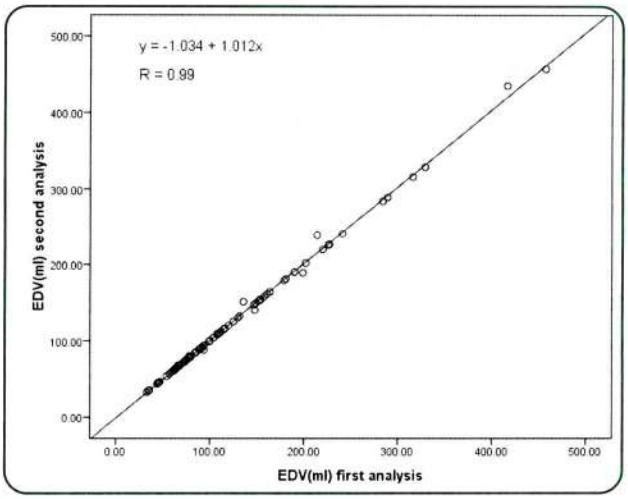

Fig.3(b)

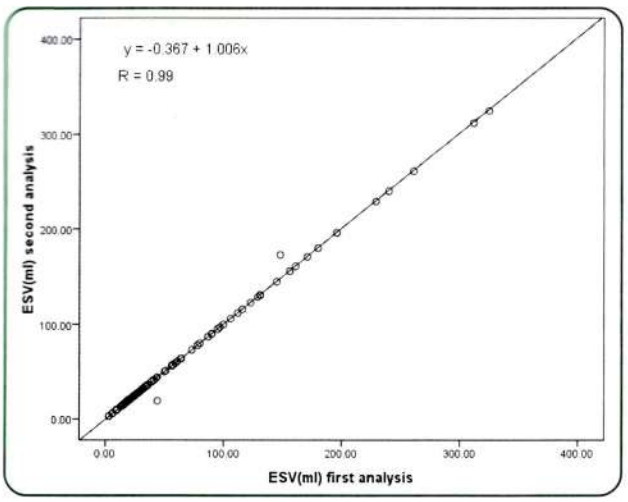

Fig.3(c)

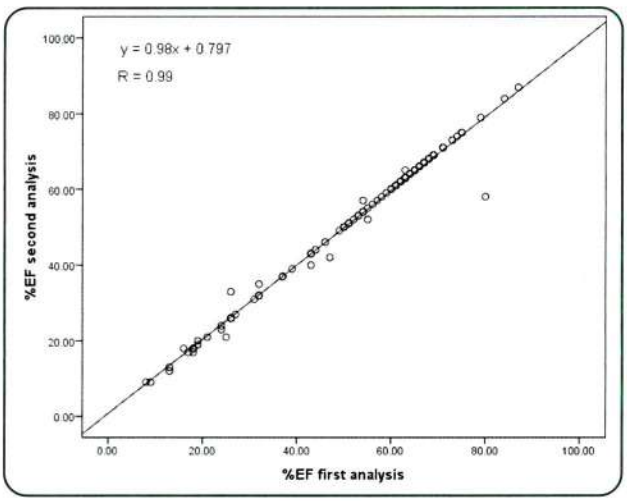

Fig.3(d)

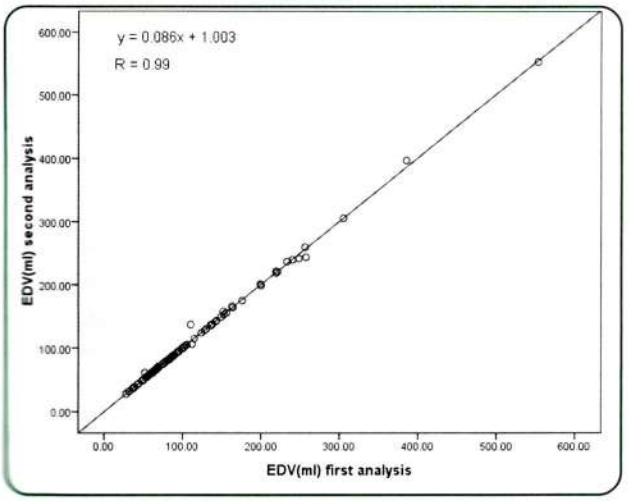

Fig.3(e)

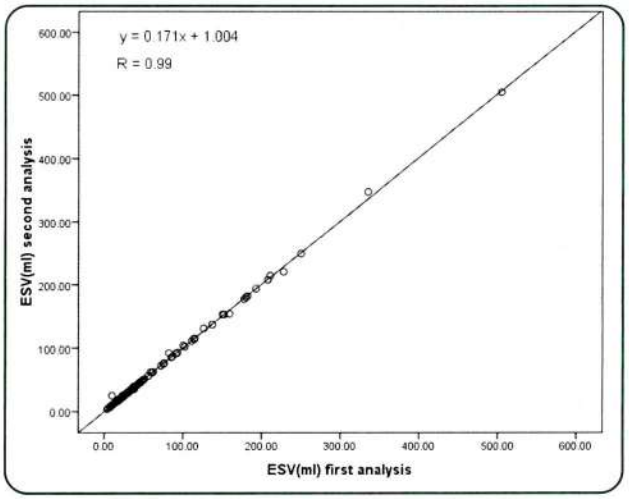

Fig.3(f)

Fig.3 Correlation analysis of %EF (a) , EDV(ml)(b) and ESV(ml) (c) calculated by 4D MSPECT and correlation analysis of %EF (d), EDV(ml) (e), and ESV(ml) (f) calculated by Myometrix for rest study in Interoperator comparison.

standard. In the Intraoperator comparison, the %EF, EDV(ml) and ESV(ml) showed the good correlation between 4D MSPECT and Myometrix for both stress and rest studies. (R=0.95-0.99) Though all these values showed a slightly different as shown in table 2 but there was no statistically different significance for this intraoperator study ($p>0.05$) as shown in table 4.

In interoperator comparison, the %EF, EDV(ml) and ESV(ml) showed the good correlation between 4D MSPECT and Myometrix for both stress and rest studies. (R=0.99) Though all these values showed a slightly different as shown in table 3 but there was no statistically different significance for this interoperator study ($p>0.05$) as shown in table 5. This comparison showed that the consistency in using these two software packages was good though the operators who used these software were different. This meant that these two software packages were reliable. Therefore, we can report the result from Myometrix software package though the physician uses the 4D MSPECT software package to diagnose the suspected CAD patients by Gated SPECT study in the Rajavithi hospital.

Conclusion

There were no statistically significant difference between all these studies. Though, the study showed a good correlation but it was not recommended to interchange these two software packages.

Acknowledgement

This study was supported by the Rajavithi hospital fund, Rajavithi hospital, Ministry of Public Health.

References

1. Paul AK, Nabi HA. Gated myocardial perfusion SPECT: Basic principles, technical aspects, and clinical applications. J Nucl Med Technol 2004;32:179-87.
2. Cwajg E, Cwajg J, He Z, et al. Gated myocardial perfusion tomography for the assessment of left ventricular function and volumes: comparison with echocardiography. J Nucl Med 1999;40:1857-65.
3. Omar W, Abdel-ghany M, Reda A. Comparison between Gated SPECT and echocardiography in evaluation of left ventricular ejection fraction. J Egyptian Nat. Cancer Inst 2000;12:301-6.
4. Lipke CSA, Kühl HP, Nowak B, et al. Validation of 4D-MSPECT and QGS for quantification of left ventricular volumes and ejection fraction from gated ^{99m}Tc-MIBI SPET: comparison with cardiac magnetic resonance imaging. Eur J Nucl Med Mol Imaging 2004;31:482-90.
5. Schaefer WM, Lipke CSA, Standke D, et al. Quantification of left ventricular volumes and ejection fraction from gated ^{99m}Tc-MIBI SPECT: MRI validation and comparison of the Emory Cardiac Tool Box with QGS and 4D-MSPECT. J Nucl Med 2005;46:1256-63.
6. Hedeer F, Palmer J, Arheden H, et al. Gated myocardial perfusion SPECT underestimates left ventricular volumes and shows high variability compared to cardiac magnetic resonance imaging -a comparison of four different commercial automated software packages. BMC Medical Imaging 2010;10 http://www.biomedcentral.com/1471-2342/10/10
7. Nakajima K, Higuchi T, Taki J, et al. Accuracy of ventricular volume and ejection fraction measured by gated myocardial SPECT: comparison of 4 software programs. J Nucl Med 2001;42:1571-8.
8. Dostbil Z, Aritürk Z, Cil H, et al. Comparison of left ventricular functional parameters obtained from three different commercial automated software cardiac quantification program packages and their intraobserver reproducibility. Ann Nucl Med 2011;25:125-31.
9. Sriwongta S, Tocharoenchai C, Pusuwan P. Validation of ejection fraction obtained from gated SPECT imaging using NCAT phantom. Asean J Radiol 2008;XIV(II): 119-25.

THE ASEAN JOURNAL OF RADIOLOGY 2012: 18(1): 9-15 9

Original Article

Tuberculum Sellae Meningioma vs Macroadenoma Hypophysis : How to Differentiate Preoperatively?

Ignatius Mardjono, MD., Muhammad Z. Arifin, MD., Ph.D., Roland Sidabutar, MD., Arwinder Singh, MD., Sevline E. Ompusunggu, MD.

Department of Neurosurgery, Faculty of Medicine Universitas Padjadjaran- Dr. Hasan Sadikin General Hospital, Bandung, Indonesia

Abstract

Background: Sellar region tumors may origin from a various number of structures and each of them have a specific clinical and radiological appearance. Among these pathological processes, one of the most challenging is to distinguish between tuberculumsellae meningioma and macroadenomahypophysis. Differentiating these two entities preoperatively is very important to decide which approach will be most suitable and beneficial. The purpose of this study is to produce a simple preoperative scoring system to differentiate these two that can be used in specific conditions where MRI is not available or could not be performed.

Methods: This analytical retrospective cohort study contains data obtained from patients treated in Neurosurgery Department of Hasan Sadikin General Hospital-Bandung from 1 January 2008 until 31 December 2010. 34 patients were enrolled in this study, in which 15 of them were diagnosed with macroadenomahypophysis and remaining 19 patients as tuberculumsellae meningioma which was confirmed with pathology examination.

Results: From clinical presentation we found that the event of endocrinopathyoccurs significantly in macroadenoma hypophysis (p=0.002). Whereas from radiological evaluation there were 7 parameters that significantly distinguish these two entities including hyperostosis, sellar floor configuration, homogeneity of mass, contrast agent enhancement, waist configuration, peritumoral edema, and duralattachment. From these findings, we propose a simple scoring system to differentiate macroadenomahypophysis and tuberculumsellae meningioma with a 84.2% sensitivity and 100% specificity.

Conclusion: Although MRI is the modality of choice in differentiating macroadenoma hypophysis and tuberculum sellae meningioma but our scoring system can be used as an aid in choosing best surgical approach.

Keywords: TuberculumSellae Meningioma; Macroadenomahypophysis; CT scan

Introduction

Neurosurgery came to developing countries over a half a century ago, yet the vast majority of population in these countries do not have equity in access to it, owing to the cost of neurosurgical care and geographical isolation of patients. Many biomedical equiments such as CT Scan and MRI are not available to most of the population in these countries.[1]

MRI is the examination of choice in pituitary and sellar region tumors because it depicts the complex anatomy around the sellar wall. Almost 30 pathologic entities occur in this region, and most can be distinguished using MRI.[2] Sellarregion tumors are one of the most challenging tumor cases for neuro-surgeons. Twoof the most common entities that should be distinguished because of their similarities especially in imaging studies are tuberculum sellae meningioma and macroadenoma hypophysis.[3] Preoperative differentiation of these tumors is important for best surgical approach. Tuberculumsellae meningioma is usually operated by craniotomy approach, wheras macroadenoma hypophysis uses transsphenoidal approach.[4,5]

We propose a simple scoring system based on clinical and radiological evaluation using CT Scan that can be used as an aid for determining surgical strategy in cases where MR imaging could not be performed.

Clinical Materials and Methods

This retrospective cohort study consists of 34 patients with sellar region tumors treated and operated in neurosurgeryward of HasanSadikin General Hospital from 1 Janury 2008 until 31 December 2010. Pathological confirmation showed 15 of these patients diagnosed with macroadenoma hypophysis and 19 patients with tuberculum sellae meningioma. Data collected included clinical presentation and various characteristics based on CT Scan imaging.

Statistical Analysis

Data were processed on a personal computer by using commercially available statistic software. These variables were compared using t test with p value ≤ 0.05. Only significant variables were then summarized into a scoring system and then tested for its specificity and sensitivity.

Results

From 34 patients in our study, there were 12 male and 22 female patients with average age slightly higher in tuberculum sellae meningioma group. Table 1 shows various clinical presentation of these patients. As shown below, there is significant correlation of endocrine abnormalities ($p=0.002$) in macroadenoma hypophysis. Whereas there is no significant correlation between sex, age, duration of symptoms, tumor size, chief complaint, and visual field defect.

Based on radiological findings shown on CT Scan, there were certain characteristics that we analyzed to differentiate these two entities. According to table 2, there is significant correlation of various radiological presentations such as homegeneity on CT scan ($p=0.017$), contrast enhancement ($p=0.001$), hyperostosis ($p=0.002$), thinning of sellar ($p<0.001$), presence of edema ($p=0.004$), size of the sellar waist ($p=0.007$) and alsodural attachment ($p<0.001$) of tumors originating as macroadenoma hypophysis or tuberculum sellae meningioma.

Table 1 Clinical presentation of patients diagnosed with Macroadenoma hypophysis and tuberculum sellae meningioma

Variables	MH (n=15)	TSM (n=19)	Total	p value
Sex				0.051*
Male	8 (66.7%)	4 (33.3%)	12 (35.3%)	
Female	7 (31.8%)	15 (68.2%)	22 (64.7%)	
Age (SD) (year)	35.80 (8.02)	39.84 (5.78)		0.097**
Tumor size (SD) (cm)	3.74 (1.53)	3.62 (0.86)		0.777**
Duration of symptoms (SD) (year)	2.24 (2.17)	1.83 (1.64)		0.539**
Clinical symptoms				0.098*
Headache	6 (66.7%)	3 (33.3%)	9 (26.5%)	
Visual Loss				0.009*
Negative	8 (100.0%)	1 (0.0%)	3 (8.8%)	
Unilateral	3 (30.0%)	7 (70.0%)	10 (29.4%)	
Bilateral	4 (26.7%)	11 (73.3%)	15 (44.1%)	
Visual field defect				0.397*
No defect	8 (53.3%)	7 (46.7%)	15 (44.1%)	
Hemianopia Bilateral	4 (33.3%)	8 (66.7%)	12 (35.3%)	
Hemianopia Unilateral	3 (66.7%)	4 (33.3%)	7 (8.8%)	
Endocrine abnormalities				0.002*
Positive	11 (73.3%)	4 (26.7%)	15 (44.1%)	
Negative	4 (21.1%)	15 (78.9%)	19 (55.9%)	

* Chi Square Test ** Mann Whitney test

Discussion

The sellae tursica which resembles a Turkish saddle if viewed from the side, forms a semicircular, central depression within the sphenoid bone. The antero-superior edge of the sella is marked by a horizontal ridge, the tuberculum sellae.[6] Two of the most frequent pathological process found in this region are macroadenoma hypophysis and tuberculum sellae meningioma.[3,7] Although according to previous reports the incidence varies according to age, gender, and ethnic group, In our series we found predilection for menigioma higher in female patients with average age of 40 years old.[7,8,9]

As shown on table 1, there were three most common symptoms in our report; headache, visual disturbance and endocrinopathy. Although almost 70% of our patients complained of visual loss in either of these tumors, there was no significancy in this data. In some series, greater than 95% of patients suffer visual acuity and/or field deficits and the pattern of vision loss can vary.[7,8,9,10] In our series, diabetes insipidus occurance was the highest endocrine abnormality present in macroadenoma hypophysis. This stalk compression effect was interestingly also present in 4 patients (26%) with tuberculum sellae meningioma.[9,11]

The gold standard for imaging is MRI as detection rate varies in the literature from 65% to more than 90% for microadenomas but computed tomography and MRI are equivalent in detecting the full extent of a macroadenoma.[9,11,12] CT scan still has a role in preoperative planning, particularly in

Table 2 Comparison of radiological presentation on CT Scan between macroadenoma hypophysis and tuberculum sellae meningioma

Variable	MH (n=15)	TSM (n=19)	Total	p value	PR(95%CI)
CT appearance				0.001*	2.74 (1.37-5.48)
Homogen	2 (13.3%)	13 (86.7%)	15 (44.1%)		
Inhomogen	13 (68.4%)	6 (31.6%)	19 (55.9%)		
CT Enhancement				0.001**	3.60 (1.75-7.42)
Minimal	9 (83.3%)	1 (16.7%)	10 (29.5%)		
Bright	6 (25.0%)	18 (75.0%)	24 (70.6%)		
Hyperostosis				0.002**	2.50 (1.54-4.04)
Negative	15 (60.0%)	10 (40.0%)	25 (73.5%)		
Positive	0 (0.0%)	9 (100.0%)	9 (26.5%)		
Thinning				<0.001**	5.75 (2.36-14.01)
Negative	4 (17.4%)	19 (82.5%)	23 (67.6%)		
Positive	11 (100.0%)	0 (0.0%)	11 (32.4%)		
Sellar Enlargement				<0.001**	7.53 (1.15-48.84)
Negative	4 (20.0%)	16 (80.0%)	20 (55.8%)		
Positive	11 (78.5%)	3 (21.5%)	14 (44.21%)		
Waist				0.008*	2.63 (1.10-6.24)
Negative	5 (25.0%)	15 (75.0%)	20 (58.8%)		
Positive	10 (71.4%)	4 (28.6%)	14 (41.2%)		
Peritumoral Edema				0.004*	2.36 (1.50-3.70)
Negative	15 (57.7%)	11 (42.3%)	26 (76.5%)		
Positive	0 (0.0%)	8 (100.0%)	8 (23.5%)		
Attachment				<0.001*	-
Negative	15 (100.0%)	0 (0.0%)	15 (44.1%)		
Tuberculum	0 (0.0%)	13 (100.0%)	13 (38.2%)		
Diaphragm	0 (0.0%)	6 (100.0%)	6 (17.6%)		
Mass Shaped				0.442	1.38 (0.56-3.44)
Round	16 (81.25%)	11 (73.3%)	27 (79.4%)		
Lobulated	3 (18.75%)	4 (26.6%)	4 (11.6%)		

* Chi Square Test ** Mann Whitney test

Table 3 Scoring system of various variables to differentiate between macroadenoma hypophysis and tuberculum sella meningioma

Variable	PA (n=15)	TSM (n=19)	Total	p value	Se	Sp	PPV	NPV
Score				<0.001*				
>3	0	16	16		84.2%	100%	100%	83.3%
≤3	15	3	18					

* Chi Square Test

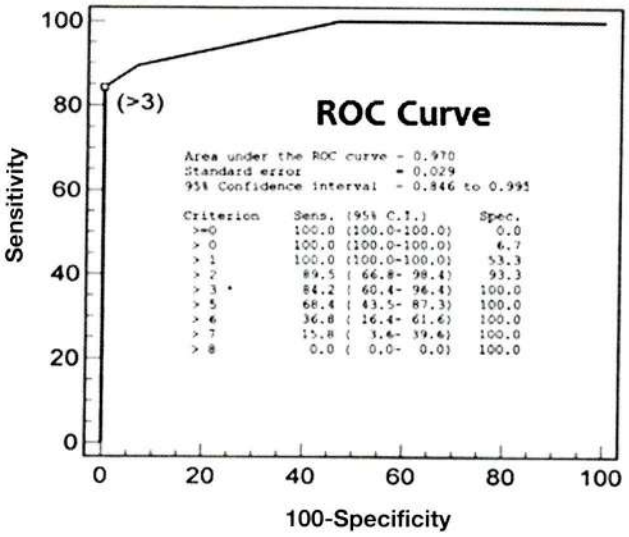

Graph.1 ROC curve showing cut off point of 3 in determining our scoring system.

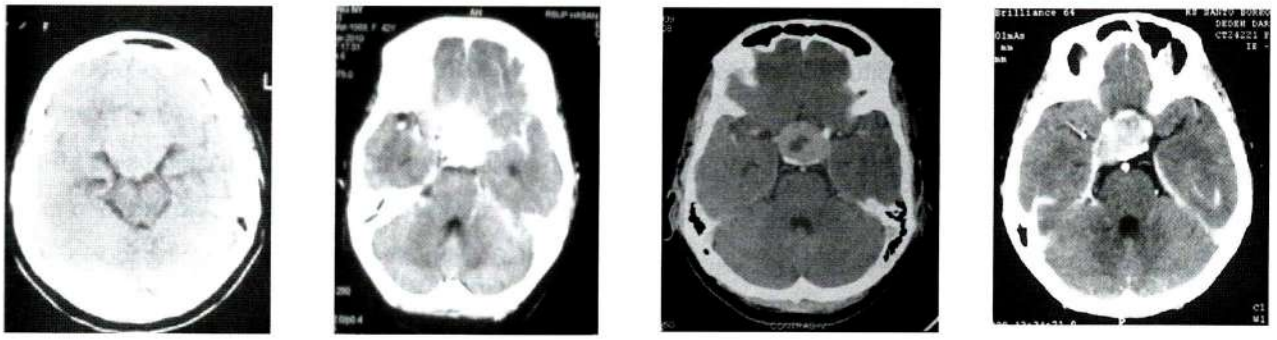

Tuberculum Sellae Meningioma

Macroadenoma Hypophysis

Fig.1 Tuberculum sellae meningiomas appear distinctively homogeneous and enhance entirely after application of contrast. On the contrary. macroadenoma hypophysis have various CT appearance with minimal contrast enhancement

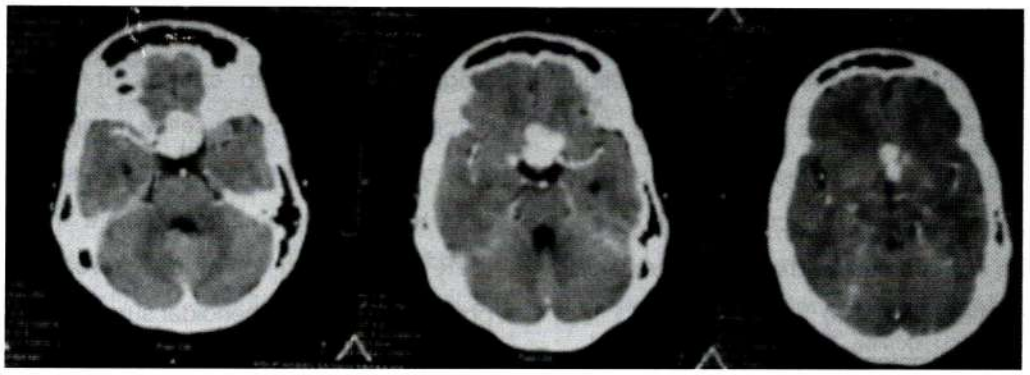

Fig.2 A CT Scan of a 44 year old lady diagnosed with tuberculum selae meningioma. Note the homogenous enhancement and lobulated configuration but no hiperostosis of the bone is present.

regard to pneumatization and the anatomy of the sphenoid sinus as not all neurological centres have MRI fasilities.[2]

In our study, we found seven radiological criterias to help recognize these two entities. Macroadenomas have variable appearances because they tend to have necrosis, cyst formation, and hemorrhage that appear as mixed attenuation. Curiously there were 6 patients (31.6%) with tuberculum sellae meningioma that show inhomegeneity of mass and 1 patient (5%) showing minimal enhancement after contrast administration. Macroadenoma hypophysis are soft tumors which usually indent at the diaphragma sellae, giving them a 'snowman' configuration. This is one feature that can help distinguish between a pituitary macroadenoma and a meningioma.[2,9] In our report,[10] (66.7%) out of 15 patients showed a positive waist configuration and also 4 patients (21%) of tuberculum sellae meningiomas also had this feature.

As shown on table 2, there were more than 50% of tuberculum sellae meningioma that did not show signs of hyperostosis (10 patients, 52%) nor peritumoral edema (11 patients, 57%) which are usually characteristics for this type of tumor. Adjacent hyperostosis, best seen on CT, is present in more than one third of cases and is a helpful sign in meningiomas.[12,13] In some previous reports, the sellae turcica is usually not expanded or only slightly enlarged in tuberculum sellae meningiomas. This is in accordance to our report where 3 patients (15.7%) with tuberculum sellae meningiomas had sellar enlargement, in contrast to macroadenoma hypophysis (11 patients, 68.7%).[9,11]

Sellar floor thinning or erosion are other criterias that could be usefulin diagnosing macroadenoma hypophysis. Eleven patients (68.7%) with macroadenoma hypophysis showed sellar floor thinning but there were 4 cases (26.7%) that did not have this feature. Obtuse dural margins and dural tail enhancementof lesions involving the sella, are helpful in the preoperative diagnosis.[12] Most of the specific CT scan features that we analyze in our series, showed significancy in helping to diagnose macroadenoma hypohysis and tuberculum sellae meningioma.

After analyzing various variables in determining difference in the two types of tumors, we can state that there were eight variables demonstrating significancy ($p<0.05$) such as; endocrine abnormalities ($p=0.002$), hyperostosis ($p=0.002$), thinning of sellae ($p<0.001$), waist configuration ($p=0.008$), peritumoral edema ($p=0.004$), dural attachment ($p<0.001$), CT homegenicity of mass ($p=0.001$) and contrast enhancement ($p=0.001$). After analizing using a ROC curve as shown on graph 1, we found a cut off point of 3 from these variables. Using our simple method, we came up with a very accurate scoring system to discern between macroadenoma hypophysis and tuberculum sellae meningioma as shown on table 3. This scoring system has a p value of <0.001 with sensitivity of 84.2% and specificity of 100%. PPV value is 100% and NPV is 83.3% with accuracy of 94.1%.

Using our simple method we can help to diagnose these two entities. It is important to differentiate tuberculum sellae meningioma from the macroadenoma hypophysis, because craniotomy is done for meningioma, whereas a transsphenoidal route is preferred for most macroadenoma hypophysis.[3,4,11,14] Transsphenoidal surgery is the approach of choice for macroadenoma hypophysis.[15] Tuberculum sellae meningiomas usually have a firm, rubbery consistency and often require sharp

dissection rather than simple suctioning for their removal.[11] Based on our preference, all of our patients diagnosed with tuberculum sellae meningioma were operated using a pterional approach.

Conclusion

The superiority and usefullnes of MRI is unquestionable as it is the gold standar imaging to distinguish macroadenoma hypophysis and tuberculum sellae meningioma but this modality is often not available in many countries. Asimple scoring system can be useful as a tool for preoperative surgicalstrategy in differentiating these two entities. A score of more than 3 is most likely to be diagnosed as tuberculum sellae meningioma whereas less than 3 is representative for macroadenoma hypophysis.

Source of support

Nil

Conflict of interest

Authors have no conflict of interests.

References

1. Black P. The Future of Neurosurgery. A Call to Leadership. Clinical Neurosurgery 54:185-91, 2007.
2. Khan Ali : Pituitary Adenoma Imaging. In :http://emedicine.medscape.com/article/343207-overview#a21, 2011.
3. Kaltsas Gregory A, Evanson Jane, Chorisoulidou Alexandra, Grossman Ashley. The diagnosis and management of paraselar tumours of the pituitary. Endocrine-Related Cancer 15:885-903, 2008.
4. Rasrassaleh, Ansari M. Javad, Ansari H. Hasan, Rahbarian Farhad, Rashidi Iran. Diaphragma sellae meningioma mimicking pituitary macroadenoma : A case report. International Journal of Collaborative Research on Internal Medicine & Public Health Vol. 2 No. 11:404-9, 2010.
5. Taylor SL, Barakos JA, Harsh GR 4th, Wilson CB. Magnetic resonance imaging of tuberculum sellae meningiomas: preventing preoperative misdiagnosis as pituitary macroadenoma. Neurosurgery 31(4):621-7; discussion 627, 1992.
6. Schubiger O. Radiology of pituitary adenomas in Landolt A.M., Vince M.L., Reilly P.L. (eds) in : Pituitary Adenomas. UK : Churchill Livingstone 1996, pp 177-219.
7. Jagannathan Jay, Kanter Adam, Sheehan Jason, Jane John, Laws Edward. Benign brain tumors : sellar/parasellar tumors. Neurol Clin 25:1231-49, 2007.
8. Al Mefty Osama, Andulrauf Saleem, Haddad Geoeges F. Meningiomas in Winn H. Richard (eds) : Youman's Neurological Surgery 6th edition. Philadelphia : Elsevier Saunders, pp 1426-49, 2011.
9. Benjamin Mc Vallo, Mc Cormack Bruce. Surgical management of tubeculumsellae and sphenoid ridge meningiomas in Schmidek (ed) : Schmidek & Sweet's Operative Neurosurgical Techniques Indications, Methods, and Results 4th edition. USA : W.B. Saunders, pp 305-324, 2007.
10. Chi John H., Mc Dermott Michael W. Tuberculum sellae meningiomas. Neurosurg Focus Vol 14 (6): Article 6, 2003.
11. Mulinda James. Pituitary macroadenoma. In: http://emedicine.medscape.com/article/123223-clinical, 2011
12. Bowers Christian, Altay Tamer, Couldwell William. Surgical decision-making strategies in tubercullum sellae meningioma resection. Neurosurg Focus 30 (5):E1, 2011.
13. Anderson JR, Antoun N, Burnet N, Chatterjee K, Edwards O, Pickard JD, Sarkies N. Neurology of the pituitary gland. Neurol Neurosurg Psychiatry 66:703-21, 1999.
14. Donovan Joseph L., Nesbit Gary. Distinction of masses involving sella and suprasellar space : Specificity of imaging features. AJR 167:597-603, September 1996.
15. Cappabianca P, Cirillo S, Alfieri A, D'Amico A, MAiuri F, MAriniello G, Caranci F, De Divitiis E. Pituitary macroadenoma and diaphragmasellae meningioma : differential diagnosis on MRI. Neuroradiology 41(1):22-6, Jan 1999.
16. Swearingen Brooke, Zeevas Nicholas. Surgical management of Cushing's Disease in Schmidek (ed) : Schmidek & Sweet's Operative Neurosurgical Techniques Indications, Methods, and Results 4th edition. USA : W.B. Saunders, pp 305-24, 2007.

THE **ASEAN JOURNAL** OF **RADIOLOGY** 2012: 18(1): 16-25

Original Article

Ultrasonographic and Mammographic Findings in Malignant Tumors of the Breast in Young Women

Cholatip Wiratkapun MD.*, Arunee Lupreechased MD.*, Panuwat Lertsittichai MD. MSc**

** Department of Radiology, ** Department of Surgery,*

Faculty of Medicine Ramathibodi Hospital, Mahidol University, Bangkok 10400, Thailand

Abstract

Objective: To evaluate the ultrasonographic (US) and mammographic findings as well as their correlation in malignant tumors of the breast in women aged 35 years or younger.

Material and methods: The subjects included 79 patients (with 85 lesions) diagnosed with breast cancer at the age of 35 years or younger and with available US and mammographic images for retrospective review during 9 and a half-year period of the study at the Breast Diagnostic Center of the University Hospital.

Results: Most young patients presented with a palpable breast mass. US showed a higher detection rate of malignant tumors in young age (99% compared to 84% in mammogram). Many US features suggested the presence of malignant tumors such as noncircumscribed borders or thickened echogenic halo. However, mammogram was still needed because not all malignant lesions were visualized by US. Mammographic size was better correlated with pathological size than US-size, which tended to be underestimate the pathological size.

Conclusion: US was a useful diagnostic tool to detect malignant tumors in young women. Its value was not only to detect the lesion but also characterize it. Similar to the older age group, interpretation of US along with mammogram increased the accuracy of diagnosis.

Keywords: Ultrasonography, mammography, malignant, breast, young women

Introduction

Breast cancer is the most common female cancer worldwide[1]. It is also the most common cancer in Thai women[1]. Thai women develop breast cancer at a younger age than the American and European women. The mean age of breast cancer in Thai women is 55 years[1]. Breast cancer is uncommon in women under 35 years, accounting for approximately 2% of all breast cancers[2]. However, palpable breast masses in this young age group are not rare. The biopsy results of breast lesions in young women are largely benign, with fibroadenoma as the most common pathology[2,3].

Ultrasonography (US) is the initial imaging modality for evaluating breast problems in young patients because it is not compromised by dense fibroglandular tissue. Moreover, this tool has nearly 100% accuracy in differentiating between cysts and solid masses[3-5]. US is also able to distinguish between benign and malignant tumors[6,7].

Mammography is not routinely performed in young patients because it has low sensitivity in dense breasts[8-10]. Mammographic sensitivity decreases from almost 100% in the fatty breasts to 45% in the extremely dense breasts[8]. Nevertheless, the value of mammography in detecting breast cancer is well established. US performed concurrently with mammography increases sensitivity compared with the use of either modality alone[8,9].

The purpose of this study was to evaluate the US and mammographic findings as well as their correlation for the diagnosis malignant tumors of the breast in women aged 35 years or younger.

Material and Methods

The study was conducted with institutional review board approval and given a waiver of patient informed consent, as it was a review of routine clinical data.

Subjects consisted of women aged 35 years and younger who were treated for breast cancer or in whom a diagnosis of breast cancer was made at the Breast Diagnostic Center, Ramathibodi Hospital, Mahidol University from January 1st, 2001 to July 31st, 2010. During the study period, eighty-five lesions in 79 patients with age 35 years old or younger had available images for review along with clinical data.

US was performed by experienced radiologists using the HDI 5000 Philips ultrasound (Bothell, WA, U.S.A.) and, beyond January 2008, using the iU22 Phillips ultrasound (Bothell, WA, U.S.A.). US was performed using a broadband linear probe (L12-5). Before November 2004, mammography was obtained with two analog mammographic units (Lorad M-IV, Danbury, CT, U.S.A., and Senographe DMR, GE, Milwaukee, WI, U.S.A.). After November 2004, mammography was obtained with digital mammography units as well (Lorad, Selenia, Hologic, Danbury, CT, U.S.A.). Routine craniocaudal (CC) and medio-lateral oblique (MLO) views were performed in all patients. All images were reviewed, and a diagnostic consensus reached, by all investigators.

The US features of each lesion were based on the American College of Radiology Breast Imaging Reporting and Data System (BI-RADS) lexicon[10]. These features included lesion shape, orientation, margin, lesion boundary, echo pattern, posterior acoustic features and associated findings which included abnormal duct, changes in Cooper's ligament, edema, architectural distortion, and skin thickening.

Mammographic findings were based on BI-RADS lexicon as well. Breast compositions were categorized as extremely dense (>75% glandular),

heterogeneously dense (51-75% glandular), scattered fibroglandular densities (25-50% glandular) and almost entirely fatty breasts (<25% glandular). The final assessments for each modality were also based on the BI-RADS[10].

Continuous variables were summarized as mean (SD) or median (range) as appropriate. Categorical variables were summarized as counts and percentages. Correlations between the size of breast lesions as measured by US, mammography and pathological examination were estimated using Pearson's correlation coefficient. Agreement between BI-RADS grading using the US and that using the mammogram was measured using the unweighted kappa statistic. All statistical analyses were performed with the statistical software Stata version 9 (StataCorp, College Station, TX, U.S.A).

Results

The mean age of the patients at diagnosis was 31.1 years (standard deviation (SD), 3.7 years); ranging from 18 to 35 years. The majority of patients (61 patients, 77%) presented with a painless palpable mass. Other presenting symptoms in the order of frequency were painful palpable mass in 6 (8%), nipple discharge in 3 (4%), palpable mass with nipple discharge in 2 (2%), palpable axillary lymph node in 2 (2%), right arm and breast edema in 1 (1%). Four patients (5%) had no symptoms. Imaging study was performed because of a high-risk history. No data were available about the presenting symptoms in 6 patients.

Most patients (89%) were investigated by both mammography and US. US was the only imaging investigation for the remaining patients (11%). Almost all malignancies presented as a mass (99%). Details of US features of 84 masses are shown in Table 1.

Mammographic evaluation was available for 73 lesions in 70 patients. There was good agreement between US and mammographic BI-RADS Classification (66 lesions, 89%) for the majority of lesions, despite dense breasts in almost all patients (extremely dense, 64%; and heterogeneously dense; 32%). Details of mammographic findings are displayed in Table 2.

In 7 patients whose lesions were retrospectively categorized as mammographic BI-RADS 0 (needing further imaging studies), malignancies presented as a focal asymmetric density and trabecular thickening, which required further investigation with US. Mammography was unable to detect any abnormality in 5 lesions (mammographic BI-RADS 1) due to extremely dense breasts.

The majority of malignant lesions were pure invasive ductal carcinoma (IDC) or included IDC (80%). Ten patients (12%) had pure ductal carcinoma in situ (DCIS). Fourteen percent of patients had stage 1 invasive cancers, 40% had stage 2 cancers, 21% had stage 3, and 6% had metastatic cancers. No staging data were available for the remaining 7% of the patients. See Table 3 for further details of pathological findings.

Mammography failed to detect 5 malignant lesions (7%) and was not assigned a category in 6 lesions (8%), which required further investigation. The histopathology of mammography-undetected lesions included 2 DCIS, 1 medullary carcinoma, 1 mucinous carcinoma and 1 IDC. All were detected by US.

The mean and median of tumor size seen on US, mammography and pathological examination

Table 1 Ultrasonographic features (n=85)

Characteristics	Summary: Number (%)	Characteristics	Summary: Number (%)
Mass lesion seen (yes)	84 (99)	Echo pattern	
Calcifications seen (yes)	41 (48)	Complex	5 (6)
Shape		Hypoechoic	79 (93)
Oval	3 (4)	No mass	1 (1)
Round	2 (2)	Posterior acoustic features	
Irregular	79 (93)	None	26 (31)
No mass	1 (1)	Enhancement	29 (34)
Orientation		Shadowing	16 (19)
Parallel to chest wall	65 (77)	Combined pattern	13 (15)
Right angle to chest wall or otherwise	19 (22)	No mass	1 (1)
No mass	1 (1)	Abnormal duct (yes)	7 (8)
Margin		Changes in Cooper's	30 (35)
Circumscribed	5 (6)	ligament (yes)	
Indistinct	56 (66)	Edema (yes)	9 (11)
Angular	5 (6)	Architectural distortion (yes)	29 (34)
Microlobulated	17 (20)	Skin thickening (yes)	16 (19)
Spiculated	1 (1)	US size (cm, n=81)	
No mass	1 (1)	Mean (SD)	2.75 (1.52)
Lesion boundary		Median (range)	2.4 (0.4 to 8.6)
Abrupt interface	10 (12)	BI-RADS for US	
Echogenic halo	74 (87)	3	2 (2)
No mass	1 (1)	4A	3 (4)
		4B	10 (12)
		4C	16 (19)
		5	54 (64)

Abbreviation: BI-RADS= Breast Imaging Reporting and Data system

are shown in Tables 1, 2 and 3. The correlation between the size of tumors measured by mammography and pathology was high (correlation coefficient, 0.838), and moderately high for US and mammogram, as was for US and pathology (correlation coefficient, 0.727 and 0.565, respectively). US tended to underestimate the true pathological size.

The unweighted kappa measure of agreement in terms of BI-RADS categorization between mammography and US was 0.466 (fair agreement). This finding suggested there were some differences between mammographic and US BI-RADS assessments for the same lesion. The BI-RADS category according to US findings were more likely to be higher than that according to the mammogram (see Table 4).

Examples of lesions are shown in Figures 1, 2 and 3.

Table 2 Mammographic features (n=73)

Characteristics	Summary: Number (%)	Characteristics	Summary: Number (%)
Correlation with US (yes)	66 (89)	Mammographic BI-RADS	
Mammographic density		0	7 (8)
Extremely dense	47 (64)	1	5 (7)
Heterogeneously dense	23 (32)	4A	1 (1)
Scattered	3 (4)	4B	10 (12)
Mammographic findings		4C	13 (18)
Ill-defined mass	14 (19)	5	37 (51)
Circumscribed mass	1 (1)	Mammographic size (cm, n=57)	
Mass with calcification	30 (41)	Mean (SD)	3.44 (1.94)
Linear branching calcification	1 (1)	Median (range)	2.9 (0.9 to 9.2)
Pleomorphic calcification	7 (10)		
Spiculated mass	3 (4)		
Lobular mass	4 (5)		
Asymmetrical density	5 (7)		
Trabecular thickening	2 (3)		
Negative	6 (8)		

Abbreviation: US= ultrasonography, BI-RADS= Breast Imaging Reporting and Data system

Table 3 Pathological features (n=85)

Characteristics	Summary: Number (%)	Characteristics	Summary: Number (%)
Pathological size (cm.)		Estrogen receptor status	
Mean (SD)	2.04 (1.64)	Positive	39 (46)
Median (range)	2.5 (0.8 to 9.5)	Negative	33 (39)
Type of cancer		Not done; loss to FU; phyllodes tumor	13 (15)
Pure DCIS	10 (12)	Progesterone receptor	
Pure IDC	53 (62)	Positive	38 (45)
IDC with DCIS	15 (18)	Negative	28 (33)
Mucinous cancer	3 (4)	Not done; loss to FU; phyllodes tumor	19 (22)
Medullary cancer	1 (1)	HER2/neu	
Papillary cancer	1 (1)	Positive	20 (24)
Malignant phyllodes tumor	2 (2)	Negative	46 (54)
		Not done; loss to FU; phyllodes tumor	19 (22)

Abbreviation: DCIS= Ductal carcinoma in situ, IDC= Invasive ductal carcinoma, FU= follow-up

Table 4 Agreement between ultrasonographic and mammographic BI-RADS (n=66)

US\Mam BI-RADS	1	3	4	5	Total
1	**0**	0	0	0	0
3	0	**0**	0	1	1
4	5	0	**14**	2	21
5	0	0	10	**34**	44
Total	5	0	24	37	**66**

Unweighted kappa measure of agreement = 0.466 (fair agreement)

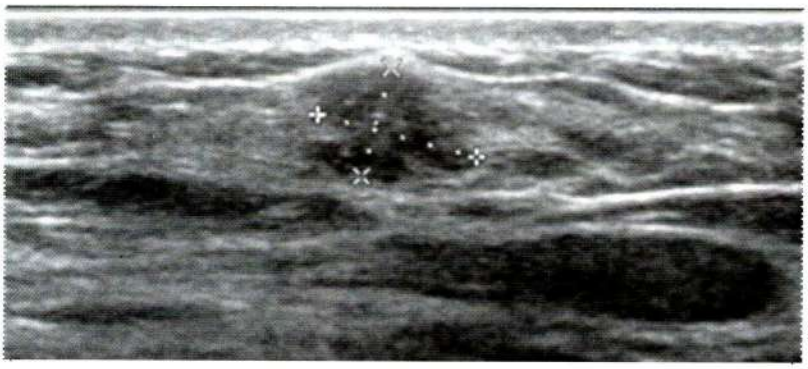

Fig.1A

A 19-year-old woman presented with painless palpable mass.

Fig 1A. US showed a 1.1-cm irregular indistinct mass with internal fine calcifications and echogenic halo.

Fig 1B. Mammography revealed extremely dense breast which totally obscured the mass. The pathology revealed ductal carcinoma in situ, grade 3 with foci of microinvasion.

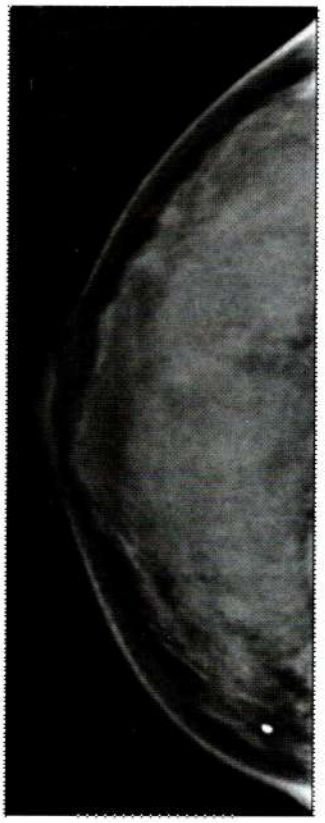

Fig.1B

Figures 2

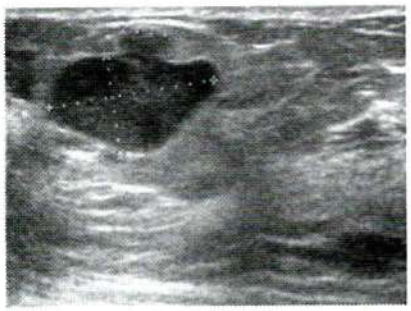

Fig.2A

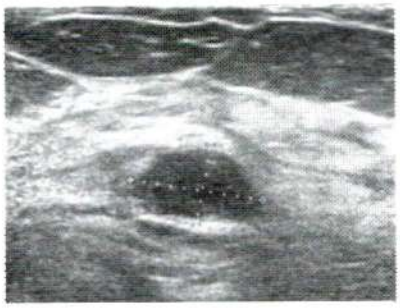

Fig.2B

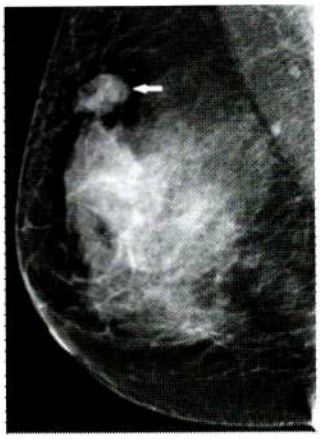

Fig.2C

A 32-year-old woman presented with a painless palpable mass. The US showed three lesions in the right breast. Fig 2A showed two contiguous solid masses with circumscribed borders, which were about 1.7 cm in total size. Heterogeneous echogenicity was noted in the larger mass. Fig 2B showed a 1.0-cm oval-shaped mass with circumscribed border. The mammography (Fig 2C) revealed heterogeneous dense breast with a lobular mass (arrow), which corresponds to the two contiguous masses seen on US. Faint internal calcifications were detected. The second mass failed to be demonstrated by mammogram. The histopathology of all lesions were mucinous carcinoma mixing with ductal carcinoma in situ.

Figures 3

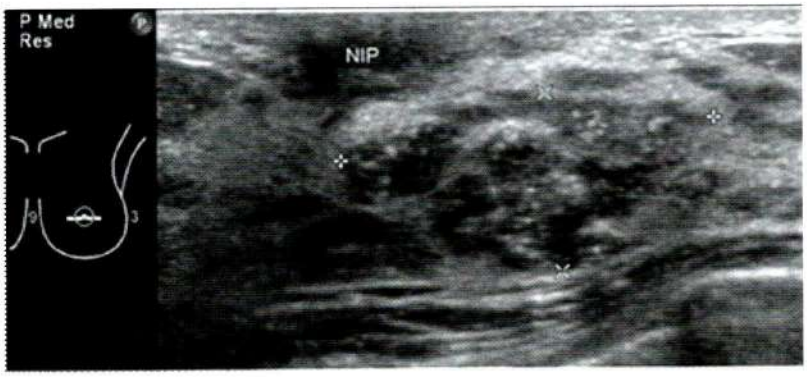

Fig.3A

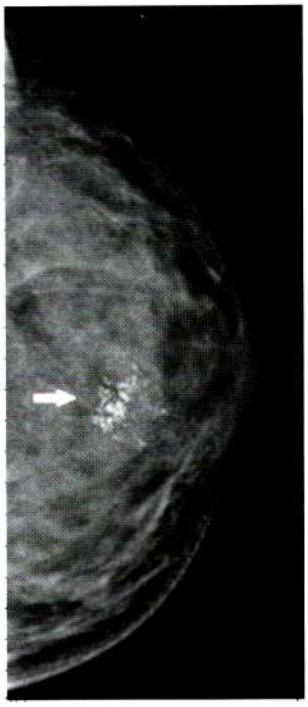

Fig.3B

A 27-year-old female presented with spontaneous left bloody nipple discharge for a few months. US revealed an ill-defined solid mass containing fine calcifications locating just beneath the left nipple (NIP) (Fig 3A). Mammography showed a cluster of linear branching and pleomorphic calcifications at the corresponding area (arrow in Fig 3B). Histopathology was intraductal papillary carcinoma and ductal carcinoma in situ, high grade. This case showed that microcalcifications were clearly visible despite extremely dense breast, unlike the cases shown in Figures 1 and 2, in which the mass was obscured by dense fibroglandular tissue.

Discussion

Diagnosing breast cancer in young women is not as straightforward as diagnosing breast cancers in the post-menopausal women. Firstly, since benign tumors such as fibroadenomas are much more common in young women, malignant breast lesions may be misinterpreted as benign lesions. Secondly, routine screening mammogram is not usually begun until the 40s in the average risk women[11-12]. Thus, DCIS, which traditionally manifests as microcalcifications, will be difficult to detect. Thirdly, the sensitivity of the mammogram declines in dense breasts, which is the typical breast pattern in young women[8-10]. US plays a major role in evaluating breast problems in young women because it is not compromised by dense breasts[3-7]. Moreover, the radiologist who performs US could correlate the US findings with the palpable mass at area of clinical concern, which is the most common presenting symptoms in young patients seeking medical attention[7]. Most patients in the present study (87%) had palpable masses. Thus, the present study emphasized the value of US in detecting and characterizing breast lesions in young women. All subjects in this study were evaluated by US and almost all malignant lesions (84 from 85 lesions, 99%) were detected as a mass by US.

Many suspicious US features are widely described in the literature[4-6], including the that on the BI-RADS lexicon[10]. These descriptors are valuable for dis-tinguishing malignant from benign lesions in the young patients in the present study as well. Most malignant lesions in the present study showed suspicious features. Seventy-nine mass lesions (93%) were irregular in shape. Most had indistinct, microlobulated, angular or spiculated margins (93%). Interestingly, echogenic halo was also an important feature, as we found 87% of lesions manifesting this US feature. This sign suggested the infiltrative nature of the tumor.

As stated previously, mammography had limited sensitivity in young patients because of their dense breast composition. However, the findings in the present study showed that mammography was still valuable in evaluating breast lesions in young patients. Most of our patients had abnormal mammograms (67 in 73 patients, 92%). This finding agreed with Paredes, et al.'s study, which reported a 89% detection rate of mammography in young patients[2].

Medullary and mucinous carcinomas constituted two out of 5 malignant tumors in the present study which were undetected by mammography. These subtypes are well-circumscribed malignancies likely to develop by pushing the surrounding breast parenchyma outwards rather than infiltrating[13]. Unlike IDC, which typically produces spiculated border or causes architectural distortion, medullary and mucinous carcinomas may easily be overlooked by mammography, particularly in the patients with dense breasts. However, these two subtypes of cancers could be detected by US.

The present study found that US-measured tumor size tended to be underestimated when compared with pathological size (correlation coefficient, 0.565), similar to findings in the literature[14-16]. Tumor size measured by mammography showed a higher correlation with pathological size (correlation coefficient, 0.838). All these findings might be explained by the fact that US could only detect the tumor nidus, but not the spicules which could represent tumor infiltration more easily seen on mammogram.

In the present study, US was unable to detect cancer in one patient. The patient had

inflammatory breast cancer, which did not manifest as a mass lesion. On reviewing the US films, the only finding was edematous breast tissue. Mammography, however, showed diffuse skin and trabecular thickening, which raised the possibility of inflammatory carcinoma. This suggested that it was prudent to interpret the US along with a mammogram. On the other hand, US finding of edematous breast without appropriate explanation should raise the concern of inflammatory breast cancer.

Breast cancer in the young is reported to have an aggressive biological behavior and is associated with less immunoreactivity for estrogen receptor and progesterone receptor[17-20]. In the present study, however, the majority of the patients (66%) presented with stage 2 cancer or lower, and almost half of all patients had positive immunohistochemistry for estrogen receptor (46%) and progesterone receptor (45%). Only one in fourth (24%) had positive HER2-neu.

There were some limitations in the present study. Because of the low incidence of breast cancer in young women, a long period of data collection was required and digital archiving of the images were not available in most of that time, thus only a quarter of all young patients with breast cancer had available images for retrospective review by the researchers. This could imply significant selection bias. Secondly, limited US images recorded on films may be not represent the true US features of the lesions. Thirdly, this study could not measure intra- and inter-observer variability. Future studies with prospective study design along with standardized mammographic and US interpretation should improve the validity of the research.

Conclusion

US showed a high detection rate for breast cancer in young patients. Many US features suggested the likelihood of the lesions being malignant. Mammography had a lower detection rate compared with US because lesions were hidden in the dense fibroglandular tissue. However, mammography was essential for diagnosis in some malignant lesions with nonspecific US findings, such as inflammatory breast cancer. Although US provided a high detection rate, it tended to underestimate the tumor size.

Acknowledgements

The authors gratefully acknowledge Amnuay Thithapandha Ph.D. and Supanee Chinnawongs Ph.D. for reviewing the manuscript.

Potential conflicts of interest

None.

References

1. Kuhaprema T, Srivatanatul, Attasara P, Wiangnon S, Sumitasawan Y. Cancer in Thailand volume 5. Bangkok 2010:47-51.
2. Paredes ES, Marsteller LP, Eden BV. Breast cancers in women 35 years of age and younger: mammographic findings. Radiology 1990;177:117-9.
3. Mendelson EB, Tobin CE. Critical pathways in using breast US. Radiographics 1995;15:935-45.
4. Venta LA, Dudiak CM, Salomon CG, Flisak ME. Sonographic evaluation of the breast. Radiographics 1994;14: 29-50.
5. Jackson VP. The role of US in breast imaging. Radiology 1990;177:305-11.
6. Paulinelli RR, Freitas R, Moreira MA, de Moraes VA, Bernardes JR, Vidal CA, et al. Risk of malignancy in solid breast nodules according to their sonographic features. J Ultrasound Med 2005;24:635-41.

7. Houssami N, Irwig L, Simpson JM, McKessar M, Blome S, Noakes J. Sydney Breast Imaging Accuracy Study. Comparative Sensitivity and Specificity of Mammography and Sonography in Young Women with Symptoms. Am. J. Roentgenol 2003;180:935-40.
8. Berg WA, Gutierrez L, Nessaiver MS, Carter WB, Bhargavan M, Lewis RS, et al. Diagnostic accuracy of mammography, clinical examination, US, and MR imaging in preoperative assessment of breast cancer. Radiology 2004;233: s830-49.
9. Kolb TM, Lichy J, Newhouse JH. Comparison of the performance of screening mammography, physical examination, and breast US and evaluation of factors that influence them: An analysis of 27,825 patient evaluations. Radiology 2002;225:165-75.
10. American College of Radiology. Breast Imaging Reporting and Data System (BI-RADS) atlas. 4th ed. Reston, VA: American College of Radiology 2003.
11. Bassett LW, Ysrael M, Gold RH, Ysrael C. Usefulness of mammography and sonography in women less than 35 years of age. Radiology 1991;180:831-5.
12. Berg, W.A., Tailored Supplemental Screening for Breast Cancer: What Now and What Next? Am. J. Roentgenol 2009;192:390-99.
13. Fattaneh A. Tavassoli, P. World Health Organization Classification of Tumors. Pathology and Genetics of Tumors of the Breast and Female Genital Organs. IARC Press: Lyon 2003.
14. Pierie JP, Perre CI, Levert LM, de Hooge P. Clinical assessment, mammography and ultrasonography as methods of measuring the size of breast cancer : a comparison. The Breast 1998;7:247-50.
15. Finlayson CA, MacDermott TA. Ultrasound can estimate the pathologic size of infiltrating ductal carcinoma. Arch Surg 2000;135:158-9.
16. Allen SA, Cunliffe WJ, Gray J, Liston JE, Lunt LG, Webb LA, et al. Pre-operative estimation of primary breast cancer size: a comparison of clinical assessment, mammography and ultrasound. The Breast 2001;10:299-305.
17. Colleoni, M. Very young women (<35 years) with operable breast cancer: features of disease at presentation. Ann. Onc 2002;13:273-79.
18. Yankaskas B. Performance of First Mammography Examination in Women Younger Than 40 Years. J Natl Cancer Inst 2010;102(10):692-701.
19. Althuis MD, Brogan DD, Coates RJ, Daling JR, Gammon MD, Malone KE, et al. Breast cancers among very young premenopausal women (United States). Cancer Causes and Control 2003;14:151-60.
20. Stanford JL, Greenburg RS. Breast cancer incidence in young women by estrogen receptor status and race. Am J Public Health 1989;79:71-3.

THE **ASEAN JOURNAL** OF **RADIOLOGY** 2012: 18(1): 26-40

Original Article

Cerebrospinal Fluid Flow Analysis in Prepontine Cistern, Foramen Magnum and 5th Cervical Spine Levels: Temporal and Spatial Patterns at MR Imaging in Volunteers and in Patients with Chiari I Malformation

Chewarat Wirojtananugoon MD.*, Parichart Somtua MD.*, Witaya Sangkarat MD.Ph.D*, Attaporn Boongerd MD., Udomchai Techavipoo, Ph.D.*****

Department of Radiology, Faculty of Medicine, Ramathibodi Hospital ** Department of Surgery, Faculty of Medicine, Ramathibodi Hospital * National Electronics and Computer Technology Center*

Abstract

Background and Purpose: The neurological signs and symptoms in Chiari I malformation patients are related to cerebrospinal fluid (CSF) flow obstruction at the foramen magnum. Previous studies show significantly higher peak CSF velocity at the foramen magnum level in these patients than in the normal population. However, recent studies report no significant difference of peak CSF velocity at the foramen magnum between symptomatic and asymptomatic Chiari I groups and suggested further studies of CSF flow outside the foramen magnum for better patient classification. The purpose of this study was to evaluate and compare CSF flow patterns in Chiari I patients and in healthy controls at the prepontine cistern, foramen magnum, and 5th cervical spine (C5) levels.

Methods: Five patients and ten healthy control volunteers were studied with a phase-contrast MRI at these levels through 20 phases of a cardiac cycle. The CSF flow patterns were analyzed for inhomogeneity using the flow velocity difference between the areas anterior and posterior to the spinal cord, the synchronous bidirectional flow, and the preferential flow direction.

Results: The peak systolic velocity means in the patients were higher than those in the controls for all three levels. However, statistical significance occurred only at the foramen magnum level. For all three levels, the flow spatial and temporal variations (flow nodes and jets and consecutive images with synchronous bidirectional flows) were more evident in the patients than in the controls.

Conclusion: No significant difference of the CSF flow occurs at the prepontine cistern and C5 levels between the patients and controls. Therefore, the CSF flow studies outside the foramen magnum may not be effective for patient evaluation

Introduction

The Chiari I malformation is a congenital hindbrain dysgenesis characterized by tonsillar ectopia, which is downward displacement of the cerebellar tonsils below foramen magnum or into the spinal canal. Multiple etiologies cause small posterior fossa relatively with the cerebellum. Chiari I patients may present with clinical findings related to brainstem compression, i.e., valsava maneuver-induced headache, ataxia or lower cranial nerve symptoms, or related to syringomyelia, i.e., pain, impaired temperature sensation or peripheral motor weakness[1,3].

However, about 1/3 of patients have no signs or symptoms related to the Chiari I malformation. In addition, clinical manifestations vary between patients with the similar amounts of tonsillar ectopia[2,4]. To our knowledge, neurological signs and symptoms in Chiari I patients related to cerebrospinal fluid (CSF) flow obstruction at foramen magnum[1,12].

Previous studies of CSF flow in the foramen magnum with phase contrast magnetic resonance imaging (MRI) show more synchronous bidirectional flows of CSF flow in symptomatic Chiari I group and show significant higher peak CSF velocity at foramen magnum than that in normal population[7]. Furthermore, in Chiari I patients, the peak CSF velocity decreases after surgical treatment by craniocervical decompression[5-9]. Then, the alteration of the CSF flow patterns in Chiari I patients may be helpful in patient screening for surgical treatment and postoperative follow-up[11-15].

However, the recent study of Krueger KD et al.[15] shows no significant difference of the peak CSF velocity in the foramen magnum between symptomatic and asymptomatic Chiari I groups and suggests that CSF flow analysis outside the foramen magnum may be beneficial for evaluation of the Chiari I patients[15].

In our study, we compared difference of CSF flow patterns at MRI in Chiari I patients and healthy controls at the prepontine cistern, foramen magnum, and 5th cervical spine (C5) levels.

Research question

Are there any differences in CSF flow patterns at the prepontine cistern, foramen magnum, and C5 levels at MRI in healthy controls and in patients with Chiari I Malformation?

Objective

To study variation in CSF flow patterns at the prepontine cistern, foramen magnum, and C5 levels through a cardiac cycle and throughout the subarachnoid space at MRI in healthy controls and in patients with Chiari I malformation.

Materials and Methods

Study design

Prospective case-control study between a Chiari I patient group and a healthy control group

Patients and Controls

Patients

Out patients with Chiari I malformation from the Departments of Neurosurgery, Neuromedicine, and Orthopedics of Ramathibodi hospital between November 2010 and October 2011 were included in our study. The inclusion and exclusion criteria were described below.

Inclusion criteria:

1. All of the patients who have been diagnosed Chiari I malformation, as determined on the basis of T2-weighted sagittal MR image (tonsillar ectopia and/or peg like cerebellar tonsils). The

patients may have or may not have signs and symptoms of Chiari I malformation.

2. No history of claustrophobia or contraindications to MRI.

3. Completed informed consent.

Exclusion criteria:

1. Contraindication for 3-Tesla MRI.

2. Not completed informed consent or cancelled informed consent

Controls

Inclusion criteria:

1. All normal volunteers who are healthy and no present or previous spinal and neurologic problems or hypertension.

2. No cerebellar tonsils below the foramen magnum level from the T2-weighted sagittal MR image.

3. No history of claustrophobia or contraindications to MRI.

4. Completed informed consent.

The MRI protocol followed ethical rules and was approved by our institutional review board, and all patients were informed and gave their consents.

MRI protocol for CSF flow study:

- Flip angle = 20°
- Repetition time (msec)/ echo time (msec)= 7.4/5.5
- Slice thickness = 5 mm
- Field of view = 150 mm
- Matrix size = 256 x 256
- Encoding velocity = 10 cm/sec

Locations of the CSF flow study (Figure 1)

1. Axial plane perpendicular to the CSF space at the mid prepontine cistern level

2. Axial plane perpendicular to the CSF space at

2.1 The foramen magnum in controls, (the mid of the slice at the line between basion (anteriorly) and opision (posteriorly)

2.2 Just below the cerebellar tonsils in patient with Chiari I malormation

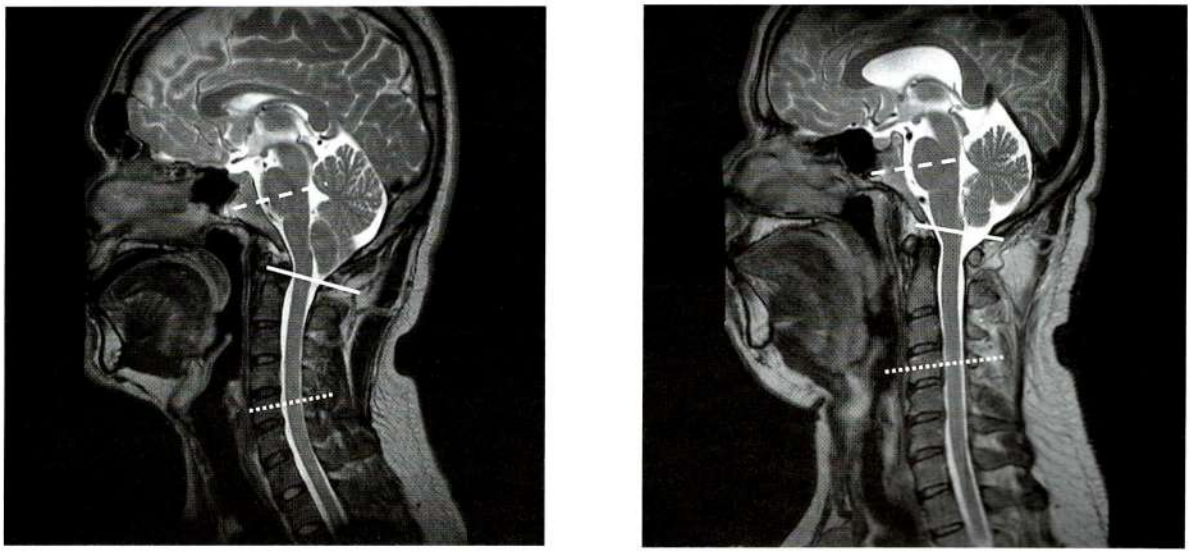

Fig.1 Axial planes are placed perpendicular to CSF space at the prepontine cistern, foramen magnum, and mid C5 levels (represented by dashed, solid, and dotted lines, respectively) on the T2-weighted images of a Chiai I patient (left) and of a healthy control volunteer (right).

3. Axial plane perpendicular to the CSF space at the mid C5 level

Total scan time was about 30-40 minutes and there was no intravenous contrast material administration.

Sample size

This study compared differences in CSF flow patterns at the prepontine cistern, foramen magnum, and C5 levels at MRI in healthy controls and in patients with Chiari I malformation.

For comparison between these two groups of data, the sample size was estimated by using estimated sample size for two-sample comparison of means, which were calculated from STATA statistical analysis program. In the previous study[10], the Chiari I patients had significant elevations of peak systolic velocity of the CSF in the foramen magnum. The average peak systolic velocity was 2.4 cm/sec (SD, 0.7) in the controls and was 3.1 cm/sec (SD, 1.0) in the Chiari I patients.

Then we set the difference between peak systolic velocity of the CSF in the foramen magnum between the controls and the Chiari I patients with statistically significant level at power = 0.800 and alpha = 0.0500.

Estimated sample size for two-sample comparison of means

Test Hypothesis: m1 = m2, where m1 is the mean in population 1 and m2 is the mean in population 2.

Assumptions:

Alpha = 0.0500 (two-sided)

Power = 0.8000

m1 = 2.4

m2 = 3.1

sd1 = 0.7

sd2 = 1.0

n2 / n1 = 2.00

Estimated required sample sizes:

n1 = 16

n2 = 32

Between November 2010 and October 2011, we estimated number of Chiari I patients that were included in the study about 5 persons. Then we recalculated estimated required sample sizes at the mean of peak systolic velocity of the Chiari I patient group at 3.5 cm/sec.

Estimated sample size for two-sample comparison of means

Test Hypothesis: m1 = m2, where m1 is the mean in population 1 and m2 is the mean in population 2

Assumptions:

Alpha = 0.0500 (two-sided)

Power = 0.8000

m1 = 2.4

m2 = 3.5

sd1 = 0.7

sd2 = 1.0

n2 / n1 = 2.00

Estimated required sample sizes:

n1 = 5

n2 = 10

Then, sample sizes in this study were 5 persons in the Chiari I patient group and 10 persons in the control group.

Data collection

Demographic data

The following demographic data, collected by interviewing or reviewing from the medical record, were recorded in data collection form.

- Age

- Gender
- Clinical presentation: sign and symptom of Chiari I malformation

CSF flow measurement and analysis

The patients and controls underwent imaging with a 3-Tesla MRI scan (Achiva; Philips medical systems, Best, the Netherlands). The T2-weighted sagittal images of the cervical spine in two groups were obtained for evaluation of tonsillar ectopia and syringomyelia by a neuroradiologist and a radiology resident. The lengths of the tonsillar ectopia in the Chiari I patient group were recorded.

The cardiac gated phase-contrast images were acquired at the prepontine cistern, foramen magnum, and C5 levels when the participant had achieved steady heart rate. The CSF flow measurement data were conduct with computer software analysis program of the Philips MRI scan. The images of 20 phases of a cardiac cycle were inspected to identify the subarachnoid space and the course of the vertebral arteries. The signal intensity within the subarachnoid space was assessed visually for the uniformity or inhomogeneity.

To measure velocity and flow volume of CSF of each voxel in the systolic and diastolic phases and to evaluate CSF flow pattern at the 3 levels, the CSF flow analysis computer program has been developed by a research scientist from the National Electronics and Computer Technology Center (NECTEC). A region of interest was manually placed to include the entire subarachnoid space (including the spinal cord), then the program removed the voxels that have absolute velocities less than 1.5 cm/s (in either caudad or cephalad directions) in all cardiac phases, indicating stationary tissue. In addition, the voxels that have all positive or all negative flow velocities in all cardiac phases, indicating vascular tissue, were also removed from the region of interest. By concensus, the investigators verify the region of interest by investigating the plots of the CSF velocities versus the cardiac phases to adjust some voxels in the regions of interest. The voxels exhibiting aliased velocities were corrected with the program. The peak systolic and diastolic velocities in the region of interest were demonstrated from color maps and surface contour plots of the CSF velocities.

The color maps and surface contour plots of the CSF velocities in both control group and patient group at three levels were analyzed for the following parameters:

1. Peak systolic velocity (PSV) and peak diastolic velocity (PDV) and their location in 6 locations of the subarachnoid space, i.e., anterior midline, anterior paramedian, posterior midline, posterior paramedian, anterolateral, and posterolateral regions
2. CSF flow in the anterior and the posterior subarachnoid space
3. Voxels that have velocity exceeded those in the adjacent region of the subaracnoid space by 100-200% (nodes) and 200-300% (jets), compared with voxels that exhibit total subaracnoid space
4. Presence of the synchronous bidirectional flow, i.e., flow images containing both cephalad and caudad flow in same image in two or more consecutive phases
5. Flow preferential direction: cephalad flow volume, caudad flow volume, and net flow volume in the subarachnoid space

Statistical analysis

Discontinuous variables, i.e., sex of patients or

controls, symptoms and signs of patients will be summarized as counts and percentages. Continuous variables, i.e., age of patients or controls, velocity or flow volume of CSF will be summarized as range) and mean ± 1 standard deviation (SD) of the groups.

To test the significance of differences in the parameters between the patients and the controls, the comparison of the mean was performed using student t-test or Mann-Whitney test, with P-value ≤ .05 considered to indicate a statistically significant difference.

Fisher's exact test was used to test the significant difference in the presence of synchronous bidirectional flows in both groups.

Results

Patients and volunteers

The Chiari I group comprised 5 patients (3 men, 2 women; age range, 16-49 years; mean age, 36 years) who have been diagnosed with Chiari I malformation, as determined on the basis of T2-weighted sagittal MR images. The control volunteers groups included 10 normal volunteers (4 men, 6 women; age range, 23-51 years; mean age, 32.1 years) who have no evidence of tonsillar ectopia or gross posterior fossa abnormalities. The age difference between the two groups was not significant (P-value = 0.4934).

In Chiari I group, tonsillar herniation ranged from 4 mm to 16 mm (mean = 11 mm). One asymptomatic Chiari I patient had unilateral tonsillar herniation about 8 mm. Four patients had symptoms and/or signs that were attributed to Chiari I malformation. Three of these patients presented with valsava maneuver-induced headache and two of which had sensory deficit (paresthesia of the upper extremity). The other patient presented with scoliosis and syringomyelia seen on MRI.

Peak systolic and diastolic velocities

All of the phase-contrast studies of two groups were considered technically adequate for the measurement of the peak velocities. For each control and patient, the subarachnoid space and vertebral artery were well identified in the foramen magnum level. The signal intensity throughout the subarachnoid space was relatively uniform in all 20 images of the cardiac phases. In both Chiari I and control groups, slightly greater velocities of CSF flow were evident in the anterior subarachnoid space in a paramedian location than those in the rest of subarachnoid space at all three levels. The signal intensity (which is the flow velocity) generally shifted from positive (cephalad flow) to negative (caudad flow) and back to positive during the cardiac cycle in both groups (Figure 2).

The peak systolic and diastolic velocities for the controls are presented in Table 1. The average peak systolic velocities at the prepontine cistern, foramen magnum and C5 levels were 3.93 cm/s (SD, 0.87), 4.10 cm/s (SD, 0.51), and 7.29 cm/s (SD, 1.38), respectively, while the average peak diastolic velocities at these three levels were 3.58 cm/s (SD, 0.94), 3.42 cm/s (SD, 0.42), and 5.76 cm/s (SD, 1.66), respectively.

The peak systolic and diastolic velocities for the Chiari I patients are presented in Table 2. The average peak systolic velocities at the prepontine cistern, foramen magnum, and C5 levels were 4.54 cm/s (SD, 1.51), 7.33 cm/s (SD, 1.62), and 8.09 cm/s (SD,1.43), respectively, while the average peak diastolic velocities at these three levels were 3.54 cm/s (SD, 0.83), 3.65 cm/s (SD, 0.79), and 5.45 cm/s (SD,1.43), respectively.

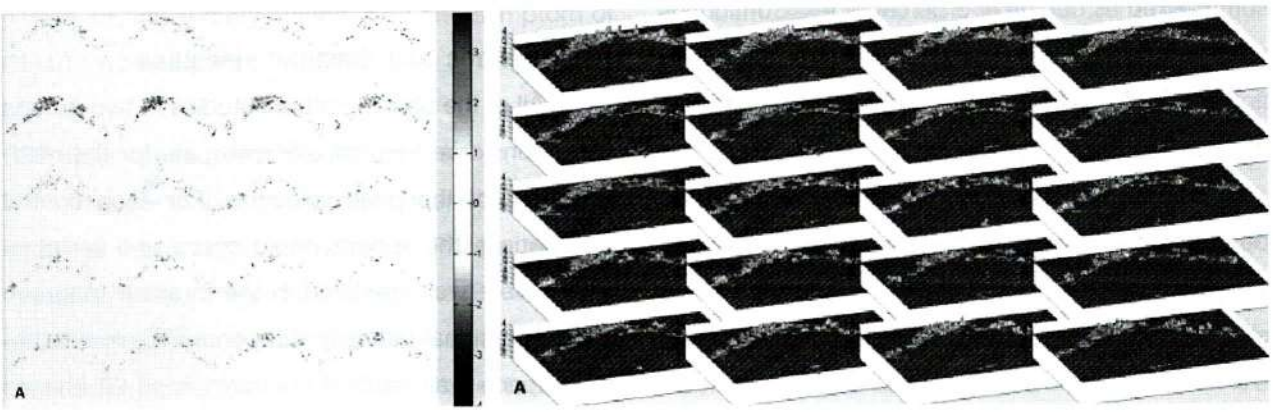

(a)

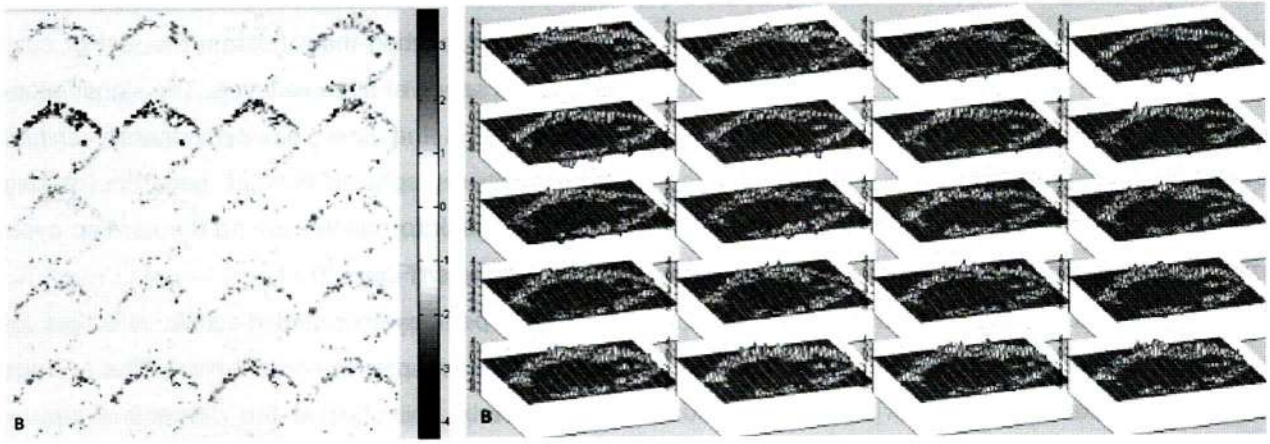

(b)

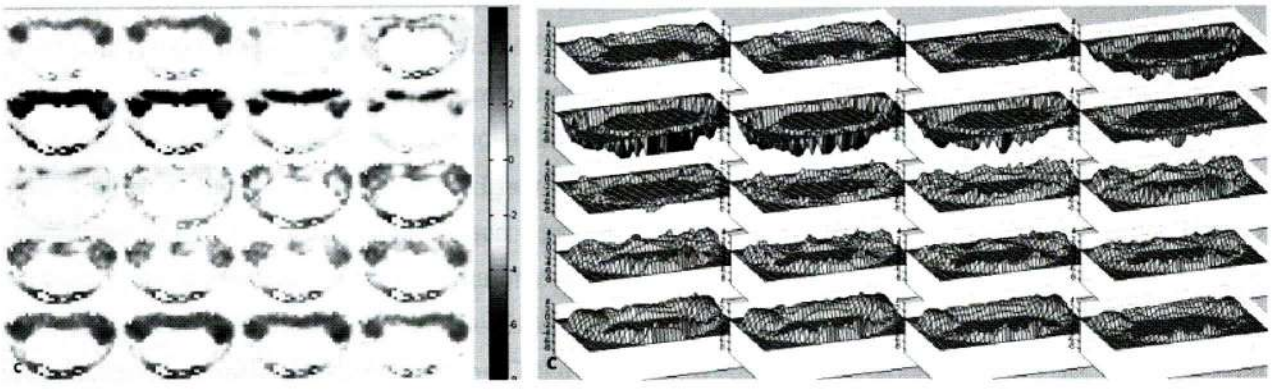

(c)

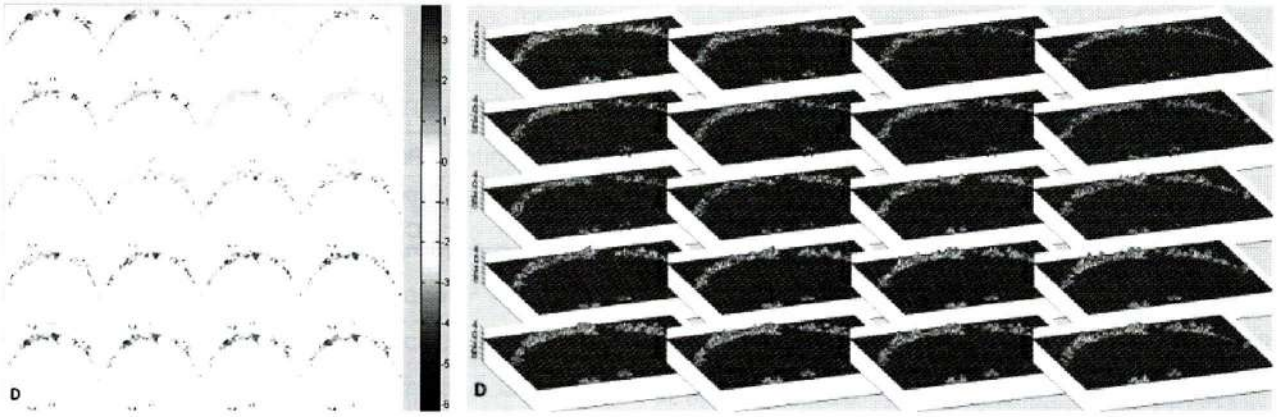

(d)

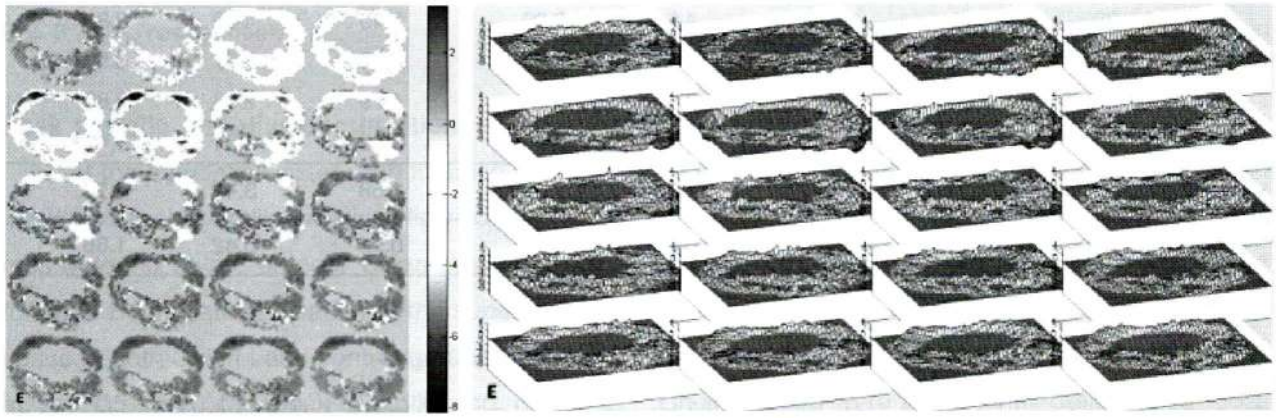

(e)

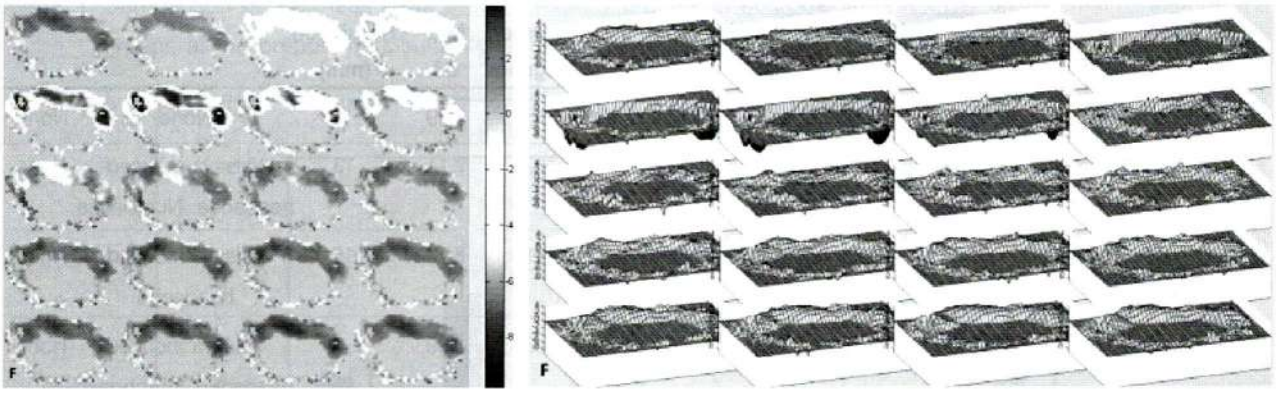

(f)

Fig.2 Color maps (left column) and surface contour plots (right column) of the CSF flow velocity during 20 cardiac phases (ordered from the left to the right and then the top to the bottom) in a control volunteer (A, B, and C) and a Chiari I patient (D, E, and F) at the prepontine cistern level (A and D), the foramen magnum level (B and E), and the C5 level (C and F). The CSF flow velocity is scaled from -8.0 to 4.0 cm/s as indicated by the colorbars and the vertical axis scales. The surfaces above the horizon plane show the cephalad flows and the surfaces below the horizon plane show the caudad flows.

Table 1 The age, sex, and peak systolic and diastolic velocities in the normal control volunteers.

No.	Age (years)	Sex	Peak Systolic Velocity (cm/s)			Peak Diastolic Velocity (cm/s)		
			Prepontine Cistern	Foramen Magnum	Mid C5	Prepontine Cistern	Foramen Magnum	Mid C5
1	51	female	3.35	3.83	8.55	4.00	3.40	5.85
2	35	male	4.19	4.13	7.31	2.88	3.33	8.36
3	34	male	3.86	3.77	8.06	3.30	3.53	5.85
4	30	female	3.21	3.94	7.81	2.66	3.54	5.10
5	30	female	2.71	4.02	4.71	2.47	3.81	4.03
6	23	female	3.28	3.81	8.54	3.15	3.12	4.80
7	28	female	4.64	4.91	8.09	5.40	4.09	8.88
8	24	female	4.05	4.35	8.00	3.79	3.67	5.50
9	37	male	5.78	3.31	5.03	4.79	2.53	3.80
10	29	male	4.26	4.97	6.76	3.32	3.21	5.40
Mean	**32.10**		**3.93**	**4.10**	**7.29**	**3.58**	**3.42**	**5.76**
SD	**8.01**		**0.87**	**0.52**	**1.38**	**0.94**	**0.42**	**1.66**

Table 2 The age, sex, and peak systolic and diastolic velocities in the Chiari I patients, including the information of the tonsillar herniation length (mm), signs/symptoms, and syrinx existance.

No.	Age (years)	Sex	Peak Systolic Velocity (cm/s)			Peak Diastolic Velocity (cm/s)			Tonsillar Herniation (mm)	Signs / Symptoms	Syrinx
			Prepontine Cistern	Foramen Magnum	Mid C5	Prepontine Cistern	Foramen Magnum	Mid C5			
1	30	male	5.49	6.58	8.39	4.11	3.52	5.09	7	None	None
2	48	female	2.68	5.88	5.96	2.64	3.24	7.11	13	Valsava induced headache, Numbness	None
3	37	female	3.23	6.23	8.51	2.67	3.13	6.79	16	Valsava induced headache	None
4	49	male	6.21	8.22	9.89	3.86	3.32	3.89	4	Valsava induced headache, Numbness	None
5	16	male	5.07	9.75	7.72	4.43	5.06	4.38	15	Scoliosis	Syrinx
Mean	**36.00**		**4.54**	**7.33**	**8.09**	**3.54**	**3.65**	**5.45**	**11.00**		
SD	**13.69**		**1.51**	**1.62**	**1.43**	**0.83**	**0.80**	**1.44**	**5.24**		

The peak systolic velocity at the foramen magnum in the Chiari I group was significantly higher than that in the control group (P = 0.0001). The peak systolic velocities at the prepontine cistern and the C5 levels in the Chiari I group were also higher than those in the control group but not statistically significant (P = 0.3398 and P = 0.3103). However, the peak diastolic velocities at the prepontine cistern, foramen magnum, and C5 levels between the Chiari I and control groups are not significantly different (P = 0.9464, P = 0.4701 and P = 0.7329, respectively).

Peak systolic and diastolic locations

At the prepontine cistern and foramen magnum levels, the peak systolic and diastolic velocities were mostly found at the anterior paramedian location, followed by the lateral location of the subarachnoid space in both Chiari I and control groups. However, at the C5 level, the peak systolic and diastolic velocities were mostly found at the lateral location of the subarachnoid space in both Chiari I and control groups. Only one control has the peak systolic velocity at the C5 level at the anterior paramedian location (Table 4).

Flow nodes and jet areas

On each image, the voxels exhibiting velocities exceeding the mode of the velocities in the subaracnoid space on that image by 100-200% were defined as nodes and those by 200-300% were defined as jets. The area of nodes or jets was then calculated in a percentage compared to the total area of the subarachnoid space on that image.

At the foramen magnum level, the node and jet areas in both cephalad and caudad directions in the Chiari I group were generally greater than those in the control group (as shown in Table 5). The node and jet areas in the cephalad direction in the Chiari I group were significantly greater than those

Table 3 Comparison of the mean peak systolic velocity and mean peak diastolic velocity of the Chiari I and control groups at the prepontine cistern, foramen magnum, and C5 levels.

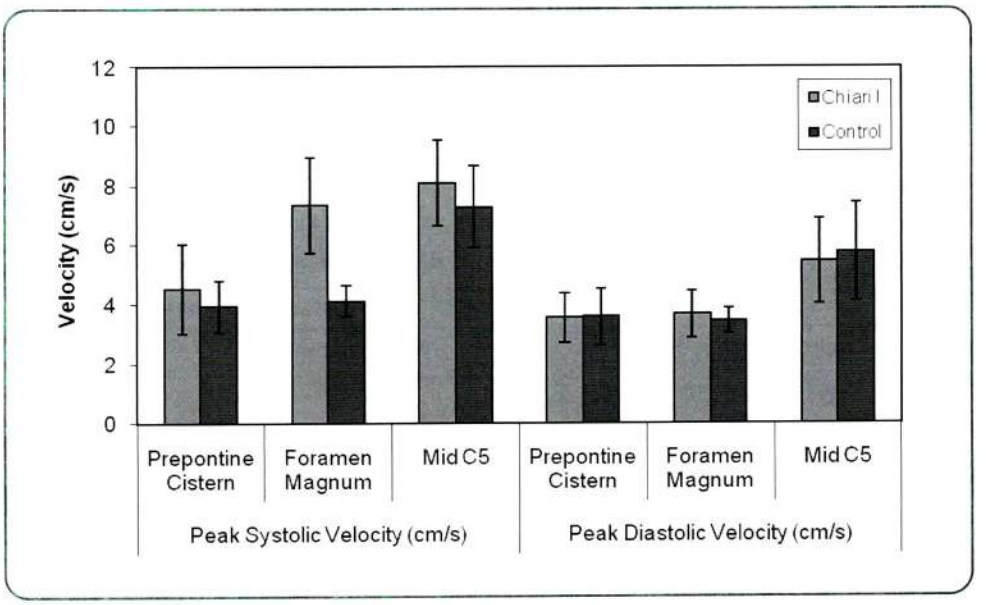

Table 4 The number of the Chiari I patients and the control volunteers categorized by their locations of the peak systolic and diastolic velocities in the subarachnoid spaces.

Location	Number of Subjects											
	Peak Systolic Velocity						Peak Diastolic Velocity					
	Prepontine Cistern		Foramen Magnum		Mid C5		Prepontine Cistern		Foramen Magnum		Mid C5	
	Chiari I	Contorl	Chiari I	Contorl	Chiari I	Contorl	Chiari I	Contorl	Chiari I	Contorl	Chiari I	Contorl
Anterior midline	-	-	-	-	-	-	-	-	-	-	-	-
Anterior paramedian	4	8	3	6	-	1	4	9	3	6	-	-
Posterior midline	-	-	-	-	-	-	-	-	-	-	-	-
Posterior paramedian	-	-	-	-	-	-	1	-	-	-	-	-
Anterolateral	1	2	2	4	5	9	-	1	2	4	5	10
Posterolateral	-	-	-	-	-	-	-	-	-	-	-	-

Table 5 The node and jet areas in percentage according to the subarachnoid at the prepontine cistern, foramen magnum, and C5 levels in the Chiari I patients and the control volunteers.

Node and Jet Areas in Subarachnoid Space	Prepontine Cistern			Foramen Magnum			Mid C5		
	Chiari I	Contorl	P-value	Chiari I	Contorl	P-value	Chiari I	Contorl	P-value
Cephalad									
Node (%)	14.54	15.62	0.807	16.98	6.72	**0.037**	9.54	11.81	0.803
Jet (%)	7.95	9.45	0.540	4.36	1.02	**0.020**	9.99	15.04	0.519
Caudad									
Node (%)	17.33	13.24	0.392	15.41	7.77	0.066	2.28	8.41	0.184
Jet (%)	5.99	4.20	0.354	13.61	1.99	**0.004**	13.63	7.64	0.662

in the control group, i.e., the node areas in the Chiari I and control groups are 16.98% and 6.72%, respectively, P = 0.0373, while the jet areas are 4.36% and 1.02%, respectively, P = 0.0200. In the caudad direction, the jet area in the Chiari I group was also significantly greater than that in the control group, i.e., 13.61% and 1.99%, respectively, P = 0.0036. The node area in the caudad direction of the Chiari I was greater than in the control group, however, it was not statistically significant, i.e., 15.41% and 7.77%, respectively, P = 0.0662.

At the prepontine cistern and C5 levels, there were no significant difference of the node and the jet areas in the cephalad and caudad directions in both groups (Table 5).

Comparison of the flow in anterior and posterior subarachnoid spaces

At the foramen magnum and the C5 levels, the cephalad and caudad flows were founded mostly in the anterior subarachnoid space in both groups.

Synchronous bidirectional flows

Synchronous bidirectional flows, i.e., simultaneous cephalad and caudad flows, were evident in both groups at all three levels. Using Fisher's exact test, the presence of synchronous bidirectional flows in both groups were not statistically different in all levels (Table 6). However, in the Chiari I group, there were more consecutive images recognized as synchronous bidirectional flows than in the control group at all three levels. In two groups, bidirectional flows were found mainly at the transitional cardiac phases from the cephalad to caudad flows or from the caudad to cephalad flows.

Preferential direction of the flow

For the variations in the flow rate over the cardiac cycles, we defined the cumulative flow through a voxel as the sum of the flow volume at that voxel over all 20 cardiac phases. The sum of the cumulative flow over all voxels in the region of interest was the net cumulative flow. The positive or negative value of the net cumulative flow assumably indicated the preferential flow direction, i.e., the cephalad or caudad flow, respectively.

At the foramen magnum, the all preferential flow directions in the Chiari I group were in the caudad (negative) direction. It was significantly different (P-value = 0.044) from the preferential flow directions of the controls, 6 of which in the cephalad (positive) direction and the other 4 of which

Table 6 The absence/presence of the synchronous bidirectional flow and the number of consecutive cardiac phases containing the synchronous bidirectional flow at the prepontine cistern, foramen magnum, and C5 levels in the Chiari I patients and the control volunteers.

Synchronus Bidirectional Flow	Prepontine Cistern			Foramen Magnum			Mid C5		
	Chiari I	Control	P-value	Chiari I	Control	P-value	Chiari I	Control	P-value
Presence (persons)	5	7	0.505	5	8	0.524	5	9	1
Absence (persons)	0	3		0	2		0	1	
Mean Number of Presence Phases	11.2	4.28	**0.007**	6.6	3.875	**0.042**	6.2	3.11	**0.008**
Range	7 to 20	2 to 8		3 to 10	2 to 7		4 to 9	2 to 5	

Table 7 The number of the Chiari I patients and the control volunteers possessing the preferential flow in the caudad and cepalad directions at the prepontine cistern, foramen magnum, and C5 levels.

Preferential Flow Direction	Prepontine Cistern			Foramen Magnum			Mid C5		
	Chiari I	Control	P-value	Chiari I	Control	P-value	Chiari I	Control	P-value
Caudad (persons)	4	5	0.58	5	4	**0.044**	2	5	1
Cephalad (persons)	1	5		0	6		3	5	

in the caudad direction. However, in the prepontine cistern and C5 levels, the preferential flow directions in the Chiari I and control groups were not significantly difference (P-value = 0.580 and 1.000, respectively) (Table 7).

Discussion

The focus of this research is on both the temporal and spatial variation of the CSF flow at MRI in Chiari I patients and healthy controls.

In control group, the peak systolic and diastolic velocities at the prepontine cistern level are not significantly different from those at the foramen magnum level. These values at the C5 level are higher compared to those at the prepontine cistern and foramen magnum levels.

In Chiari I group, the peak systolic velocity tends to increase progressively from the superior to inferior levels, i.e., from the prepontine cistern level to the foramen magnum level and to the C5 level. The peak diastolic velocities at the prepontine cistern and foramen magnum levels are not significantly different; however, it increases at the C5 level. In addition, there is no significant relation between the length of tonsillar herniation and the peak velocity at the foramen magnum in the Chiari I group. This finding supports the result from the previous study that isolated finding of tonsillar herniation is of limited prognostic utility and must be considered in the context of clinical and radiographic data[4].

At the foramen magnum level, we found a significant increase in the peak systolic velocity in the Chiari I group compared to the control group. However, there is no significant difference in the peak diastolic velocity between the two groups. This finding is similar to the previous studies[4,10]. The results support the hypothesis that the presence of the tonsils in the foramen magnum alters the CSF flow patterns due to the CSF flow obstruction.

Difference in section location at the foramen magnum in volunteers and just below cerebellar tonsils in Chiari I patients has been thought to diminish differences in CSF velocities between patient and control groups[7]. In our study, we found that the CSF velocities tend to increase from superiorly to inferiorly (prepontine cistern down to C5 level). So, CSF velocities at just below cerebellar tonsils may not be significantly lower than those at the foramen magnum, and this should not affect the result.

However, at the prepontine cistern and C5 levels, the peak systolic and diastolic velocities are not significantly different between the two groups. The finding implies that the altered CSF flow from the cerebellar tonsils at the foramen magnum in the Chiari I group does not influence the CSF flow at

the level above or below the foramen magnum.

For the location of the peak velocity at the foramen magnum level, in our study both the peak systolic velocity and the peak diastolic velocity are mostly found at the anterior paramedian location of the subarachnoid space, followed by the lateral location. In contrast to the previous studies[4,10], the peak systolic velocity and the peak diastolic velocity are found only at the anterior paramedian location.

We find the number of consecutive images of the synchronous bidirectional flows in the Chiari I group is higher than that in the control group in all three levels. In addition, the areas of nodes and jets are much larger in the Chiari I group at the foramen magnum level, compared to the control group. These suggest that the CSF flow in the Chiari I group is more inhomogeneous than that in the control group, agreeing with the previous studies[7,10].

Significant preferential CSF flow in caudad direction at the foramen magnum in the Chiari I group found the our study supports theory of CSF obstruction at the foramen magnum as a pathophysiology of syringomyelia[12].

Limitation of study

The result of this study is limited to the Philips 3T MRI scanner and the provided software to evaluate the phase contrast MR images for the velocity of the CSF flow. The partial volume artifact on the image pixels due to the thick slice thickness and the pixel value interpolation from the image reconstruction could also impair the results. In addition, the investigators' decisions on the segmentation of the ROI could bias the results. The result of this study is also based on a small number of Chiai I patients and normal control volunteers. Therefore, further data collection from large population should be obtained for adequate information for conclusion.

Conclusion

There is significantly higher degree of peak systolic velocity and the inhomogeneity of the CSF flow at the foramen magnum level in the Chiari I group compared to the control group. There is no significant difference in the quantitative analysis of the CSF flow at the prepontine cistern and C5 levels between the Chiari I group and the control group. Then, CSF flow studies outside the foramen magnum may not be useful enough for evaluation and differentiation between symptomatic and asymptomatic Chiari I patients. Conclusion about relationship between the CSF flow patterns and the clinical deficits in association with Chiari I malformations requires additional data from larger population.

References

1. Milhorat TH, Chou MW, Trinidad EM, et al. Chairi I malformation redefined: clinical and radiographic findings for 364 symptomatic patients. Neurosurgery 1999;44: 1005-17.
2. Elster AD, Chen MYM. Chiari I malformations: clinical and radiologic reappraisal. Radiology 1992;183:347-53.
3. Barkovich AJ, Wippold FJ, Shermam JL, Citrin CM. Significance of cerebellar tonsillar ectopia on MR. AJNR Am J Neuroradiol 1986;7:795-99.
4. Meadows J, Kraut M, Guamieri M, et al. Asymptomatic Chiari I malformations identified on magnetic resonance imaging. J Neurosurg 2000;92:920-6.
5. Wolpert SM, Bhadelia RA, Bogdan AR, et al. Chiari I malformation: assessment with phase-contrast velocity MR. AJNR Am J Neuroradiol 1994;15:1299-308.
6. Roldan A, Wieben O, Haughton V, et al. Characterization of CSF hydrodynamics in the presence and absence of tonsillar ectopia by means of computational flow analysis, AJNR Am J Neuroradiol 2009;30:941-6.

7. Quigley MF, Iskandar B, Quigley ME, et al. Cerebrospinal fluid flow in foramen magnum: temporal and spatial patterns at MR imaging in volunteers and in patients with Chiari I malformation. Radiology 2004;232:229-36.
8. Hofman E, Warmuth-Metz M, Bendzus M, et al. Phase-contrast MR imaging of the cervical CSF and spinal cord: volumetric motion analysis in patients with Chiari I malformation. AJNR Am J Neuroradiol 2000;21:151-5.
9. Iskandar BJ, Haughton V. Age-related variations in peak cerebrospinal fluid velocities in the foramen magnum. J Neurosurg 2000;103(6 suppl):508-11.
10. Haughton VM, Korosec FR, Medow JE, et al. Peak systolic and diastolic CSF velocity in the foramen magnum in adult patients with Chiari I malformations and in normal control participants. AJNR Am J Neuroradiol 2003;24: 169-76.
11. Iskandar BJ, Quigley M, Haughton VM, Foramen magnum cerebrospinal fluid flow characteristics in children with Chiari I malformation before and after craniocervical decompression, J Neurosurg 2004;101(2 suppl):169-78.
12. Heiss JD, Patronas N, DeVroom HL, et al. Elucidating the pathophysiology of syringomyelia. J Neurosurg 1999; 91:553-62.
13. Pinna G, Alessandrini F, Alfieri A, Rossi M, et al. Cerebrospinal fluid flow dynamics study in Chiari I malformation: implications for syrinx formation. Neurosurg Focus 2000;8(3):E3.
14. Dolar TM, Haughton VM, Iskandar BJ, et al. Effect of Craniocervical Decompression on Peak CSF Velocities in Symptomatic Patients with Chiari I Malformation, AJNR Am J Neuroradiol 2004;25:142-5.
15. Krueger KD, Haughton VM, Hetzel S. Peak CSF Velocities in Patients with Symptomatic and Asymptomatic Chiari I Malformation, AJNR Am J Neuroradiol 2010;31:1837-41.

THE ASEAN JOURNAL OF RADIOLOGY 2012: 18(1): 41-56 41

Original Article

Infected Aneurysms in Thai Patients: Computed Tomography Findings

Krisdee Prabhasavat, MD.
Chomsiri Segsarnviriya, MD.

Department of Radiology, Faculty of Medicine Siriraj Hospital, Mahidol University, Bangkok, Thailand

Abstract

Objectives: To determine the CT characteristics of infected aortic and visceral aneurysms and evaluate the difference between Salmonella and non-Salmonella infections by radiography.

Materials and Methods: Records of patients with surgical and/or pathological/microbiologic proof of infected aortic aneurysm collected over a 5-year period were reviewed. Computed tomography (CT), demographics and clinical data were studied. Twenty-eight aneurysms were found in 24 patients including 18 men and 6 women between the age of 35-78 years (mean = 63.29 years). The size, shape and location of aneurysm, aortic wall calcification, gas, and periaortic findings were evaluated.

Results: Aneurysms were located in the thoracoabdominal aorta (n=1; 4.2%), juxtarenal aorta (n=7; 29.2%), infrarenal aorta (n=13; 54.2%), superior mesenteric artery (n=1; 4.2%), and Iliac arteries (n=2; 8.3%). One patient had 2 infected aortic aneurysms and one patient had 4 infected aortic aneurysms. All 28 aneurysms were saccular with a mean diameter of 4.2 ± 2.4 cm (range, 0.6-10.4 cm). Paraaortic stranding, and/or fluid retention was present in 28 aneurysms (100%), paraaortic soft tissue mass in 21 aneurysms (75%), enhancing irregular wall thickening in 19 aneurysms (67.9%), disruption of calcification in the aortic wall in 13 aneurysms (46.4%), and perianeurysmal gas in 5 aneurysms (20.8%). Other findings included ruptured/ concealed ruptured aneurysm (n=9, 32.1%), adjacent vertebral body erosion/osteomyelitis (n=5, 20.8%), renal abscess (n=1, 4.8%) and psoas abscess (n=3, 14.3%).

Conclusion: Saccular aneurysms especially those with adjacent stranding,/fluid, and mass were highly suspicious of infection. Perianeurysmal gas and patients with relatively older age were found more common in salmonella infection than those with non-salmonella infection. Whereas, multiple aneurysms were more common in non-salmonella infection.

Keywords: infected aneurysms, mycotic aneurysms, computed tomography

Introduction

Infected aneurysm (or mycotic aneurysm) was first described by Osler in 1885. It is defined as an infectious break in the wall of an artery with the formation of blind, saccular outpouching that is contiguous with the arterial lumen. It is currently estimated that 0.7% to 2.6% of all aortic aneurysms are complicated by infection[3]. In addition to being a rare occurrence, it can be fetal if not diagnosed and treated early. Patients commonly present nonspecific symptoms, and the diagnosis is usually delayed until aneurysm has ruptured or until fulminant sepsis. Infected aneurysms are prone to rupture, with reported rupture rates of 53% to 75%. Prompt recognition and early detection are important for the timely treatment with antibiotics and surgical intervention. Still, the reported clinical experiences are limited to a few small series and case reports.

Staphylococcus aureus and *Streptococcus spp.* are the most common causative pathogens associated with infected aneurysm in Western countries[5], whereas non-typhoidal *Salmonella spp.* and *S. aureus* are more commonly responsible for cases that occur in East and Southeast Asian countries[3]. *Burkholderia pseudomallei* causing infective endarteritis in areas in which melioidosis is endemic has been documented in Northeast Thailand[4].

Computed tomography (CT) is widely available and routinely accessible to all patients with aortic aneurysms as it is noninvasive and safe with few contraindications. This method is useful for patients who cannot undergo magnetic resonance imaging (MRI). Multislice CT scans can be displayed as axial, multiplanar reconstructed, reformatted, or surface-rendered images. Furthermore, CT angiography is also possible.

The purpose of this study is to determine the radiographic characteristics of infected aneurysms of aorta and its branches obtained with CT scan or CT angiography and assess whether radiographic findings of Salmonella infection are different from non-Salmonella infection.

Material and Methods

Patients

This retrospective study was conducted at Siriraj hospital (Bangkok Thailand). The medical records of patients who received a diagnosis of infected (mycotic) aneurysm of aorta and its branches from January 2005 through December 2011 were reviewed.

Patients were enrolled in the study if they received a diagnosis of infected aneurysm, which was defined by the presence of the followings: (a) clinical evidence of infection (fever and/or leukocytosis), (b) bacteremia with radiographic findings that were compatible with infected aneurysm, (c) intraoperative findings suggestive of infected aneurysm, such as inflammation or pus collection around the aneurysm, or (d) pathological evidence of infected aneurysm or septic arteritis from the resected aneurysm, such as acute or chronic inflammation, acute suppurative inflammation, abscess formation, and/or bacterial clumps from the excised aneurysm.

We excluded patients with iatrogenic or traumatic aneurysms.

Record and Image Review

Demographics, clinical characteristics, surgical, microbiological and pathological findings were collected from the patient records by one resident. CT studies were reviewed by a vascular radiologist

with 27 years of experience and a senior resident in radiology.

The patients in our study included 18 men and 6 women between the ages of 35 and 78 years (mean = 63.29 years). The demographic information of patients: age, sex, underlying diseases, clinical features, operative findings, causative organisms, site of vascular involvement, and complications was recorded. Computed tomographic (CT) scans were performed by Definition; Siemens and Light Speed VCT; GE Medical Systems. Twenty-four CT studies (all patients underwent CT once) were available for review. In all 24 patients, CT examinations were performed before and after the administration of intravenous contrast material, with a section thickness of 1.25 to 5 mm. We evaluated CT scans for the location, shape (saccular or fusiform), size and number of the aneurysms. Additionally, we examined images for additional findings including adjacent soft tissue masses, stranding/fluid, enhancing irregular wall thickening, gas, calcification in the adjacent or involved aortic wall and its complications such as bony erosion/ osteomyelitis, abscess and ruptured aneurysms.

The microbiological findings of infected aneurysms were correlated with the presence of gas, vertebral body erosion, abscess, ruptured aneurysm, multiplicity of aneurysms, paraaortic soft tissue masses, stranding, and fluid accumulation observed on CT scans.

A comparison of these characteristics between patients with infected aneurysm caused by *Salmonella* and patients with infected aneurysm caused by other pathogens was performed to evaluate clinical and radiolographic differences between groups.

Data analysis was performed using SPSS software, version 17 (SPSS). Comparison was performed using Fisher's exact test, as appropriate. Two-tailed tests of significance were used to assess statistical significance at $p < 0.05$.

Result

During the 7-year study period, 30 cases were registered as mycotic aneurysm of aorta and its branches. Of these, 24 patients had medical records that were available for review.

Demographics

The majority of the patients were male (19 cases; 79%) and elderly (mean age, 63.29 years). Nineteen patients (79.1%) had preexisting diseases, of which the two most common were hypertension (13 patients; 54.1%), and diabetes mellitus (9 patients; 37.5%). The remaining preexisting diseases included gout, cerebrovascular disease, ischemic heart disease, chronic obstructive pulmonary disease, and SLE.

Clinical Characteristics

Most of the patients presented with localized pain at the site of the aneurysm (abdominal and/or back pain) (18 cases; 75.5%). Fever (11 cases; 45.8%) and palpable, pulsatile mass (3 cases; 12.5%) were common clinical features. (Fig.1)

Demographics, clinical characteristics, microbiological and pathologic findings in 24 patients with infected aneurysm are shown in Table 1.

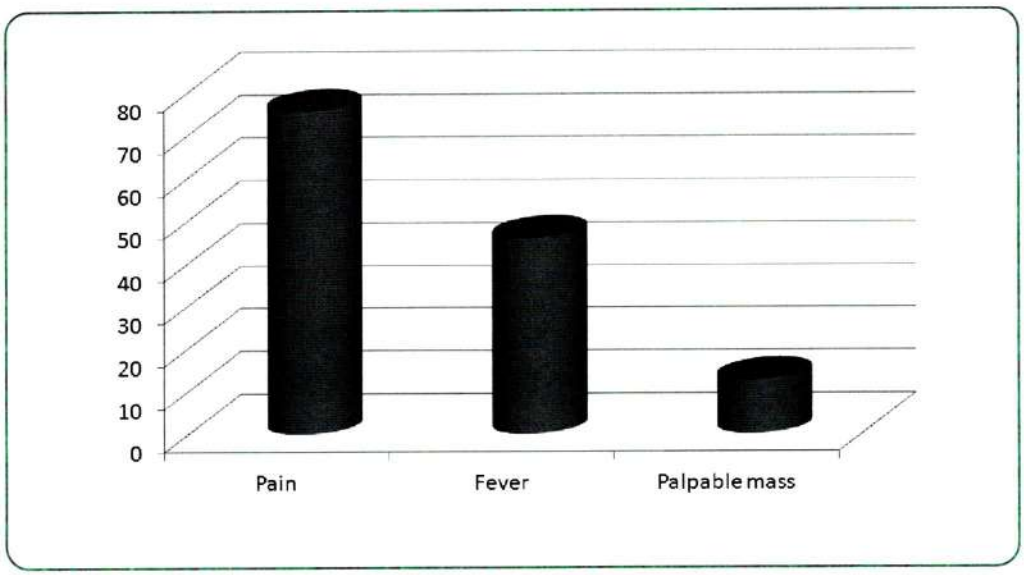

CT Scan Findings

The abdominal aorta was involved in 21 cases (87.5%); infrarenal aorta (13 cases; 54.2%), juxtarenal aorta (7 cases; 29.2%), and thoracoabdominal aorta (1 case; 4.2%). The minority of cases involved common/ external iliac arteries (2 cases; 8.3%), and superior mesenteric artery (SMA) (1 case; 4.2%).

We found multiple aneurysms in 2 patients: one patient had 4 infrarenal aneurysms (Figure 1) and the another one had 2 infrarenal aneurysms.

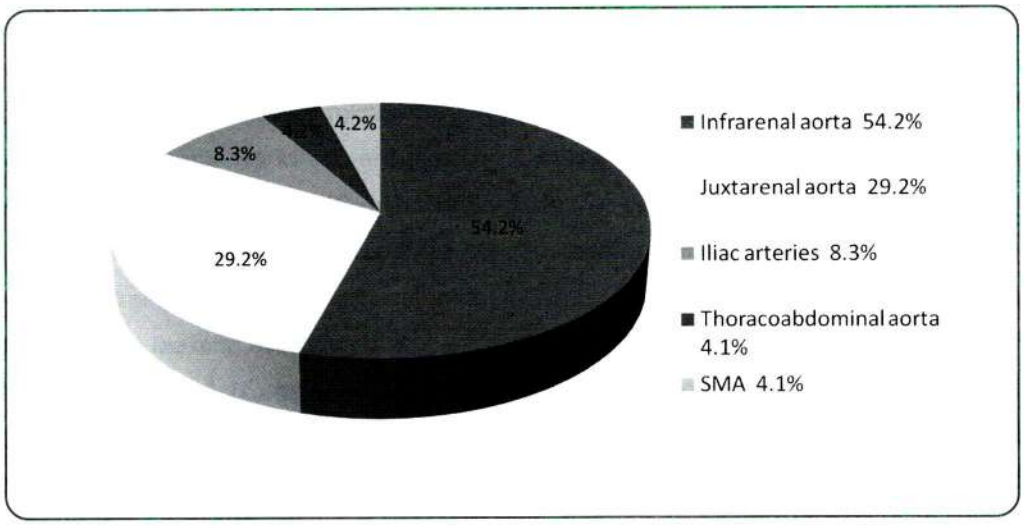

Table 1 Demographics, clinical characteristics, microbiological and pathologic findings in 24 patients with infected aneurysm

Age/sex	Clinical presentation	Aneurysm location	Underlying disease/ Predisposing factor	Primary source	Microbiology and pathology
M/70	Fever	Infrarenal aorta	HT, renal insufficiency, old CVA	UTI	Blood: *Salmonella spp.*
M/69	Fever	Infrarenal aorta	HT, History of aneurysmorrhaphy 1 year ago	Septic arthritis	Left knee effusion, blood: *Burkholderia pseudomallei*
M/62	Acute fever, abdominal distension, left hip pain	Left CIA	HT, DM, mild MR	-	Blood: negative (aneurysm wall: chronic inflammatory cells)
M/70	Acute fever	Juxtarenal aorta, right CIA	HT, DM	-	Blood: *Salmonella* group D (organize thrombus, dissecting aneurysm)
M/73	Abdominal pain, palpable mass	Juxtarenal aorta, renal pedicle involvement	DM	-	Blood: *Salmonella* group C1
M/67	Acute fever, abdominal pain	Infrarenal aorta	HT, CAD	-	Blood: negative, Melioid titer 1: 80
M/68	Abdominal pain	Infrarenal aorta, both CIA	HT	-	Thrombus, pus: *Streptococcus agalactiae*
M/59	Abdominal pain	Juxtarenal aorta, both CIA	HT, DM	-	Pus: *Shewanella spp.* (Thrombus: acute inflammation, necrotic debris)
F/73	Abdominal pain	Thoracoabdominal aorta above celiac trunk	-	-	H/C: *Streptococcus agalactiae*
M/78	Chronic fever	Infrarenal aorta	HT, DM, CAD, old CVA	-	Wall aorta, blood: *Salmonella* group C1
M/55	Acute fever, back pain	Juxtarenal aorta	HT	-	Blood: *Staphylococcus hemolyticus*
M/35	Palpable mass	Right EIA,CFA	Thalassemia trait	Chronic wound at right groin	Hematoma at aneurysm wall: *Pythium insidiosum* (active arteritis of femoral a, chronic arteritis obliterans of ATA,PTA, peroneal a., infected thrombus, fungal hyphae)

Table 1 Demographics, clinical characteristics, microbiological and pathologic findings in 24 patients with infected aneurysm *(cont.)*

Age/sex	Clinical presentation	Aneurysm location	Underlying disease/ Predisposing factor	Primary source	Microbiology and pathology
M/70	Chronic abdominal pain, acute fever	Infrarenal aorta	DLP, gout	-	Blood: negative, melioid titer<1:160
F/50	Abdominal pain, chronic fever	Infrarenal aorta	HT, erythema nodosum	-	Blood: negative (aortic wall: acute necrotizing inflammation of aortic wall)
M/57	Chronic abdominal pain	Infrarenal aorta, left CIA	DM, HT, COPD	-	Thrombus at aortic wall: *Burkholderia pseudomallei* (Blood clot: chronic, acute inflammation, aortic wall: chronic inflammation, necrosis)
M/45	Chronic abdominal pain	Infrarenal aorta	DM, TB	-	Wall of aneurysm: *Burkholderia pseudomallei*
M/61	Leg pain	Juxtarenal aorta	DM, HT, DLP, CAD, gout	-	Blood: negative (focal necrosis of wall, acute suppurative inflammation)
F/61	Abdominal pain	Juxtarenal aorta	DM, HT, epidermolysis bullosa acquiritica on prednisolone, cyclophosphamide	-	Blood: *Salmonella* group D
M/69	Acute fever	Infrarenal aorta	-	-	Pus, L4: *Salmonella* group D (aorta: focal necrosis, acute suppurative inflammation, L4: chronic osteomyelitis)
M/78	Abdominal pain, fever, palpable mass	Juxtarenal aorta, Left CIA	-		Blood clot G/S: gram positive cocci in pair (aortic wall: focal necrosis, acute inflammation)
F/58	Chronic abdominal pain	Infrarenal aorta	SLE, CAD S/P PCI, chronic AF	Septicemia	Blood, aortic wall: *Salmonella* group D
F/51	Abdominal pain, chronic anorexia	Superior mesenteric artery	HT	-	Blood: *Streptococcus alpha hemolyticus* (Focal acute inflammation)
M/75	Abdominal pain, chronic fever	Infrarenal aorta	Gout, BPH	-	Blood: *Salmonella* group C2 (blood clot: mixed many RBC, some WBC)
M/65	Chronic left hip pain, fever	Infrarenal aorta	-	-	Blood: *Salmonella* group D

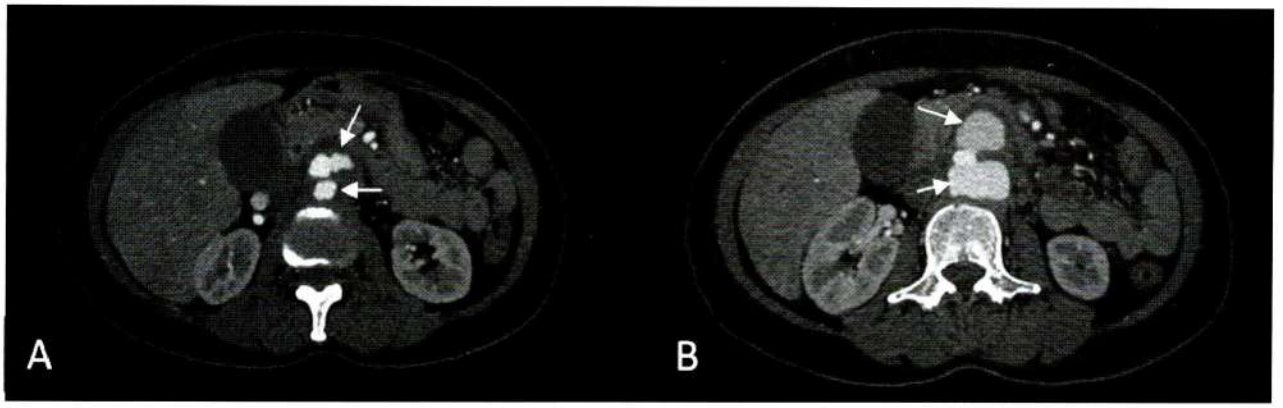

Fig.1 A 50-year-old female with non-*Salmonella* infected aneurysm presented with intermittent fever, radiating pain to the back and pulsatile mass at abdomen. A. and B. Multiple irregular saccular dilatation (arrows) with surrounding fat stranding and soft tissue thickening of infrarenal abdominal aorta

Maximal diameters were greater than 10 cm in 1 aneurysm (3.6%), 5 to 10 cm in 9 aneurysms (32.1%), and less than 5 cm in 18 aneurysms (64.3%). The mean average diameter of the infected aneurysms were 4.2 ± 2.4 cm. (range, 0.6 -10.4 cm.).

Aneurysm shape was saccular in all 28 aneurysms and no aneurysm was with fusiform shape.

Paraaortic stranding, and/or fluid retention was presented in 28 aneurysms (100%), paraaortic soft tissue mass in 21 aneurysms (75%), irregular wall thickening in 19 aneurysms (67.9%), disruption of calcification in the aortic wall in 13 aneurysms (46.4%), and perianeurysmal gas in 5 aneurysms (20.8%) (Figure 2).

In addition, we found groups of reactive small intraabdominal lymph nodes around the infected aneurysm in 15 cases (62.5%). Twelve cases (50%) had evidence of associated atherosclerotic change of the aorta.

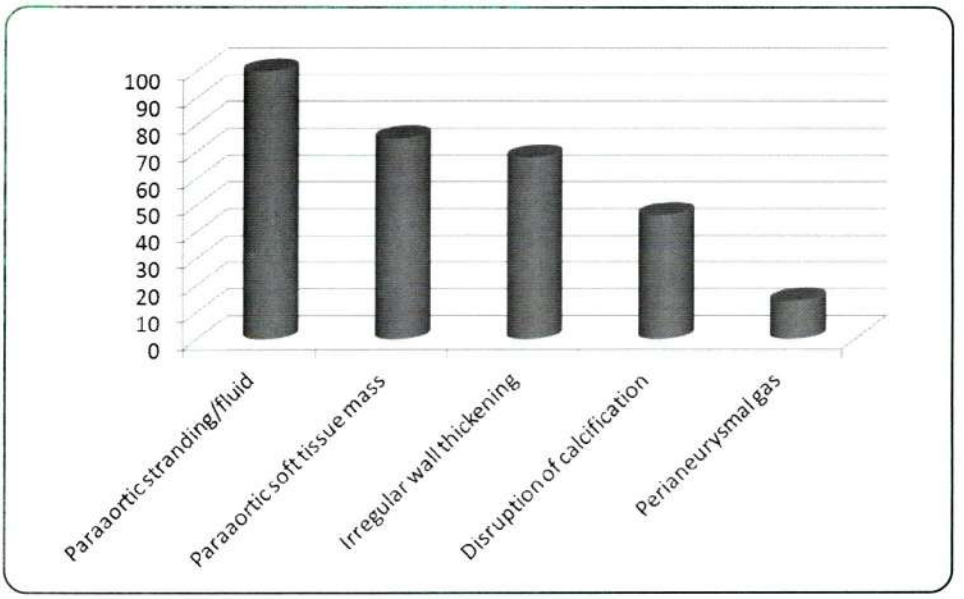

Complications related to infected aneurysms

The majority of infected aneurysms in this study were located at the abdominal aorta. Their complications were identified on CT scan in 10 out of 24 cases. These included rupture/concealed ruptured in 9 cases (37.5%) (Figure 3), adjacent vertebral body erosion/ osteomyelitis in 5 cases (20.8%) (Figure 4), secondary ureteral involvement in the inflammatory process or compression by hematoma with resultant hydronephrosis (Figure 5) in 2 cases (8.3 %), psoas abscess (Figure 6) in 3 cases (12.5%), and renal abscess in 1 case (4.2%). In our study, there was no coexistent aortic dissection, kidney infarct and aortoenteric fistula that were found in the prior literature[1-3].

Isolated inflammatory iliac artery aneurysms were found in 2 cases with negative culture and Pythium insidiosum, whereas isolated inflammatory superior mesenteric artery aneurysm (Figure 7) was found in 1 case with *Streptococcal* infection. In a patient with Pythiosis, we found a severe occlusion of distal arteries which was caused by invasion of the organism, resulting in gangrene (4.2%) (Figure 8). Therefore, the patient underwent amputation of the affected extremities and the pathology showed acute arteritis of the aneurysm with chronic arteritis obiterans of the distal arteries.

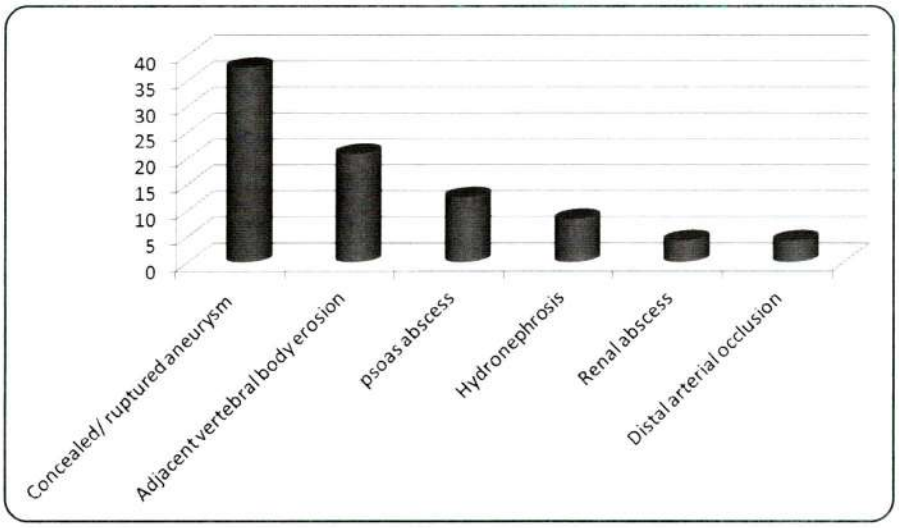

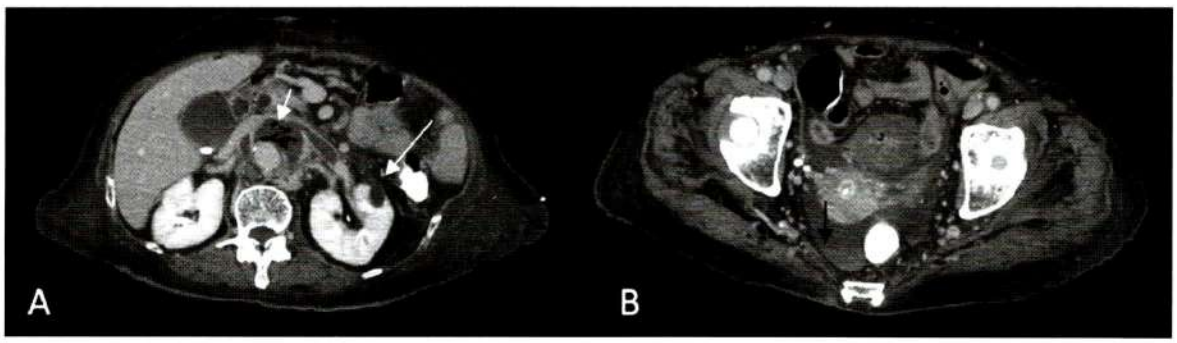

Fig.2 A 73-year-old woman with Salmonella infected aneurysm presented abdominal pain and palpable mass. A. Saccular aneurysm at juxtarenal aorta surrounding by enhancing periaortic hypodensity rim with large amount of periaortic gas (short white arrow). B. Hemoperitoneum (black arrow) All these finding are consistent with ruptured infected aortic aneurysm with periaortic and left renal abscess formation (long white arrow).

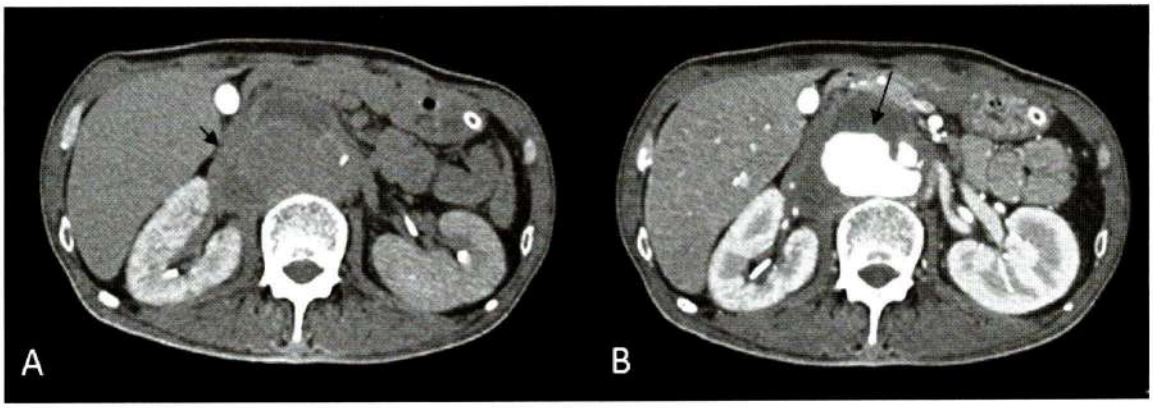

Fig.3 A 59 year old male with non-*Salmonella* concealed ruptured infected aneurysm (*Shewanella spp.*) presented with abdominal pain. A. Crescents shaped hyperdensity intramural thrombus in precontrast phase (short arrow). B. Diffuse periaortic soft tissue thickening and stranding surround the aneurysm (long arroow).

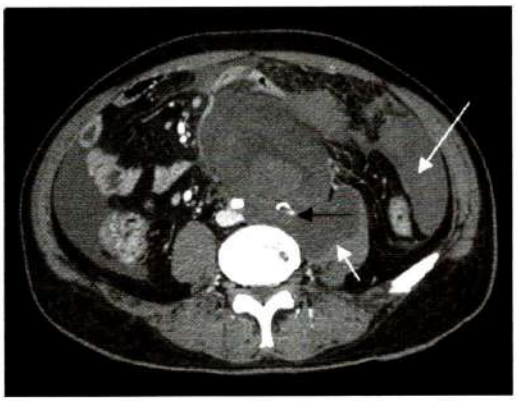

Fig.4 A 57-year-old male with ruptured Melioidosis infected aneurysm presented with acute alteration of consciousness and hypotension. There is a large irregular mixed hypo-hyperdensity lesions with peripheral enhancement surrounding infrarenal abdominal aorta. Disrupted wall of left common iliac artery associated markedly obliterated its lumen (black arrow). This hematoma at left iliopsoas muscle (arrow) and hemoperitoneum (long arrow) are visualized.

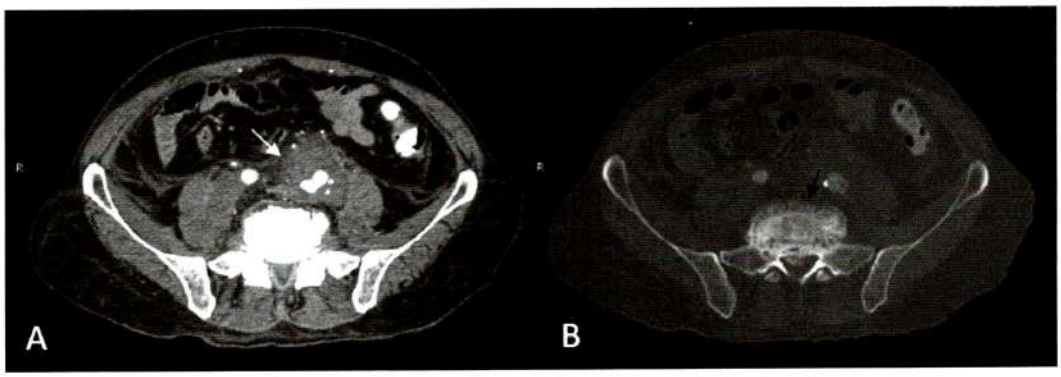

Fig.5 A 62-year-old man with culture-negative infected aneurysm presented with left lower abdominal pain with fever. A. An outpouching of contrast medium at left common iliac artery surrounding with irregular thickened soft tissue and perilesional stranding (white arrow). B. Minimal bony erosion at L5 and S1 vertebral body (balck arrow).

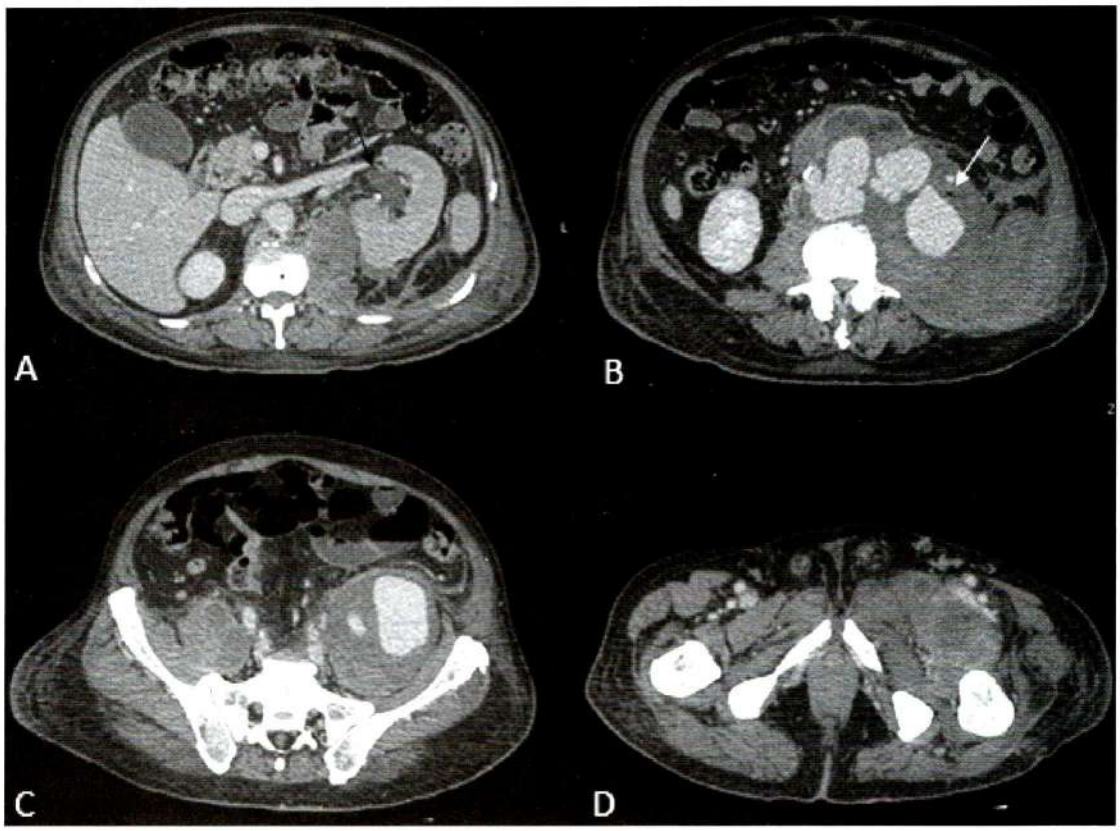

Fig.6 A 65-year-old man with ruptured *Salmonella* infected aneurysm presented with fever with chronic left hip pain. B. Saccular aneurysm with enhancing periaortic soft tissue thickening. B., C., D. Large left retroperitoneal hematoma with internal air bubbles (white arrow) extending along bilateral psoas, iliopsoas, and muscles of left upper thigh, compatible with infected hematoma. A. The aneurysm and hematoma have pressure effect and cause left kidney anterolaterally with abrupt narrowing at left proximal ureter, causing mild left hydronephrosis (black arrow).

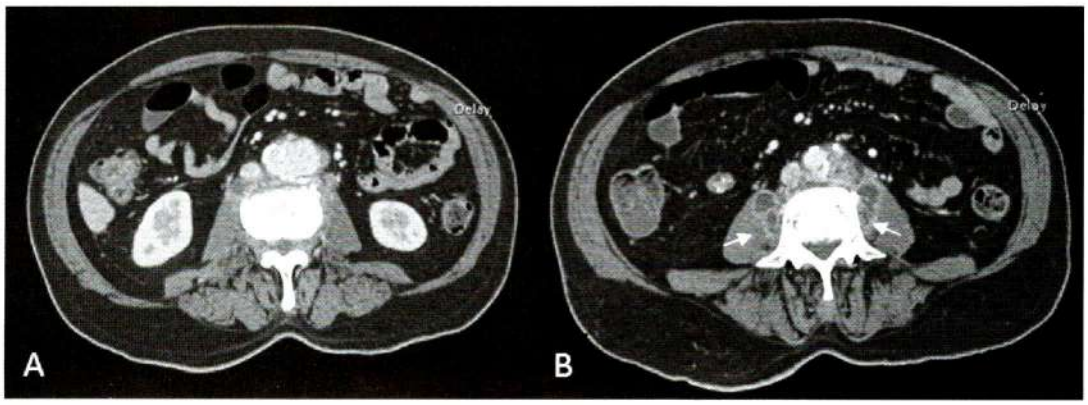

Fig.7 A 69-year-old man with *Salmonella* infected aneurysm presented with acute fever. A. An irregular shape saccular aneurysm at left side of abdominal aorta with soft tissue thickening. B. Multiple rim enhancing hypodensity lesions in both psoas muscles, compatible with bilateral multiple psoas abscesses (arrow).

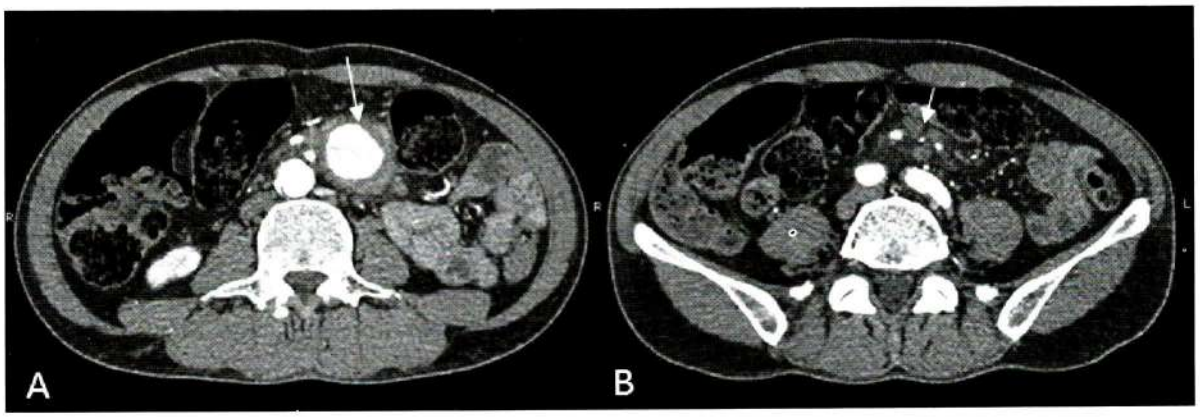

Fig 8 A 51-year-old man with non-*Salmonella* infected aneurysm (*Streptococcus* spp.) presented with abdominal pain. A. A saccular outpounching lesion at intestinal branch of superior mesenteric artery with soft tissue thickening and fat stranding (long arrow) B. Adjacent multiple lymphadenopathies are pathological proven of reactive lymph nodes (short arrow). All of these findings are suggestive of mycotic aneurysm of SMA.

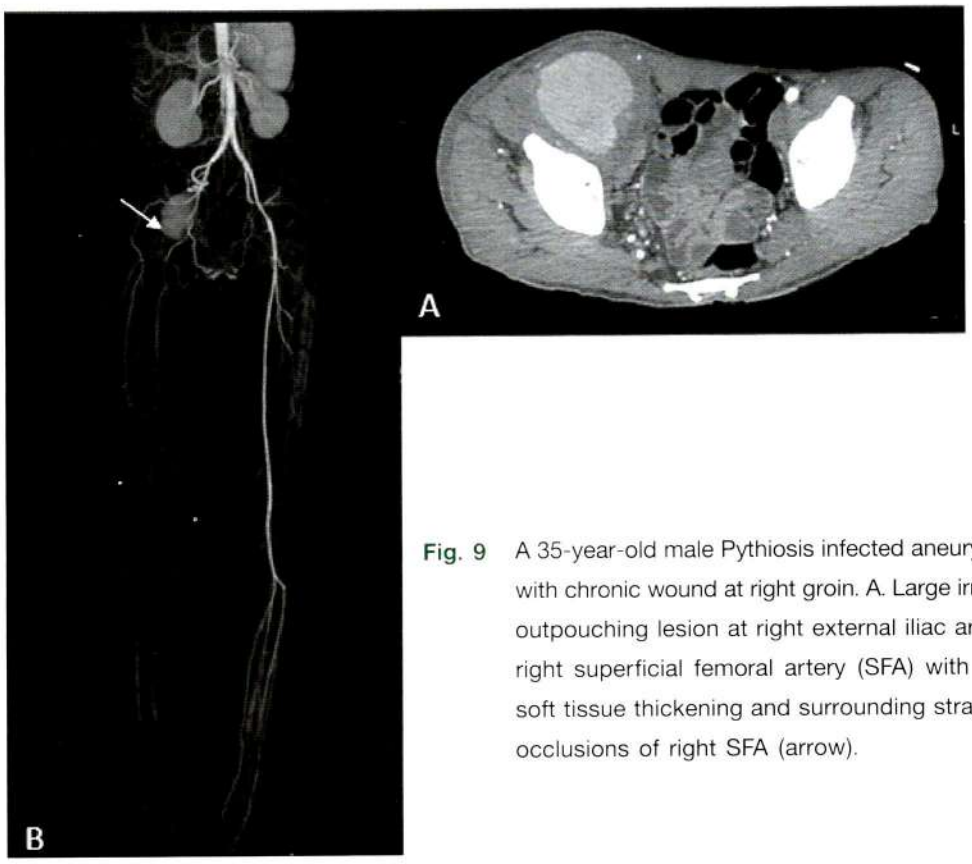

Fig. 9 A 35-year-old male Pythiosis infected aneurysm presented with chronic wound at right groin. A. Large irregular shaped outpouching lesion at right external iliac artery (EIA) and right superficial femoral artery (SFA) with enhancement soft tissue thickening and surrounding stranding. B. Total occlusions of right SFA (arrow).

Pathogens

Eighteen cases (75%) were culture-proven infected aneurysms (from aneurysm or blood). The most common etiological pathogens were non-typhoidal *Salmonella spp.* (9 cases; 37.5%) and *Streptococcus spp.* (3 cases; 12.5%), Burkholderia pseudomallei (3 cases; 12.5%). *Staphylococcus spp.*, *Shewanella spp.*, and *Pythium insidiosum* were found once each.

Only 16 aneurysms were excised. These pathogens were isolated from blood (16 cases; 66.7%) and excised aneurysms (11 cases; 45.8%). The remaining isolates of the pathogens were from samples obtained from intraabdominal (psoas and renal) abscesses (4 cases; 16.7%) and another disseminated site of infection such as joint effusion (1 cases; 4.2%).

The rest of the 6 cases (25%) were culture-negative. Therefore, the diagnosis of infected aneurysm was convincing by surgical and pathological findings.

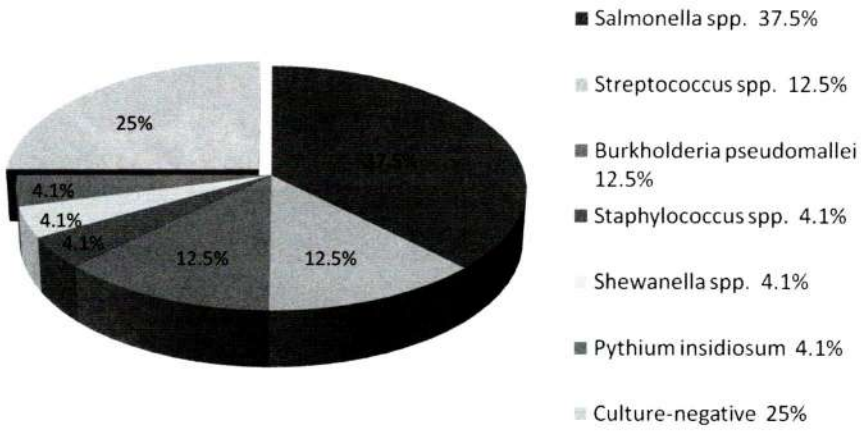

Table 2 Correlation of Infected Aortic Aneurysms causing by various pathogens with Imaging Findings

	Microbiologic Finding						
Imaging Characteristics	***Salmonella*** **(n=9pt)**	***Staphylococcus*** **(n=1pt)**	***Burkholderia*** **(n=3pt)**	***Streptococcus*** **(n=4an,3pt)**	***Pythium*** **(n=1pt)**	***Shewanella*** **(n=1pt)**	**Negative (n=9an,6pt)**
Periaortic soft-tissue mass (n=20pt)	8	1	2	3 (4an)	1	1	3 (3an)
Periaortic stranding, and/or fluid (n=28pt)	9	1	3	4	1	1	9
Multiple aneurysms (n=2pt)	0	0	0	1 (2an)	0	0	1 (4an)
Gas (n=5pt)	5	0	0	0	0	0	0
Bony erosion (n=5pt)	2	1	0	1	0	0	1
Abscess (n=4pt)	3	0	1	0	0	0	0
Rupture (n=9pt)	3	0	1	1	0	1	3

an= aneurysms, pt= patients

Salmonella versus non-Salmonella

Of the 18 cases of culture-proven infected aneurysm, 9 were associated with *Salmonella spp.*, and 9 were associated with other pathogens. Six cases of infected aneurysms were culture-negative. There were no statistically significant difference with respect to sex, underlying diseases, clinical presentations, site of aneurysm or positive-culture sample site between patients with infected aneurysm caused by *Salmonella* and patients with infected aneurysm caused by non-*Salmonella*.

We found that *Salmonella* infected aneurysm were significantly related with older age (mean age 68.8 ± 6.5 year in *Salmonella* vs. 60.0 ± 11.5 year in non-*Salmonella*; $p = 0.049$) and perianeurysmal gas was significantly more common among patients with *Salmonella* infected aneurysm (56% in *Salmonella* vs. 0% in non-*Salmonella* group) ($p = 0.003$).

Table 3 Comparison between causes of mycotic aneurysms due to Salmonella and non-Salmonella

Variable	Patients with mycotic aneurysm		P-value
	Salmonella **(n=9 pt)**	**non-*Salmonella*** **(n=15 pt)**	
Age, mean years ± SD	68.8 ± 6.5	60.0 ± 11.5	0.049
Male sex	7/9 (78%)	12/15 (80%)	1
Underlying disease			
Any	7/9 (78%)	12/15 (80%)	1
DM	4/9 (44%)	5/15 (33%)	0.678
HT	4/9 (44%)	9/15 (60%)	0.675
Clinical feature			
Localized pain	6/9 (77%)	12/15 (80%)	0.635
Palpable mass	1/9 (11%)	2/15 (13%)	1
Fever	5/9 (56%)	6/15 (40%)	0.675
Site of aneurysm			
Abdominal aorta	9/9 (100%)	12/15 (80%)	0.266
other site	0/9 (0%)	3/15 (20%)	
Site of positive culture sample			
Aneurysm	2/4 (50%)	9/12 (75%)	0.547
blood	6/9 (67%)	10/15 (67%)	
Radiological findings			
Infra/juxtarenal aortic aneurysm	9/9 (100%)	11/15 (73%)	0.259
Periaortic soft-tissue mass	8/9 (89%)	12/15 (80%)	1
Periaortic stranding and/or fluid	9/9 (100%)	15/15 (100%)	1
Multiple aneurysms	0/9 (0%)	2/15 (13%)	< 0.001
Gas	5/9 (56%)	0/15 (0%)	0.003
Bony change	2/9 (22%)	3/15 (20%)	1
Abscess	3/9 (33%)	1/15 (7%)	0.130
Rupture	3/9 (33%)	6/15 (40%)	1

Pt= patients

Intraabdominal (renal or psoas) abscess was found more common in *Salmonella* group (33% in Salmonella vs 7% in non-*Salmonella* group), though, there is no statistically significant difference (p = 0.130).

Multiple aneurysms were significantly more common in non-*Salmonella* group (0% in Salmonella and 13% in non-*Salmonella* group, p <0.001).

Discussion

Because of an infected aortic aneurysm is not always aneurysmal by conventional criteria (more than 50% luminal diameter dilatation), therefore, we use the term infected aortic aneurysm to include any aortic dilatation of infectious origin, regardless of size and pathogens.

In practice, the infected aortic aneurysm is often not suspected during clinical evaluation because of non-specific symptoms and inconclusive laboratory data. If diagnosed, however, the common treatment usually consists of antibiotics and urgent surgical intervention. With the treatment, the overall mortality rate is 16-40%[9,10].

Our study shows that *Salmonella spp.* are the most common causative pathogen found in infected aneurysms of aorta and its branches accounting for up to one-third of all cases (37.5%). As with infected aneurysm due to non-typhoidal *Salmonella spp.*, the major pathogenesis of other bacterial aneurysm is most likely to be a complication of bacteremia caused by hematogenous seeding in elderly patients with preexisting atherosclerotic diseases such as DM, HT and 50% of patient had evidence of associated atherosclerotic change of the aorta. This often leads to the formation of infected aneurysm. The demographics and clinical features of *Salmonella* infected aneurysm are not significant different from those caused by other pathogens.

In our study, up to 66.7% of infected aneurysms result in bacteremia and it must be noted that the primary source of the bacteremia is often unknown. Negative blood cultures have been reported in up to 47% of cases[8] and may be caused by antibiotic pretreatment and anaerobic organisms.

The most common location of aneurysm was different between atherosclerotic aneurysm and infected aortic aneurysm as reported in the literatures with infrarenal aorta (85%-87%) in atherosclerotic aneurysm[11] and descending aorta (47.6%) in infected aneurysm[3]. In our study, the distribution of infected aortic aneurysms were similar to the more common location of atherosclerotic aneurysm. About 54% of infected aneurysms located in infrarenal aorta and multiple aneurysms were uncommon.

Cross-sectional imaging is valuable to demonstrate the characteristic adjacent findings such as paraaortic soft tissue stranding and/or fluid, mass, and enhancing irregular wall thickening. Helpful findings such as gas, disruption of calcification and adjacent vertebral body change were seen less commonly. In the early stage, subtle paraaortic inflammatory changes may be overlooked.

The complications are dependent upon the location of infected aneurysm, branch/ adjacent organ involvement, and progression of the disease. The more common complications in the literature were hydronephrosis and coexistent aortic dissection[2]. The most common complication in our study is ruptured/ concealed rupture aneurysm.

Ming et al[3] reported 21 cases of infected aortic aneurysm. Periaortic gas was found in 7 cases (33.3%) in various bacterial pathogens. However, our study results that perianeurysmal gas found only in *Salmonella* infection.

Relatively old age and perianeurysmal gas were significantly more common among patients with *Salmonella* mycotic aneurysm than the non-*Salmonella* group. Renal/ psoas abscess are more common in *Salmonella* infected aneurysms rather than non-*Salmonella* group, though this was not statistically significant. Prior studies found that *Salmonella* infected aneurysm has a high fatality rate. Antibiotics alone are not sufficient, and complete excision of the affected aorta is the key to curative treatment[7].

The infected aneurysms caused by *Pythium insidiosum* (Pythiosis) is associated with chronic arterial inflammation and occlusion by invasion of the organism, which can result in gangrene, aneurysm formation and resection of affected arteries or amputation of the affected extremities. The disease is not uncommon in Thailand and Southeast Asia and predisposing factors are thalassemia and agricultural occupation[6].

There are a few limitations associated with this study. Firstly, the reviewer knew the diagnosis of infected aneurysm before evaluation of images, so we directly attended to the specific involved organs and findings Secondly, we had no control case to calculate sensitivity and specificity. Thirdly, this was a retrospective study of patients from a single institution and fourthly, infected aortic aneurysm was uncommon diagnosis. Therefore, the number of cases was small. The statistical significance of some findings cannot be predicted with this small number. The evaluation of causative organisms was based on an aerobic culture, so we could not explore the role of anaerobic bacteria or other uncommon organisms under this condition.

Conclusion

Infected aneurysms of aorta are not uncommon but can be fatal if untreated. A high degree of clinical awareness followed by computed tomography allows early detection of infected aneurysm, adjacent organ involvement and its complications. The recognition of imaging findings associated with an infected aneurysm is critical for early diagnosis and adequate therapy. Saccular aneurysm with paraaortic stranding and/or fluid retention or mass constitutes the imaging findings that are highly suggestive of an infected aortic aneurysm. Perianeurysmal gas, disruption of calcification and adjacent vertebral change are other helpful features in the diagnosis of infected aortic aneurysm. In conclusion, *Salmonella* infected aneurysms might have a poorer prognosis than non-*Salmonella* group because of more common in perianeurysmal gas, abscess and relatively old age of the patients.

References

1. Macedo TA, Stanson AW, Oderich GS, et al. Infected aortic aneurysms: imaging findings. Radiology. 2004; 231:250-7.
2. Misako I, Sachio K, Satoshi I, et al. Sensitivity and Specificity of CT in the Diagnosis of Inflammatory Abdominal aortic aneurysms. Journal of computer assisted tomography. 2002;26(6):1006-12.
3. Ming PL, Shih CC, Reng HW. A comparison of computed tomography, magnetic resonance imaging, and digital subtraction angiography findings in the diagnosis of infected aortic aneurysm. Journal of computer assisted tomography. 2008;32:616-20.
4. Siriluck A, Ploenchan C, Churairat K. Mycotic aneurysm in northeast Thailand: The importance of Burkholderia pseudomallei as a causative pathogen. Clinical infectious diseases. 2008;47:1436-9.

5. Wai-Kit L, Peter JM, Andrew FL, et al. Infected (Mycotic) Aneurysms: Spectrum of imaging appearances and management. Radiographics. 2008;28:1853-68.
6. Theerapong K, Boonmee S, Roongnapa P, et al. Clinical and epidemiological analyses of human Pythiosis in Thailand. Clinical infectious diseases. 2006;43:569-76.
7. Azlina AB, CS Ngiu, Mohamad S, Petrick P. Salmonella related mycotic aneurysm with psoas and paraortic abscess treated conservatively. Annals academy of medicine. 2011;40:467-68
8. Bennett DE. Primary mycotic aneurysms of the aorta: report of case and review of the literature. Arch Surg. 1967;94:758-65.
9. Oderich GS, Panneton JM, Bower TC, et al. Infected aortic aneurysms: aggressive presentation, complicated early outcome, but durable results. J Vasc Surg. 2001;34: 900-8.
10. Castaneda-Zuniga WR, Nath PH, Zollikofer C, et al. Mycotic aneurysm of the aorta. Cardiovasc Intervent Radiol. 1980;3:144-9.
11. Coselli JS, LeMaire SA. Diseases of the thoracic aorta. In: Dean RH, Yao JST, Brewster DC, eds. Current diagnosis and treatment in vascular surgery. Norwalk, Conn: Appleton & Lange, 1995;118-32.

THE ASEAN JOURNAL OF RADIOLOGY 2012: 18(1): 57-71 57

Case Report

Post-Transplant Lymphoproliferative Disorder of the Brain Mimics Brain Abscess: Case Report and Review Literature.

Wiboon Suriyajakryuththana, MD.[1], Pat Suntarawipath Kwankaew, MD.[1], Noppadol Iarbcharoensub, MD.[2]

[1] Departments of Radiology and [2] Department of Pathology,

Faculty of Medicine Ramathibodi Hospital, Mahidol University, Thailand.

Abstract

Post-transplant lymphoproliferative disorder (PTLD) is a spectrum of hematological diseases arising in context of immunosuppression after organ transplantation. PTLD can involve any organ. We have studied two cases of polymorphic PTLD of the brain that developed in patient with relapsed acute lymphoblastic leukemia (ALL) following two times of bone marrow transplantation ongoing immunosuppressive therapy and end stage renal disease with renal transplantation. Additionally, case of PTLD in the brain was reviewed in 2004. The neoplasm showed large cell morphology and B-cell phenotype. In situ hybridization for Epstein-Barr virus (EBV) was positive. Complete remission was obtained after decreasing immunosuppressive therapy. The patient remained in remission at almost 2-years' follow up. This rare case increased our awareness of PTLD in the brain of patients following organ transplantation and immunosuppressive therapy.

Introduction

Post-transplant lymphoproliferative disorder (PTLD) is well-recognized complication after solid organ or bone marrow transplantation. As currently defined by the World Health Organization (WHO), post-transplant lymphoproliferative disorders (PTLDs) are lymphoid proliferations or lymphomas that develop in immunosuppressed recipients of solid organ or bone marrow allograft. They are best considered as a spectrum of pathologic patterns ranging from reactive Epstein-Barr virus (EBV)-driven lymphocytic/ plasmacytic hyperplasia to high-grade malignant lymphomas that can be EBV+ or EBV-. The vast majority is of the B-cell phenotype; rare T-cell PTLDs have been described. Patient outcome generally depends on the histological grading, organ sites involved, tumor burden, and response to therapy. PTLD may involve the lymph nodes or extranodal tissue at any site, including organ allograft.

The incidence of PTLDs in the transplantation population has been estimated at less than 2%, with slightly higher rates in the pediatric population. Patients undergoing heart-lung or liver-bowel transplantation are at highest risk (5%). Risk is lower following liver, cardiac, and bone marrow allograft (1%-2%) and is lowest after kidney transplantation (<1%).

The anatomic distribution of PTLDs varies with patient age and the type of immunosuppressive therapy. Childhood PTLDs often involve lymphoid tissues including lymph nodes and adenoids and arise in the abdomen (64%), thoracic cavity (50%), and head and neck (25%). PTLDs in adults tend to localize to the liver, lung, lymph nodes, and gastrointestinal tract. In most cases, the transplanted organ is involved. PTLDs that arise following azathioprine-based immunosuppressive therapies are more common in the allograft and also might involve the central nervous system (CNS); those that follow FK-506- or cyclosporine-based regimens most frequently involve lymph nodes and the gastrointestinal tract.

A series of 90 PTLD cases occurring in 4283 solid organ transplantations over a nine-year period revealed that two thirds of the patients presented with disease in a single site, and uncommon of the cases presented in the brain. Dr Frank Gaillard[1] on September 4, 2009 contributed Post transplant lymphoproliferative disorder (PTLD) that the time between transplant and development of PTLD is variable, ranging from one month to seven years, with most occurring within a year. As a general rule, patients who present late (more than one year) have more aggressive tumors with poorer prognosis. This report showed that radiographic features are similar to lymphoma in the setting of HIV infection. Necrosis and hemorrhage were more common than in run-of-the-mill primary CNS lymphoma.

Among CNS disorders after transplantation, PTLDs follow cerebrovascular disease and infection in frequency. CNS PTLDs were seen in 2% to 7% of brains in the largest autopsy series of posttransplant patients (which most likely overestimates the incidence of clinical disease). Partly owing to their rarity, the spectrum of pathologic features of CNS PTLDs has not been characterized fully, nor has their range of biologic behavior. Case reports and small series seem to indicate that CNS PTLDs are more aggressive as a group than PTLDs involving other organ systems. Recognizing CNS PTLDs and distinguishing them from other nontransplant primary CNS lymphomas is critical because therapeutic options and clinical outcomes can vary sub-

Introduction

Post-transplant lymphoproliferative disorder (PTLD) is well-recognized complication after solid organ or bone marrow transplantation. As currently defined by the World Health Organization (WHO), post-transplant lymphoproliferative disorders (PTLDs) are lymphoid proliferations or lymphomas that develop in immunosuppressed recipients of solid organ or bone marrow allograft. They are best considered as a spectrum of pathologic patterns ranging from reactive Epstein-Barr virus (EBV)-driven lymphocytic/ plasmacytic hyperplasia to high-grade malignant lymphomas that can be EBV+ or EBV-. The vast majority is of the B-cell phenotype; rare T-cell PTLDs have been described. Patient outcome generally depends on the histological grading, organ sites involved, tumor burden, and response to therapy. PTLD may involve the lymph nodes or extranodal tissue at any site, including organ allograft.

The incidence of PTLDs in the transplantation population has been estimated at less than 2%, with slightly higher rates in the pediatric population. Patients undergoing heart-lung or liver-bowel transplantation are at highest risk (5%). Risk is lower following liver, cardiac, and bone marrow allograft (1%-2%) and is lowest after kidney transplantation (<1%).

The anatomic distribution of PTLDs varies with patient age and the type of immunosuppressive therapy. Childhood PTLDs often involve lymphoid tissues including lymph nodes and adenoids and arise in the abdomen (64%), thoracic cavity (50%), and head and neck (25%). PTLDs in adults tend to localize to the liver, lung, lymph nodes, and gastrointestinal tract. In most cases, the transplanted organ is involved. PTLDs that arise following azathioprine-based immunosuppressive therapies are more common in the allograft and also might involve the central nervous system (CNS); those that follow FK-506- or cyclosporine-based regimens most frequently involve lymph nodes and the gastrointestinal tract.

A series of 90 PTLD cases occurring in 4283 solid organ transplantations over a nine-year period revealed that two thirds of the patients presented with disease in a single site, and uncommon of the cases presented in the brain. Dr Frank Gaillard[1] on September 4, 2009 contributed Post transplant lymphoproliferative disorder (PTLD) that the time between transplant and development of PTLD is variable, ranging from one month to seven years, with most occurring within a year. As a general rule, patients who present late (more than one year) have more aggressive tumors with poorer prognosis. This report showed that radiographic features are similar to lymphoma in the setting of HIV infection. Necrosis and hemorrhage were more common than in run-of-the-mill primary CNS lymphoma.

Among CNS disorders after transplantation, PTLDs follow cerebrovascular disease and infection in frequency. CNS PTLDs were seen in 2% to 7% of brains in the largest autopsy series of posttransplant patients (which most likely overestimates the incidence of clinical disease). Partly owing to their rarity, the spectrum of pathologic features of CNS PTLDs has not been characterized fully, nor has their range of biologic behavior. Case reports and small series seem to indicate that CNS PTLDs are more aggressive as a group than PTLDs involving other organ systems. Recognizing CNS PTLDs and distinguishing them from other nontransplant primary CNS lymphomas is critical because therapeutic options and clinical outcomes can vary sub-

stantially. The report was described the features of 12 primary CNS PTLDs with the aim of better characterizing their clinical, radiographic, and pathologic features and distinguishing them from other primary CNS lymphomas.

Here we report rare cases of polymorphic PTLD of the brain in patient after second bone marrow and renal transplantation with immunosuppressive therapy, which was improved by reduction of the immunosuppression. This review summarizes the current knowledge of EBV-PTLD and, as a result of international meetings on this topic, differential diagnostic point by imaging findings and provides recommendations for future area of study.

Case presentation

Case number one

A 13-year-old Thai female (Body weight = 27 kg, height = 144 cm) with history of second relapsed acute lymphoblastic leukemia (ALL) S/P second time for bone marrow transplantation, the last one performed on February 6, 2009. She also had chemotherapy, systemic fungal infection (hepatosplenic candidiasis and invasive pulmonary aspergillosis. At admission (from June 18, 2009 to August 5, 2009) she presented with fever, diarrhea, nausea, neutropenia and CMV reactivation for one day before admission. Vital signs showed low fever (38.3°C), respiratory rate was about 24/minute and pulse rate was 120 beats/minute. Skin showed hypopigmented and erythematous patch at face. On Neurological examination; she was no significant finding. CBC showed WBC=8,400 cells with PMN=41 (neutropenia), Hb=10.9, Hct=32.1, Platelet= 23,000. Stool examination showed WBC 5-10 cells per high field and RBC 10 cells per high field (infectious diarrhea, stool cultures & sensitivity showed *Salmonella*). Electrolyte showed Na=135, K=3.32, Cl=99, CO_2=25.7 (hypokalemia). 6 days after admission, she developed alteration of her consciousness level and complex-partial seizure. EEG showed normal study. Lumbar puncture performed on June 24, 2009 showed high protein and low glucose, cannot be excluded encephalitis. MRI of her brain performed on June 25, 2009 showed small ring enhancing lesion with associated mild perilesional edema at medial left temporal lobe. (Figure 1-5). She undergone operation on June 26, 2009, place-

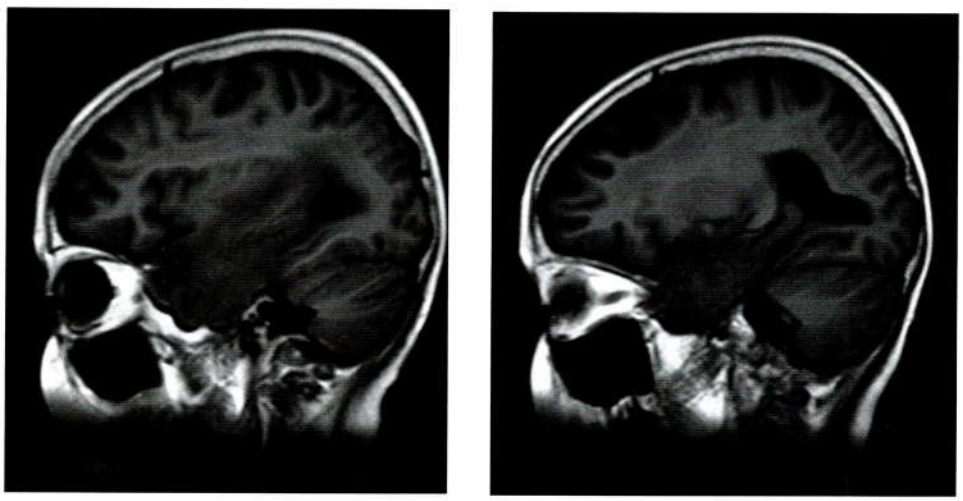

Fig.1 Sagittal T1W showed small well-defined mass with near uniform isointense-T1W wall and hypointense-T1W at central portion. Hypointensity in T1W signal surrounding this lesion could be associated perilesional edema.

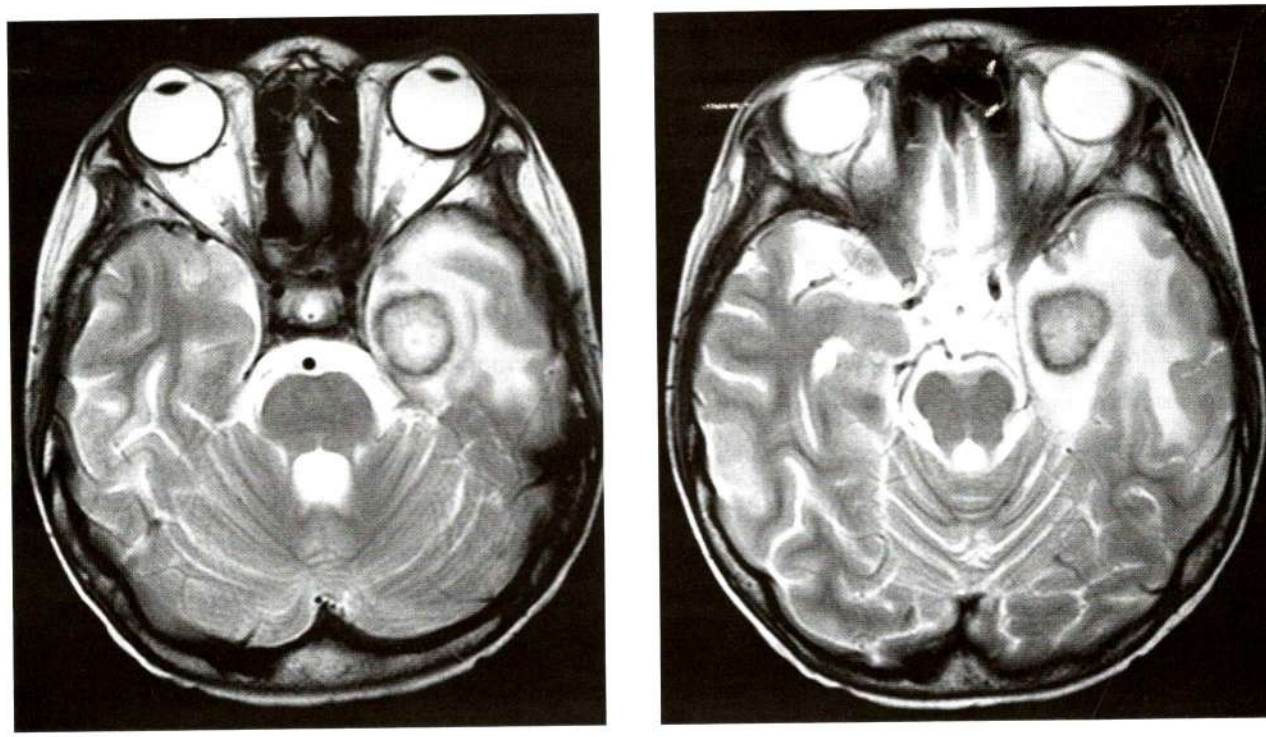

Fig.2 Axial T2W showed dark T2W signal wall with mild-hyperintense-T2W signal change in central portion. The lesion and an associated perilesional edema produce mass effect to the cortical sulci, sylvian fissure and obliteration of temporal horn of the left lateral ventricle.

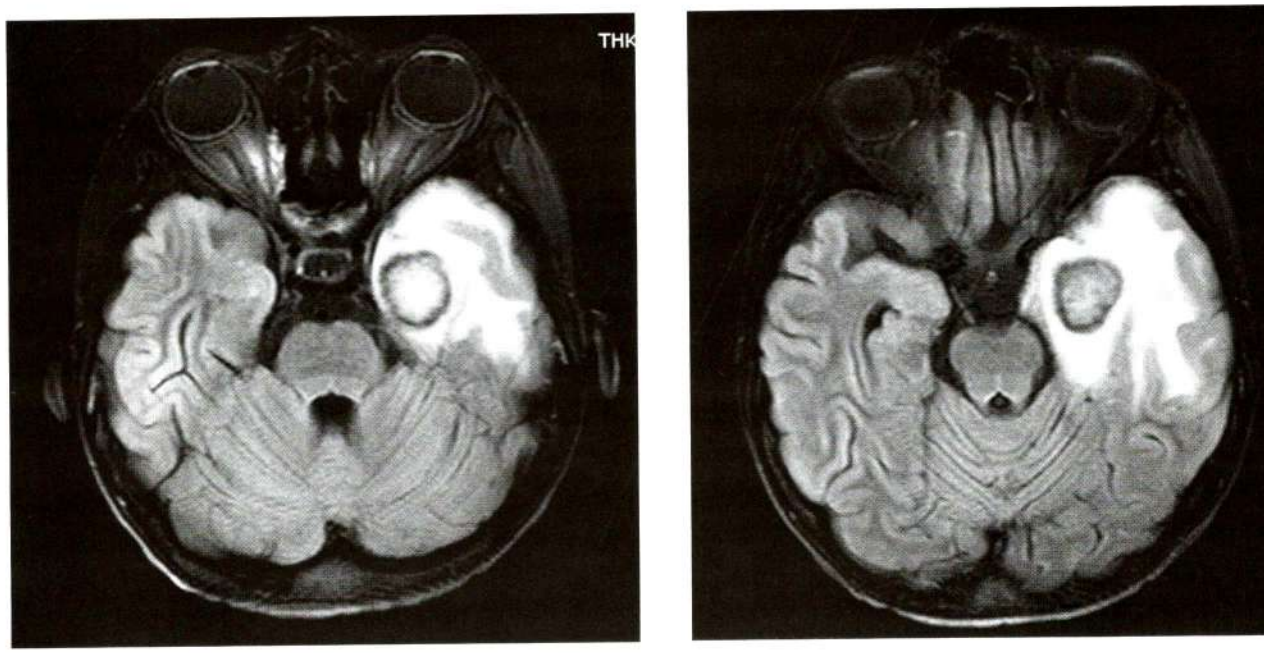

Fig.3 Axial FLAIR showed better demonstration of the signal intensity change as described in Figure 2

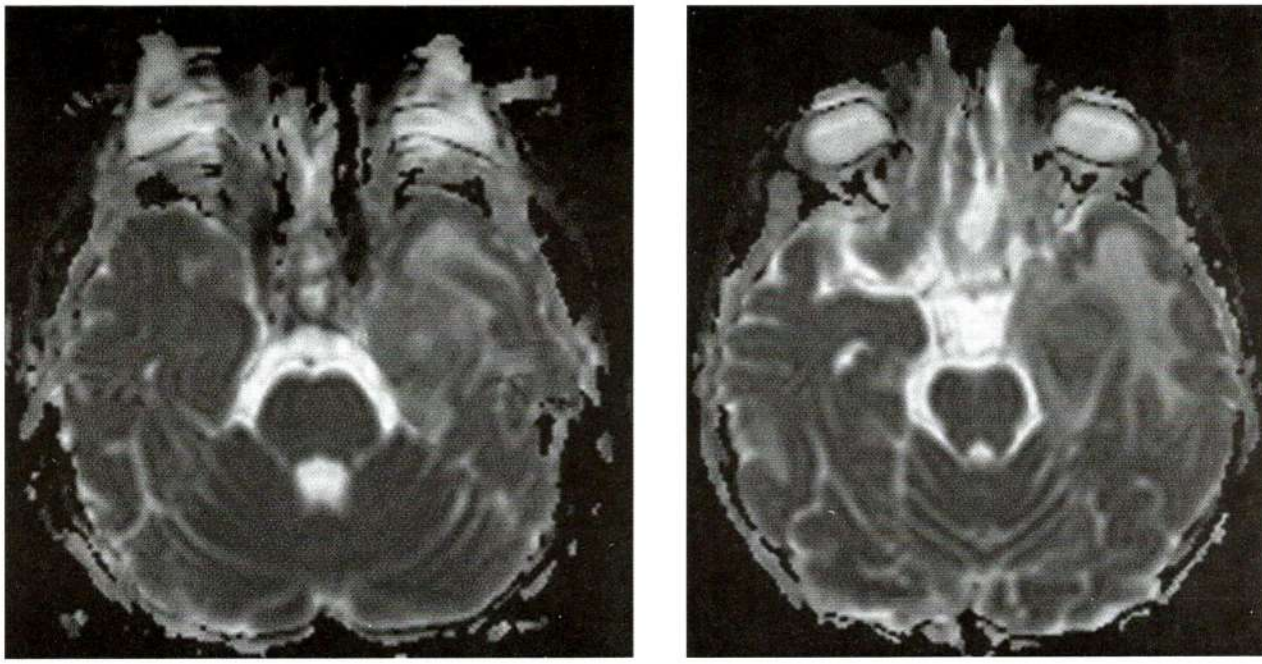

Fig.4 ADC mapping from DWI showed partial restricted diffusion at posterior wall and partly left anterolateral wall as well as some area in central portion.

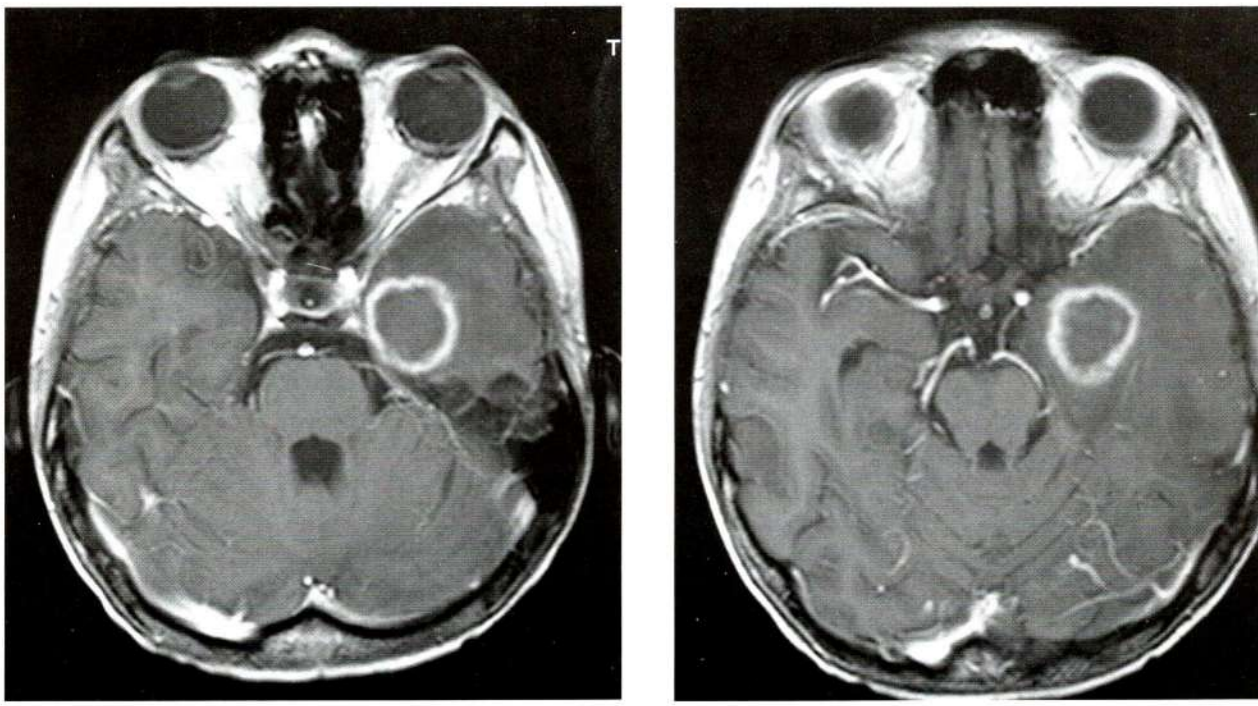

Fig.5 Axial T1W post-contrast showed complete, smooth near-uniform enhanced wall. The suspicious associated perilesional edema was not enhanced.

ment of the intracranial catheter via burr hole craniotomy with lesion biopsy under navigator. Pathologic report showed focal necrosis with focal polymorphous lymphoid cell infiltration including small lymphoid cells, immunoblasts and plasma cells, suggestive of polymorphic post-transplant lymphoproliferative disorder (PTLD). Echocardiography was performed on June 29, 2009 appeared normal. Bone marrow biopsy performed on June 19, 2009 showed marked hypo cellular marrow showing severely decreased trainer hematopoiesis. There is no residual lymphoblast.

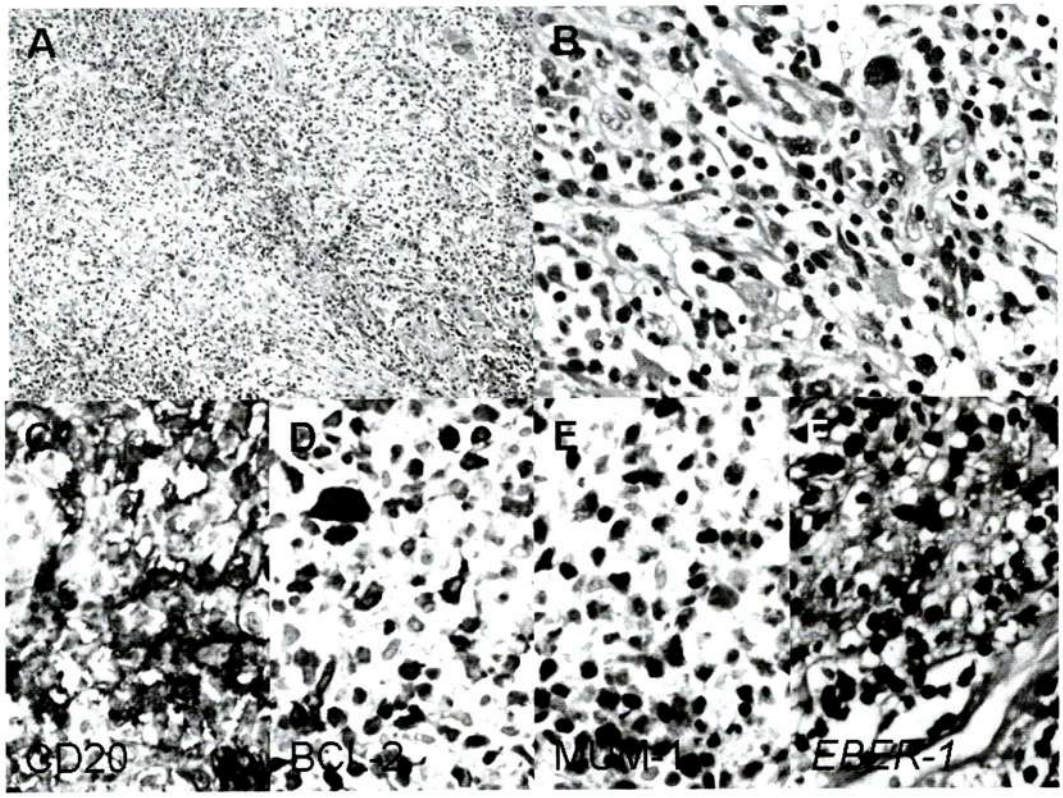

Fig.6 Histologic features of polymorphic post-transplant lymphoproliferative disorder. (A) Brain biopsy showing dense infiltration of polymorphic cells (H&E, x 100). (B) Mixed proliferation of immunoblasts, plasma cells and medium-sized lymphoid cells and large atypical lymphoid cell (H&E, x 400). Immunohistochemistry showing tumor cells are strongly positive for CD20 (C), BCL-2 (D), and MUM-1 (E) (x 400). (F) EBV in situ hybridization showing all the tumor cells are positive for EBER-1 (x 400).

The results of the immunohistochemical stains are

CD3 : negative in large lymphoid cells
CD 10 : negative in large lymphoid cells
CD 20 : Positive in large lymphoid cells
CD 30 : Positive in large lymphoid cells
CD138 : positive in large lymphoid cells
MUM-1 : positive for large lymphoid cells
Bcl-2 : positive in large lymphoid cells
Bcl-6 : positive 30% in large lymphoid cells

The EBV in situ hybridization (EBER) is positive in large lymphoid cells.

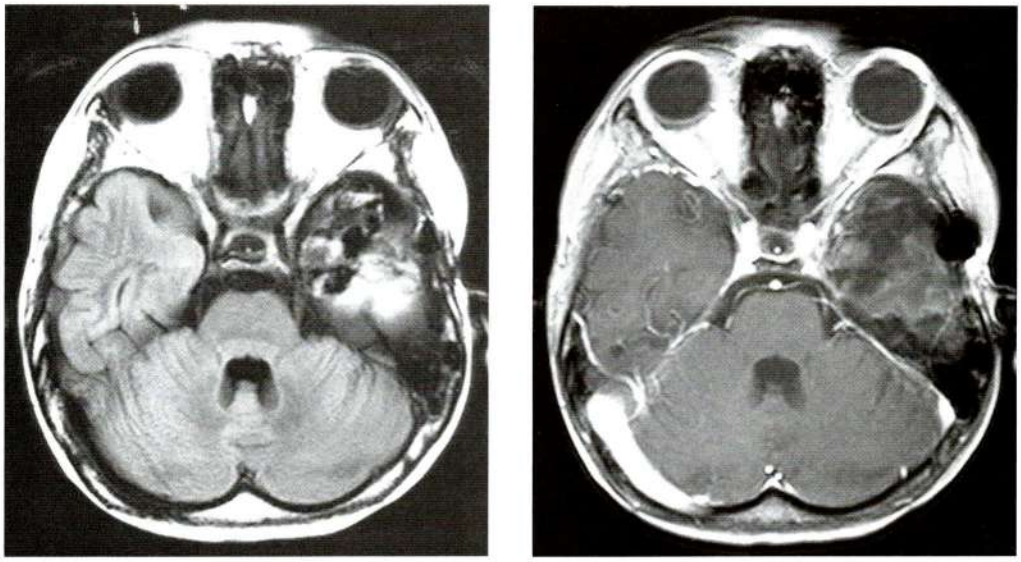

Fig.7 Follow up MRI 5 months post treatment. Axial FLAIR and Post contrast T1W. Complete resolution of the prior seen rim-enhancing lesion.

Case number two

A 51-year-old Thai male, who is a case with history of end stage renal disease (ESRD) post-renal transplantation and chemotherapy, presented with numbness of the right hand. MRI of his brain performed on April 24, 2009 showed small ring enhancing lesion with associated mild perilesional edema at left fronto-parietal lobe.

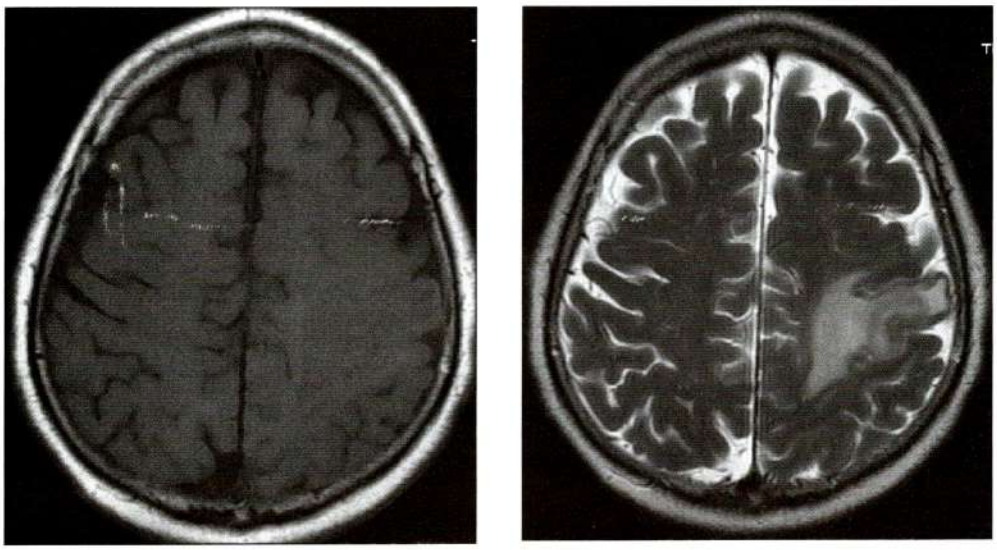

Fig.8 Axial T1W and T2W showed iso-intense-T1W/ dark T2W signal wall lesion with mild-hyperintense-T2W signal change in central portion. The lesion and an associated perilesional edema produce mass effect to the cortical sulci of the left post-central gyrus.

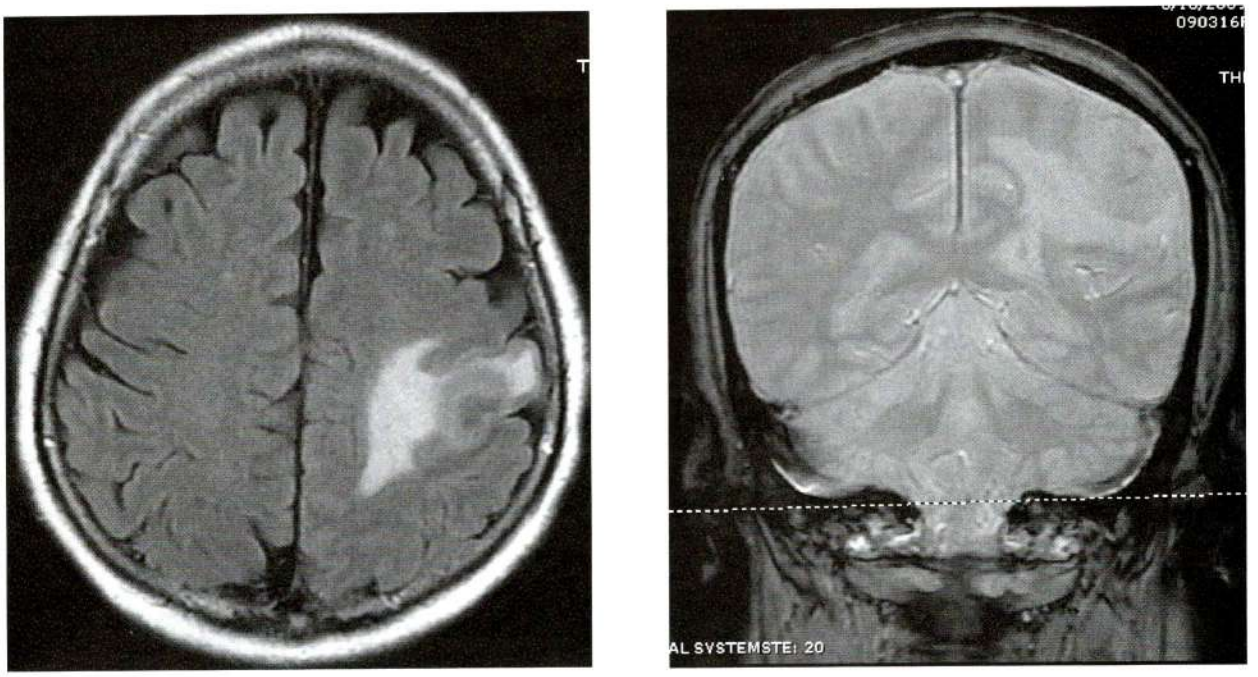

Fig.9 Axial FLAIR and coronal GRE-T2W better demonstrated dark T2W signal wall lesion with mild-hyperintense-T2W signal change in central portion.

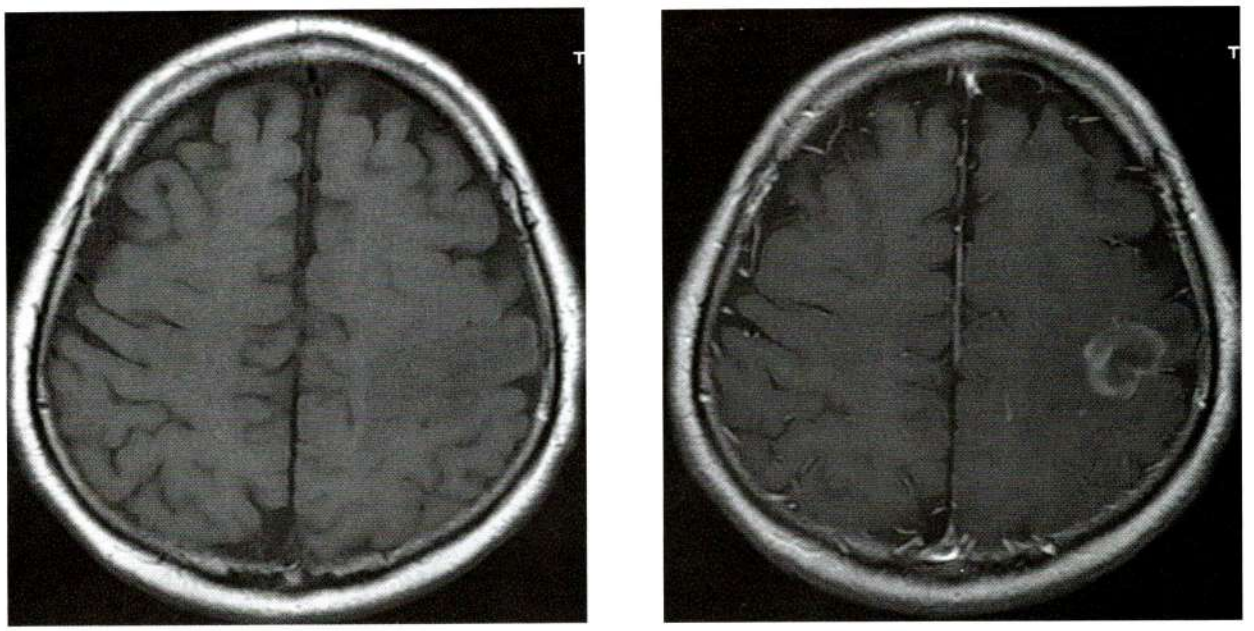

Fig.10 Axial T1W post-contrast showed complete, smooth near-uniform enhanced wall. The suspicious associated perilesional edema was not enhanced.

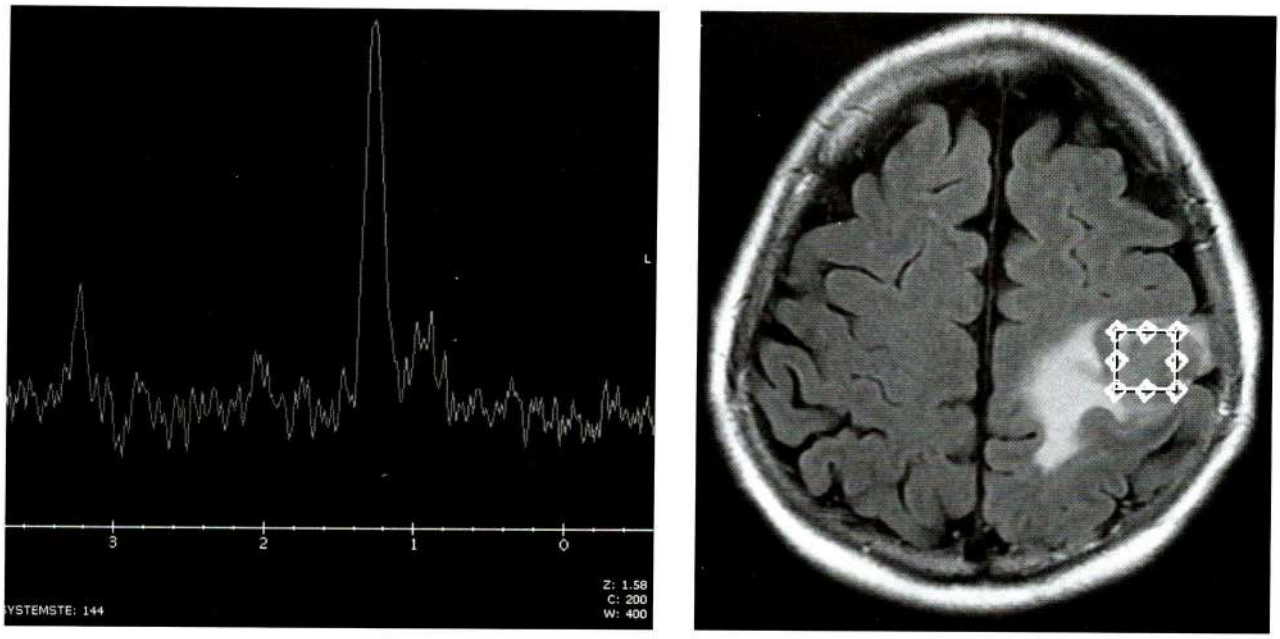

Fig.11 Single voxel MR spectroscopy in long TE showed high lactate peak at the rim-enhanced lesion.

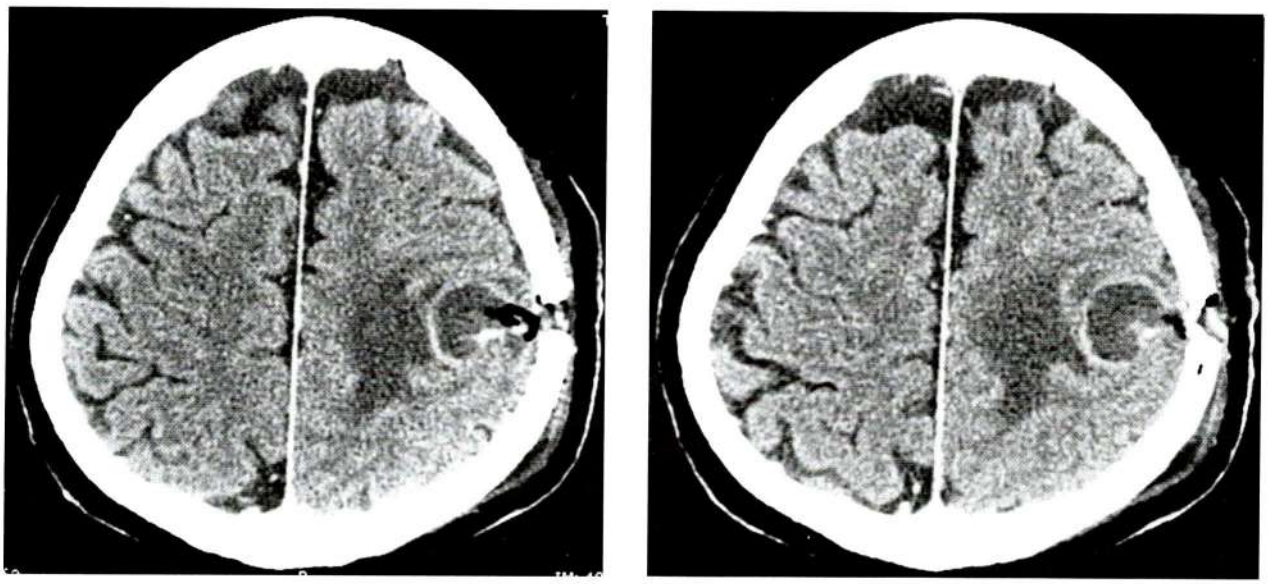

Fig.12 Follow up axial enhanced CT of the brain showed rim-enhanced lesion with persisted perilesional edema.

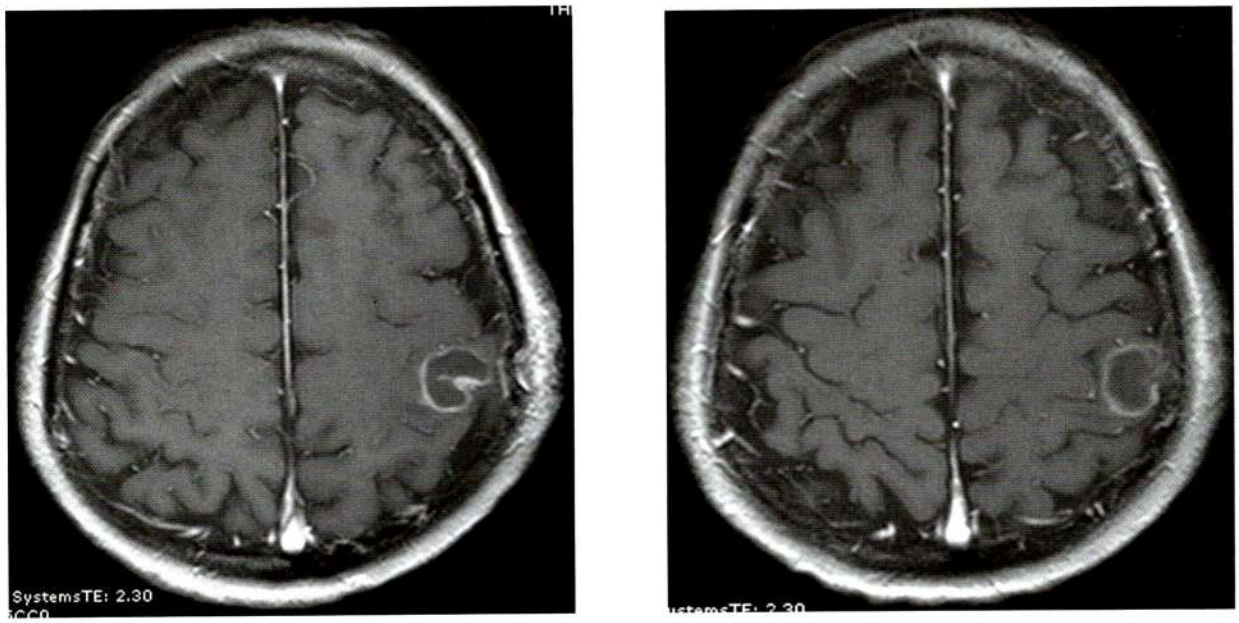

Fig.13 6-months follow up axial enhanced T1W MRI of the brain showed decreased size of the rim-enhanced lesion without perilesional edema.

Treatment: reduction of immunosuppressive therapy, the patients have complete resolution of the brain lesion.

Literature review of Primary Central Nervous System Posttransplant lymphoproliferative disorders (PTLD) by Amilcar A. Castellano-Sanchez, MD; Shiyong Li, MD, PhD; Jiang Qian, MD, PhD; Anand Lagoo, MD, PhD; Edward Weir, MD; Daniel J. Brat, MD, PhD Authors and Disclosures Posted: 02/27/2004; American Journal of Clinical Pathology. 2004; 121(2) © 2004 American Society for Clinical Pathology[2]. Posttransplant lymphoproliferative disorders (PTLDs) represent a spectrum ranging from Epstein-Barr virus (EBV)-driven polyclonal lymphoid prolife-rations to EBV+ or EBV- malignant lymphomas. Central nervous system (CNS) PTLDs have not been characterized fully. They reviewed the clinical, radiologic, and pathologic features of 12 primary CNS PTLDs to define them more precisely. Patients included 10 males and 2 females (median age, 43.4 years) who were recipients of kidney (n=5), liver (n=2), heart (n=2), peripheral blood stem cells (n=2), or bone marrow (n=1). All received immunosuppressive therapy. CNS symptoms developed 3 to 131 months (mean, 31 months) after transplantation. By neuroimaging, most showed multiple (3 to 9) intra-axial, contrast-enhancing lesions. Histologic sections showed marked expansion of perivascular spaces by large, cytologically malignant lymphoid cells that were CD45+, CD20+, EBV+ and showed light chain restriction or immunoglobulin gene rearrangement. In distinction to PTLDs in other organ systems, CNS PTLDs were uniformly high-grade lymphomas that fulfilled the World Health Organization criteria for monomorphic PTLDs. Extremely short survival periods were noted for each CNS PTLD that followed peripheral blood stem cell transplantation. Survival of others with CNS PTLD varied; some lived more than 2 years.

Radiologic and Pathologic Features

By neuroimaging that included magnetic resonance imaging (MRI) or computed tomography (CT) scan, CNS PTLDs were seen as multiple, contrast-enhancing, intra-axial lesions in 10 of 12 cases and as solitary lesions in the remaining 2 cases. In all cases, the lesions were associated with extensive peritumoral edema. CNS parenchymal lesions were distributed in highest frequency in the cerebral hemispheres (44/54 [81%]), brainstem (8/54 [15%]), and cerebellum (2/54 [4%]). In the cerebral hemispheres, lesions were most common in the cortex and white matter (18/54 [33%] each), basal ganglia (7/54 [13%]), and corpus callosum (1/54 [2%]). No spinal cord involvement was noted in the 12 cases.

By immunophenotype, all tumors were CD20+. Three tumors so tested showed expression of additional B-cell markers (CD19, CD22, or CD79a). The T-cell marker CD3 demonstrated admixed lymphocytes in the background. Results from immunohistochemical analysis for light chains were available for 7 cases. Among these, all 7 were light chain-restricted, 3 for k and 4 for l. Of 12 tumors, 11 showed evidence of EBV infection within tumor cells.

Discussion

PTLDs are clinically and morphologically heterogeneous lymphoid tumors, their common elements being a history of organ transplantation and immunosuppression. These lesions arise most often in the allograft, but also frequently affect other organs, including the gastrointestinal tract, lung, lymph nodes, and bone marrow. Although their occurrence in the brain is relatively rare, it is critical for the pathologist to distinguish them from other CNS lymphomas and lymphoid proliferations. This is especially true for CNS PTLDs: the brain was the first and only manifestation of PTLD in all patients in this study. Since immunosuppressive therapy is highly relevant to the pathogenesis of PTLDs, treatment of these disorders nearly always involves its reduction.

We have presented two rare cases of polymorphic PTLD at medial left temporal lobe and left fronto-parietal lobe of the brain with successful treatment by reduction in immunosuppression. Both two cases showed rim-enhanced lesions by CT and MRI, which were similar imaging findings to brain abscess. MR spectroscopy did not differentiate between abscess and tumor. Clinical information includes history of organ transplantation with immunosuppressive agents and chronic onset should be warning us to diagnose PTLD. As review literature by Amilcar A. et al who reviews 12 cases of Primary Central Nervous System Posttransplant lymphoproliferative disorders (PTLD) suggests that CNS PTLDs are monomorphic by WHO criteria and have histopathologic features similar to the diffuse large cell lymphomas that occur in the HIV-infected population and elderly people--so-called primary CNS lymphoma (PCNSL). CNS PTLD and PCNSL are aggressive, large cell lymphomas, nearly always with a B-cell phenotype. Both have a marked predisposition to grow within perivascular spaces, to invade vascular walls, and to display a concentric, laminar pattern around central vessels that can be highlighted by stains for reticulin or collagen IV. PCNSLs and CNS PTLDs also are similar in their ability to infiltrate CNS parenchyma, and both typically demonstrate extensive necrosis. Similar to CNS PTLDs, the PCNSLs that arise in the HIV-infected population are EBV+. PCNSLs that arise in elderly people usually do not show evidence of EBV expression. The distinction between PCNSLs and

monomorphic CNS PTLDs lies in the clinical history, response to therapy, and clinical outcomes. The requirement for transplantation--solid organ or bone marrow allograft--together with post-transplant immunosuppression is absolute for the diagnosis of PTLDs. The majority of PTLDs in other organ sites occur within 1 to 4 years after transplantation, with slightly shorter latency periods after azathioprine therapy. Similar latency periods (3-131 months) were seen for PTLDs that arose in the CNS.

The majority of CNS PTLDs were multifocal on neuroimaging studies, often with large numbers of discrete, contrast-enhancing masses. When the lesions of CNS PTLDs were multiple, the number varied from 3 to 9, and most were confined to the supratentorial compartment. In 4 cases, both infratentorial and supratentorial lesions were seen. The solitary lesions (cases 6 and 7) involved the pons and the parietal lobe, respectively. In contrast, PCNSLs can be solitary or multifocal, depending mostly on the immunologic status of the patient. Up to 80% of PCNSLs that arise in immunocompromised patients are multifocal. In contrast, the majority of PCNSLs that arise in non-immunocompromised patients are solitary. Thus, neuroimaging features of CNS PTLDs overlap most with those of PCNSLs that arise in immunocompromised patients. It has been suggested that PCNSL is a "whole brain" disease, with diffuse involvement of CNS structures manifesting as solitary or multiple masses on neuroimaging, and the same may be true of CNS PTLDs. 32 Most neuroimaging studies of PCNSLs, as well as the clinical review of PTLDs by Phan et al, have stressed the intimacy of these lymphomas with the ependymal lining and distribution in the periventricular region. Distinguishing the contrast-enhancing lesions of CNS PTLDs or PCNSLs from infection by neuroimaging is not always possible, and a tissue-based diagnosis usually is required.

The term Epstein-Barr virus (EBV) induced post-transplant lymphoproliferative disorders (PTLD) describes a heterogeneous group of lymphoproliferative disease associated with EBV infection in solid organ and bone marrow transplant recipients. Lymphoid tumors were first described in transplant patients in 1968 and were called "reticulum cell sarcoma"; or as a subgroup of termed "pseudolymphomas" in light of their ability to undergo regression. *Frizzera et al*[3] first recognized the variable histologic appearances of these tumors and in 1981 introduced a pathologic classification to accommodate this histological heterogeneity. Clinically, these disorders may differ markedly in growth rates, and patients may manifest a spectrum of presentation varying from localized to disseminated involvement, and nodal to extranodal, including the allograft organ itself. Reported incidence of PTPD ranges from 0.8 to 20% and varies with the type of solid organ transplant, the age of patients transplanted, individual transplant centers and type of immunosuppression. The diagnosis of PTLD may convey mortality rates that range up to 50-80%.

In 1969 *Penn et al*[4] reported a case of a renal transplant patient on azathioprine and prednisolone who developed a rapidly progressive left hemiparesis. Brain biopsy revealed a tumor of lymphoid origin. The patient was given radiotherapy with synchronous dosage reduction of the immunosuppressive therapy. He demonstrated marked neurologic improvement with shrinkage of the mass. Two decades later Stariz et al[8] first used the term post-transplant lymphoproliferative disorder (PTLD) and suggested that reduction and/or discontinuation of immunocompressive medications could lead to

regression of the post-transplant malignancies.

Defining the clinical course, risk factors, and therapeutic results of PTLD have been severely limited due to the lack of: 1) a standard definition of PTLD; 2) an understanding of the pathogenesis of EBV-induced lymphocyte transformation and proliferation in transplant recipients; 3) standardized diagnostic techniques, and 4) randomized multicenter trails that examine effective prophylactic and therapeutically strategies. Two separate meetings have been organized of discussion and define future direction in the management of EBV-PTLD. The following document is a summary of the current knowledge of PTLD and of recommended areas that needs further development under the suspicious effects.

In addition, there are several practical aspects regarding the diagnosis of PTLD. Tissue biopsy is necessary to establish the diagnosis of PTLD. Excisional biopsy is preferred to provide adequate tissue for evaluation of cell type, clonality, virological studies, and architectural background. Needle biopsy should only be employed when larger biopsies are not practical. Cytology has a limited role in the diagnosis of PTLD, and should not be used to subclassify PTLD. The histological sample should be interpreted by a hematopathologist or a pathologist familiar with the histopathological features of PTLD. Communication between clinicians and pathologists is essential in directing the diagnostic work-up and ensuring that appropriate tissue for evaluation as expeditiously as possible. Ancillary diagnostic tests are primarily DNA-based and it is not necessary to preserve RNA except for research purposes. The single RNA-based diagnostic test currently in use employs in situ hybridization for EBV early RNA. Because this RNA species has extensive secondary structure, it is capable of surviving routine tissue handling and processing.

Although no specific staging system exists for PTLD, the ANN Arbor Staging Classification with Cotswold Modifications, which is currently used to stage non-Hodgkin's lymphomas, has been used for PTLD. It should be noted that although most EBV-PTLDs are of B cell origin, a small proportion arise from T cells. Finally, lymphomatous PTLD can be indistinguishable from the typical lymphoma or myeloma in which EBV is not present. Thus, these diseases should be recorded but not categorized as EBV negative PTLD, as it is currently unknown whether their incidence is higher in transplant patients versus the general population.

Quantitative EBV polymerase chain reaction technology is a promising innovation that may allow for an earlier diagnosis of PTLD and identification of those patients likely to develop PTLD. However, additional study is required before recommending it for routine clinical use. Important consideration includes the standardization of specimen type and the methodology of quantitation. Efforts should be directed at correlating quantitative PCR values in relation to: 1) outcome as related to level of EBV copies in peripheral blood at the time of PTLD diagnosis; 2) genome levels and response to therapy; 3) predicting development of PTLD for different types of organ allograft. Other areas for further study include EBV protein expression in PTLD and the role of lytic virus in PTLD.

Prospective multi-institutional studies are necessary to accrue sufficient case material to assess the usefulness of present reporting systems, and examine the applicability of systems such as the international Prognostic Index for non-Hodgkin's lymphoma in PTLD. Such studies could also uncover

other features of clinical significance, which should be incorporated into the diagnostic evaluation of PTLD. Although current definition of PTLD are solely focused on histological classification, nonhistological classification such as those that address clinical features of PTLD, could be of additional value in the prognosis of PTLD and therapeutically interventions.

Ho and colleagues[6] reported on a series of pediatric kidney transplant recipients. Patients who were EBV seronegative at time of transplantation had a 10% frequency of PTLD compared with patients who were EBV positive at the time of transplantation, who had a 0% frequency of PTLD. At the same institution, PTLD frequencies in adults who were EBV seronegative and EBV seropositive were 4.9% and 1.6%, respectively. Despite these figures, Harwood and colleagues[21] were unable to document any increase in PTLD in a series of EBV-seronegative pediatric thoracic transplant patients who received organs from seropositive donors. They concluded that EBV matching was not justified in this population.

Most patients with PTLD present with at least 1 tumor. About two thirds of these tumors are extranodal, and about one third are nodal. There is a tendency to involve specific sites. The gastrointestinal tract is involved in about 26% of cases and CNS in about 27% of cases. The allograft can also be involved. In this case, the frequency of involvement varies according to the specific type of allograft. PTLDs that arise in lung or intestinal transplant recipients involve those allografts in up to 80% of cases. The reason for this is not known. However, it is interesting that the lung and bowel are transplanted with a large indigenous lymphoid population. PTLDs that occur in patients receiving other types of allografts, such as liver and kidney, involve the allograft in about one third of cases. In contrast, the transplanted heart is only rarely involved with these tumors.

Imaging findings by MRI showed ring-enhancing lesion, which its wall appeared smooth, uniform, with dark T2W signal, favored brain abscess. However, on diffusion weight imaging (DWI), typical pyogenic brain abscess commonly showed restricted diffusion, due to presentation of inflammatory cells in its central core. Contrast to neoplasm, it appeared irregular thickened hyperintense-T2W signal change at its wall, may re restricted diffusion but at its central core which are contained tumor necrotic fluid collection must be not restricted diffusion. The reported cases showed incomplete restricted diffusion in its wall and partly in central core, caused equivocal differentiation between brain abscess to brain tumor. So biopsy of the lesion was performed for the definite diagnosis.

Initial treatment for PTLD is to reduce immunosuppression. A response is usually seen within 2-4 weeks of withdrawal of immunosuppression, and reduction in immunosuppression alone leads to long-term disease-free remission in 25-73% of adults. The chances of complete remission seem to be directly related to the degree of differentiation of neoplasm. Early and infectious mononuleosis-like lesions tend to regress more often with reduction in immunosuppression alone, compared to monomorphic PTLD. A proportion of cases of both types, however, require chemotherapy. The benefit of withdrawing immunosuppression and the risk of transplant rejection need to be carefully reconciled. The institution of chemotherapy also brings inherent risks of infections and *de novo* malignancies. Antiviral agents seem to have some effects on the early hyperplastic lesions. However, these agents do not

have significant effects on the lesion once monoclonality has emerged.

Another common dilemma is differentiation opportunistic infections and PTLD. Patients with immunosuppression after organ transplantation are at increased risk of infections and sepsis. However, it should be noted that opportunistic infections with positive tissue and/or blood cultures might mask an underlying hematological malignancy. Since immunosuppressed patient are at increased risk of developing opportunistic infections and hematological malignancies, both possibilities need to be considered on the differential diagnosis. This cases report stress the importance of biopsies of brain lesion in immunosuppressed patient following bone marrow and renal transplantation to direct appropriate treatment in an expedition fashion.

Conclusion

In conclusion, we have learned much about PTLD, but much cooperative work remains to be done before this disease can be conquered. EBV positive PTLD has served as a model of virus-associated lymphomagenesis, and the lessons learned here may have applicability in other tumor systems as well. As EBV-positive lymphomas are prevented or successfully treated, our attention will turn to EBV-negative tumors and other forms of neoplasia that continue to plague transplant recipients. For the present, however, awareness of PTLD and an aggressive stance toward the diagnosis of this disease, together with graded therapy using the best means available for the individual disease, remain our best form of defense against this theoretically fascinating yet deadly enemy.

References

1. Dr Frank Gaillard. Post transplant lymphoproliferative disorder (PTLD): September 4, 2009.
2. Castellano-Sanchez AA, Li S, Qian J, Lagoo A, Weir E, Brat DJ. Primary central nervous system posttransplant lymphoproliferative disorders. Am J Clin Pathol 2004 Feb;121(2):246-53.
3. Penn I. The changing pattern of post-transplant malignancies. Transplant Proc 1991 Feb;23(2):1101-3.
4. Starzl TE, Poster KA, Iwatsuki S, et al. Reversibility of lymphomas and lymphoproliferative lesions developing under cyclosporine-steroid therapy. Lancet 1984;1:583(8)
5. Ho M, Breinig MK, Dummer JS, et al. Epstein-Barr virus infections and DNA hybridization studies in post-transplantation lymphoma and lymphoproliferative lesions: the role of primary infection. J Infect Dis 1985 Nov;152(5): 876-86.
6. Harris NL, Ferry JA, Swerdlow SH. Posttransplant lymphoproliferative disorders (PTLD): Summary of Society Hematopathology Workshop. Semin Diagn Pathol 1997 Feb;14(1):8-14.
7. Michael Nalesnik, MD, Anthony J. Demetris, MD, John J. Fung, MD, PhD, Posttransplantation Lymphoproliferative Disorders.
8. Parmjeet Randhawa, MD, Adriana Zeevi, PhD. Authors and Disclosures Published: 03/31/2000

THE ASEAN JOURNAL OF RADIOLOGY 2012: 18(1): 72-77

Case Report

Benign Symmetric Lipomatosis (Madelung's disease); A Case Report

Luckana Girapongsa MD.[1], Pravitpong Kiatkungwankai MD.[2]
Orawan Autravisitkul MD.[1], Pariyanoot Deesuwun MD.[1]

[1] Department of Radiology, [2] Department of Surgery,
Samutsakorn Hospital, Samutsakorn, Thailand.

Abstract

Benign multiple symmetric lipomatosis (Madelung's disease) is a rare disease and characterized by non-capsulated accumulations of fat in a symmetrical manner around the neck and the shoulder, rarely involving the lower limbs and the lower body[1]. The prevalence is increased among the mediteranean population[2] and very rare in the oriental area[3]. The etiology is still unknown. We have presented with a case of madelung disease type I associated with avascular necrosis at both femoral heads and gynecomastia at the right breast.

Keywords: Benign symmetrical lipomatosis, Madelung's disease.

Introduction

Benign symmetric lipomatosis is a rare disease first described in 1846 by Brodie[4]. Madelung subsequent reported 33 patients with cervical lipomatosis in 1888[5], the classical description of the disease was published by Launois and Bensuade in 1893[6] defined this syndrome as presence of multiple symmetric unencapsulated fatty accumulations diffusely involving the cervical and the upper dorsal regions, the abdomen and the groin.

Historically, Madelung's disease has been more frequently observed in men (male to female ratio about 15 : 1 to 30 : 1)[7] and aged between 30-60 years old. The disease prevalence is increased among the Mediterranean population (incidence in italy : 1/ 25,000 men)[2,7]. There is clear relationship between this disease and excessive consumption of alcohol especially red wine[10,11]. Our case was diagnosed Madelung's disease with avascular necrosis at both hips and right gynecomastia.

Case report

History

A 39-years-old male were referred from the surgical outpatient clinic for searching cause of palpable neck masses. He found that there were some painless lumps at his right posterior neck, both cheeks and the right breast for a year before presentation. He felt that they were slowly growing and he started to worry about their natures.

His past history was that he just had been avascular necrosis at bilateral femoral heads S/P bilateral bipolar hemiarthropathy. His alcohol intake was excessive past 6 years but he tries to quit now. There is no family history of this condition and no continuous medication.

Physical examination revealed normal vital sign, no pallor or jaundice. There were ill-defined soft consistency mass-like lesions at the bilateral posterior neck and the anterior part of both ears. They measured about 15 cm and 4 cm in diameter; respectively. No sign of inflammatory process was demonstrated. The right breast was enlargement without definite mass or sign of inflammation. The left breast was unremarkable.

The liver and the spleen were not palpable. No sign of chronic liver disease was seen. The cardiovascular systems, the respiratory systems and the nervous systems were unremarkable.

The routine screening blood work up as CBD, BUN, creatinine and electrolytes analysis were unremarkable. Subsequently, He was underwent ultrasonography and computed tomography.

Image findings

The ultrasonography at the neck and both breasts.

The neck study

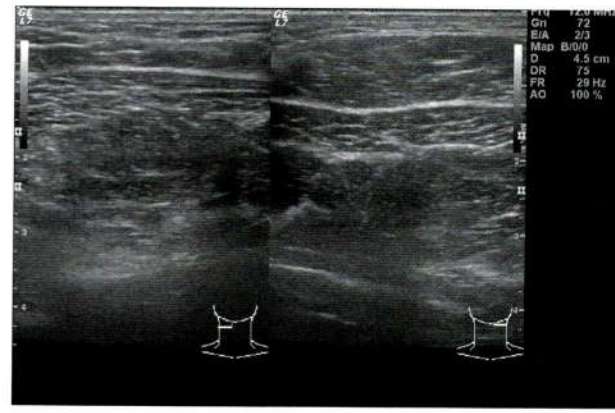

Fig.1 Ultrasound finding showed no definite mass at the posterior necks.

THE ASEAN JOURNAL OF RADIOLOGY
January-April 2012, Volume XVIII No.I

Both breasts study

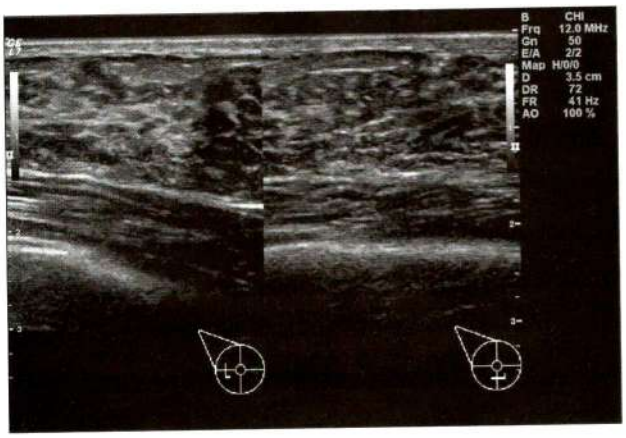

Fig.2a Ultrasound finding show fibroglandular tissue at the retroareolar area of the left breast.

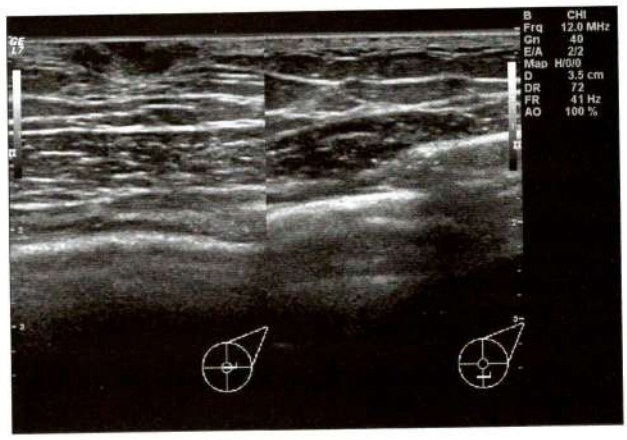

Fig.2b Ultrasound finding show normal nipple without retroglandular tissue of the right breast

The computed tomography of the neck

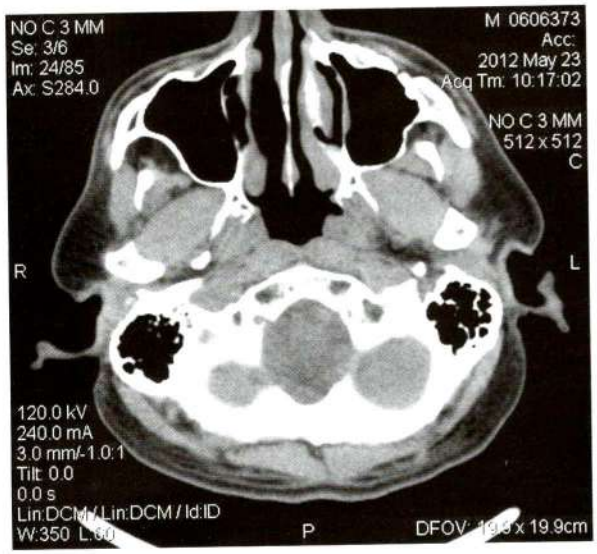

Fig.3a Axial non-contrast CT scan showed excessive fat filtration at bilateral cheeks

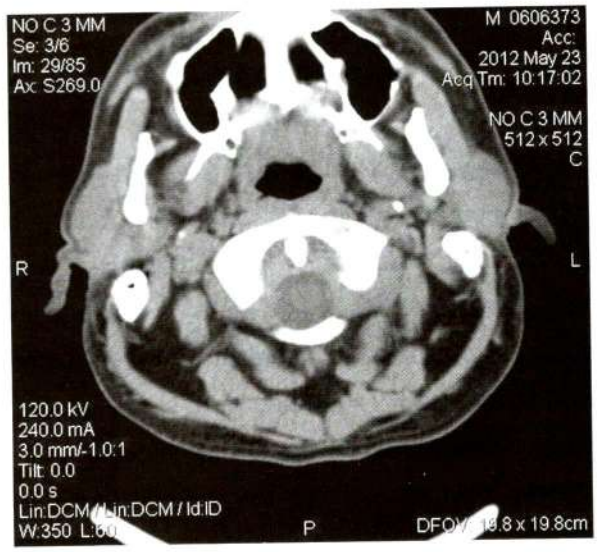

Fig.3b Axial non-contrast CT scan showed excessive fat filtration at posterior cervical space.

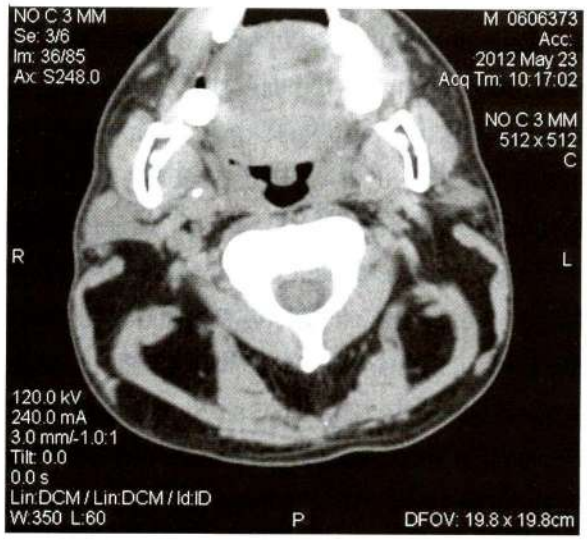

Fig.3c Axial non-contrast CT scan showed thinning of sternocleidomastoid muscles and paraspinal muscles with symmetrical fatty infiltration.

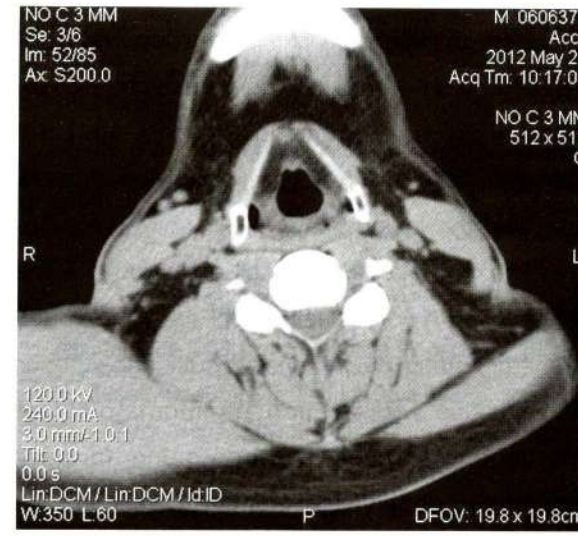

Fig.3d Axial non-contrast CT scan showed excessive fatty infiltration in submental area. No vascular invasion was seen.

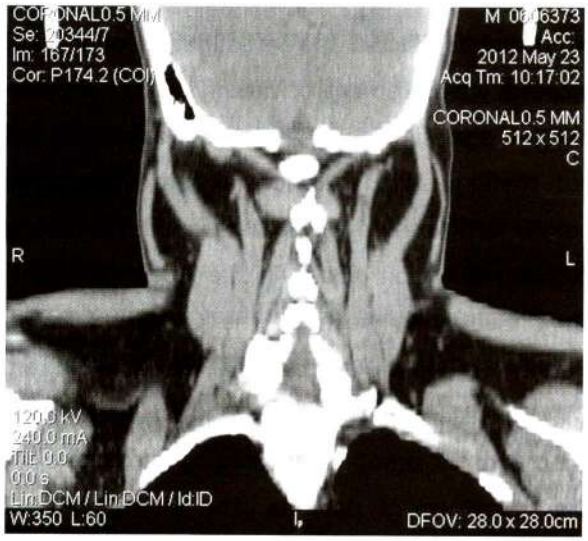

Fig.3e

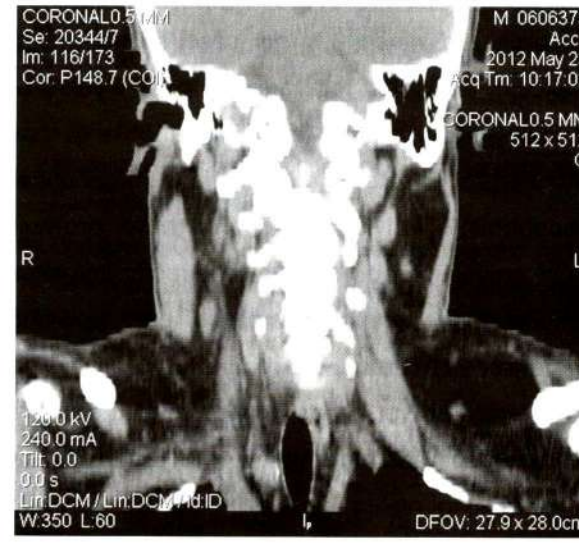

Fig.3f

Fig 3e and 3f Coronal non-contrast CT scan showed thinning of the sternocleidomastoid muscles and the paraspinal muscles with symmetrical fatty infiltration in the posterior cervical spaces. the perivertebral space and bilateral supraclavicular fossa.

He was underwent biopsy and his pathology revealed small piece of fibrofatty tissue as well as striated muscle. No inflammatory reaction or malignant was seen.

He was diagnosed as having multiple symmetric lipomatosis (Madelung disease). Finally; he was referred to Siriraj hospital.

Discussion

Benign symmetric lipomatosis is a rare disease characterized by non-capsulated accumulations of fat in a symmetrical manner around the neck and the shoulder, rarely involving the lower limbs and the lower body[1].

The pathogenesis is still unknown but there are several hypothesises such as defect in the adrenergic-stimulated lipolysis resulting in autonomy and massive proliferation of lipomatous cells, embryogenic brown fat undergoing functional sympathetic denervation, primary defect in brown fat mitochondrial DNA and recently it is found that 80% of patients with HIV -I infection treated with protease inhibitor develop this syndrome[8].

There is clear relationship between this disease and excessive consumption of alcohol especially red wine[10,11]. In our case, he had history of excessive alcohol intake in the past 6 years but he tries to quit now. Alcohol is known to have determen-tal effects on many organs. In genetically susceptibility individuals, alcohol have profound effect on fat metabolism which directly influences blood supply to marginal areas of perfusion such as the femoral heads[12] resulting avascular necrosis of bilateral femoral heads. Ingestion of the alcohol can also decreased in the serum testestorone level by increasing clearance from circulation through enhanced hepatic testosterone A-ring reductase activity resulting in gynecomastia[13]. Asymmetrical gynecomastia is common and unilateral gyneocomastia may actually represent a stage in the development of bilateral disease[17]. Our case diagnosed of the avascular necrosis of bilateral femoral heads and gynecomastia of the right breast. His physical examination showed no other evidence of chronic liver disease and also the liver study showed normal LFT. There are also associated of medelung's disease with liver disease, hyperlipidemia including elevated LDL, hypertriglyceride, hypothyroidism, diabetes mellitus and neurological changes[11,13].

The symptoms of this disease are variable although the patients may complain of interference with neck motion, difficulty in obtaining a proper fit cloths or respiratory difficulty. The fat deposits never spontaneous disappear and the disease is usually progressive over a period of years[1]. Our case seeked for medical help due to progression in size of his palpable masses.

Diagnostic is usually made of history and physical examination and confirmed by sonography, computed tomography (CT) and fine needle aspiration cytology. The sonographic finding of lipomatosis are typical however despite the frequent ulitization of the ultrasound in the investigation of the neck masses, measurement of density by CT provide a higher diagnostic fidelity[11,15,16]. In our cases, we could not distinguish the abnormal fatty tissue from normal fatty tissue by using ultrasound. We detected only some lymph nodes in the deep part of the neck. But when we used the CT, the CT could display the typical character of disease. Currently CT is considered to be the method of choice for the diagnosis; preoperative staging and post operative follow up of patients. The utilization of CT allows the investigator to rule out relevant differential diagnosis such as lymphoma and metastasis lymph nodes involvement. Also it allows the tumor staging in cases of multiple systemic lipomatosis associated with malignant disease[11]. The MR imaging can also provide the surgeon with adequate information[16].

The multiple symmetric lipomatosis is classified into three types, type I or diffuse lipomatosis of the

neck (horsecollar lipomata) lipomatous deposits maintain the aspect of the circumscribed protruding masses affecting primary the nape of the neck as well as the supraclavicular and the deltoid regions[1]. In advances cases, there will be mediastinal involvement with trachea and vena cava compressing as well as erodigestive tract compression. Type II or multiple systemetric lipomata of the shoulder girdle, the upper arms, the thorax, the thighs and sometimes the abdomen giving the patients so call pseudoathetic appearance and type III or a rare type with preponderance of the lipomatosis in the pelvic girdle (hips and thighs): gynecoid type[9]. Our case had characteristic of type I.

At the present time point there is no causal therapy available and dietetic intervention are not successful. Removal therapy is the only successful treatment although relapse may occur. Two main procedures are lipectomy or liposuction[7]. Our case was referred to Sirirajj hospital for proper management.

In conclusion; we presented with a case of madelung's disease type I associated with avascular necrosis at both femoral heads and gynecomastia at the right breast resulting from excessive alcoholic consumption without definite evidence of chronic liver disease.

Acknowledgement

The authors would like to thank Miss Chantana Wiriyasajja for computed tomography processing.

References

1. Chih-Chieh Chuang,Yen-Fu Cheng, Hsin-Pin Chang, Ching-Zong Lin. Madelung's Disease. J Chin Med Asset 2004; 67:591-4.
2. Feliciani C, Amerio P. Madelung's Disease: Inherited from an Ancient Mediterranean Population?. N Engl J Med 1999;340:1481.
3. Wu WH, Fang RH. Multiple symmetrical lipomatosis (Madelung's Disease): a case report. J Chin Med Assoc 1996;58:139-42.
4. Brodie BC. Lectures illustrative of various subjectd in pathology and surgery. Longman: London 1846:275-6.
5. Madelung OW. Über den fetthals (diffuses lipom des halses). Archiv Klin Chir 1888;37:106-30.
6. Launois PE, Bensaude R. De l'adeno-lipomatose symmetrique. Bull Mem Soc Med Hôp 1898;1:298.
7. M. Zuber, D. Pittasch. Benign symmetric lipomatosis (Launios-Bensauade syndrome)- A rare cause of muscular weakness. Eur J Med Res 2006;11:174-7.
8. Hengel RL, Watts NB, Lennox JL. Benign symmetric lipomatosis associated with protease inhibitors. Lancet 1997;350:1596.
9. Busetto, L., Strater, D., Enzi, G., Coin, A., Sergi, G., Inelmen, E. M. and Pigozzo, S. Differential clinical expression of multiple symmetric lipomatosis in men and women. Int J Obes Relat Metab Disord 2000;27:1419-22.
10. Landis MS, Etemad-Rezai R, Shetty K, et al. Case 143: Madelung disease. Radiology 2009;250:951-4.
11. Ligia Persici Rodrigues, Ernesto Lima Araujo Mel. Madelung's disease: a case report and literature review. Radiol Bras 2012;45.
12. Christopher Chang M and Eric Gershwin. Alcohol-Induced Osteonecrosis; critical review in the physical and rehabilitation medicine 2004;16:102.
13. Glenn D. Braunsein. Gynecomastia: N ENGL J MED 1993; 490-5.
14. Pollock, M., Nicholson, G. I., Nukada, H., Cameron, S., and Frankish, P. Neuropathy in multiple symmetric lipomatosis. Madelung's disease. Brain 1988;1157-71.
15. Gritzmann N, Schratter M, Traxler M, Helmer M. Sonography and computed tomography in deep cervical lipomas and lipomatosis of the neck. J Ultrasound Med 1988;7(8):451-6.
16. A.T. Ahuja, A.D. King, E.S. Y. Chan, J. Kew, W.W.M. Lam, P. M. Sun, W. King and C. metreweli. Madelung disease: Distribution of cervical fat and preoperative findings at Sonography, MR and CT. AJNR Am J Neuroraiol 1998;19: 707-10.
17. Wilson JD, Aiman J, MacDonald PC. The pathogenesis of gynecomastia. Adv Intern Med 1980;25:1-32.